THESIS

GEOSTATISTICAL METHODS FOR ESTIMATING SNOWMELT CONTRIBUTION TO THE SEASONAL WATER BALANCE IN AN ALPINE WATERSHED

Submitted by

Douglas M. Hultstrand

Department of Forest, Rangeland, and Watershed Stewardship

In partial fulfillment of the requirements

For the Degree of Master of Science

Colorado State University

Fort Collins, Colorado

Fall 2006

COLORADO STATE UNIVERSITY

JULY 24, 2006

WE HERBY RECOMMEND THAT THE THESIS PREPARED UNDER OUR SUPERVISION BY DOUGLAS M. HULTSTRAND ENTITLED GEOSTATISTICAL METHODS FOR ESTIMATING SNOWMELT CONTRIBUTION TO THE SEASONAL WATER BALANCE IN AN ALPINE WATERSHED BE ACCEPTED AS FULFILLING IN PART REQUIREMNTS FOR THE DEGREE OF MASTERS OF SCIENCE

Committee of Graduate Work

____
Nolan Doesken

____
Robert Musselman

____
Advisor: Steven Fassnacht

____
Co-Advisor: John Stednick

____
Department Head

ABSTRACT OF THESIS

GEOSTATISTICAL METHODS FOR ESTIMATING SNOWMELT CONTRIBUTION TO THE SEASONAL WATER BALANCE IN AN ALPINE WATERSHED

The performance of nine spatial interpolation models was evaluated to estimate snowmelt contributions to streamflow in the West Glacier Lake watershed (0.61 km^2), in the Snowy Range Mountains of Wyoming. Streamflow from the West Glacier Lake watershed has been previously estimated at 40% to 130% greater than measured precipitation inputs. Additional input into the watershed had been attributed to a permanent snowfield in the upper portion of the watershed covering approximately 2.4% of the watershed area. However, the excess output may be a result of inaccurate estimation of water quantities using current precipitation and stream gauging methods.

In April 2005, near peak accumulation snow depth measurements and snow density measurements were collected within West Glacier Lake watershed. The distribution of snow water equivalent (SWE) was calculated as the product of snow depth, snow density, and snow-covered-area (SCA). Snow depths were spatially distributed throughout the watershed through nine spatial interpolation models. Snow densities were spatially distributed through a multiple linear regression. The nine spatial snow depth models explained 18% to 94% of the observed variance in the measured snow depths. Co-kriging with solar radiation produced the best results explaining 94% of the observed variance in snow depth measurements. The annual water balance, expressed as equivalent water depths for water year 2005, was total precipitation (1,481 mm), snowpack sublimation (251 mm), and streamflow (1,000 mm), resulting in an evapotranspiration estimate of 230 mm. Estimated SWE from the field survey data was 67% greater than precipitation gauge estimates and accounted for 85% of the annual streamflow. Summer precipitation was not a significant contributor to the annual hydrograph and was also less than snowpack sublimation. Precipitation gauge values were unrepresentative of actual precipitation depths, and several spatially distributed snow depth models provided better estimates of precipitation inputs.

Douglas M. Hultstrand
Department of Forest, Rangeland, and Watershed Stewardship
Colorado State University
Fort Collins, CO 80523
Fall 2006

ACKNOWLEDGEMENTS

Appreciation goes to Robert Musselman and John Korfmacher of the Rocky Mountain Research Station (US Forest Service) for their help and support at GLEES, and Robin Reich (Colorado State University) for spatial modelling support. Special gratitude to everyone who contributed to the field data collection: Jeff Derry, Dr. Steven Fassnacht, Dena Hicks, John Korfmacher, Scott McKim, Dr. Bob Musselman, Julie Repass, Wendy Ryan, and Alex Schaaf, Dr. John Stednick. I would like to acknowledge members of my graduate committee, Steven Fassnacht, John Stednick, Robert Musselman, and Nolan Doesken, who provided support, insightful comments, and guidance. Special thanks are extended to my family and friends as they have provided continuous support in my personal and academic endeavors.

TABLE OF CONTENTS

LIST OF FIGURES

LIST OF TABLES

CHAPTER 1

1.1 INTRODUCTION

Knowledge of the variables composing annual inputs and outputs in a water balance are essential to understanding watershed level processes. The components of a water balance are precipitation, streamflow, evapotranspiration, and storage. Precipitation is the primary input of water to a watershed. Streamflow and evapotranspiration are the major outputs of water. The most basic water balance equation can be evaluated as the difference between the volume of water entering the watershed and leaving the watershed. The difference is equal to the change in the volume of water stored. Quantifying these water flux variables, especially winter precipitation, through measurement and estimation are crucial to understanding the basic hydrology and hydrochemistry of a watershed.

In the mountainous regions of the western United States, the majority of annual precipitation falls as snow and is stored in high-elevation mountain snowpacks. Mountain snowfall can be stored on the surface for time periods ranging from hours to months before melting and continuing through the hydrologic cycle. The annual hydrograph in high-elevation areas is driven primarily by the melting of deep seasonal snowpacks. In the western United States, stream runoff during the snowmelt season (May-July) accounts for more than 75% of total annual flow [e.g., *Kattelmann and Elder*, *1991; Doesken and Judson, 1996*]. In high-elevation seasonally snow-covered basins, obtaining accurate estimates of the amount of water contained within the snowpack is important for the purposes of river and flood forecasting, and in terms of correctly representing the inputs into a snow-dominated system.

A challenging problem in snow hydrology is to understand and quantify winter precipitation in mountain catchments. Accurate precipitation data are essential for quantifying water balance studies and/or streamflow; therefore measurements need to be as accurate as possible. Within a small-scale watershed ($<10^3$ km^2), rainfall, snowfall, and snowcover are not homogenous, are highly variable, and hard to estimate in complex terrain [*Johnson and Hanson, 1995*]. Snow water equivalent (SWE) is an important input into any high elevation hydrologic model because it affects streamflow [*Luce et al., 1998*] and hydrochemistry [*Ruess et al., 1995*] of a watershed. SWE is defined as the depth of water that would result from melting the snow, and is expressed as a unit of length. Spatial and temporal estimates of SWE are limited due to the extreme spatial variability snow exhibits. To better quantify and estimate snowmelt runoff, it is essential to account for the spatial differences in SWE distribution [*Elder et al., 1998; Luce et al., 1998; Erickson et al., 2005*].

In snow dominated watersheds, such as alpine and subalpine regions, it is important to gain an understanding of precipitation quantity, variability, and the distribution of SWE. Rugged mountain topography can produce complex patterns of snow distribution, controls snow accumulation, and snow ablation [*Elder and Dozier, 1990*]. First and foremost, accurate estimates of winter precipitation, distribution, and ablation are fundamental toward understanding the drivers of watershed processes in mountainous regions.

1.2 HYPOTHESIS

High elevation, snow-dominated watersheds provide an opportunity to estimate the accumulation, distribution, and melting of deep seasonal snowpacks. Net winter precipitation is usually a significant component to the seasonal water balance in an alpine watershed.

It was hypothesized that by combining intensive field measurements with spatial interpolation techniques, a better estimate of winter precipitation in an alpine watershed can be made.

1.3 OBJECTIVES

The objective of this study was to quantify net winter precipitation stored within the mountain snowpack that was available for snowmelt runoff.

Specific study objectives were:

i) To take field measurements of snow depth, snow density, and snow-covered area in an alpine watershed.

ii) To develop several geostatistical models that represent the measured snow depth and snow density distribution.

iii) To calculate evaporation and sublimation losses from the watershed using meteorological data collected within the watershed.

iv) To take field measurements of streamflow and compile annual streamflow data.

v) To calculate the annual water balance using the above components and conduct an error analysis on each term.

In this study, the performance of nine interpolation methods was evaluated. The nine spatial snow depth models used were: 1) inverse distance weighting 2) ordinary kriging 3) modified residual kriging 4) binary regression tree 5) a combined method of binary regression tree and kriging 6) co-kriging snow depth with elevation 7) co-kriging snow depth with solar radiation 8) co-kriging snow depth with slope, and 9) co-kriging snow depth with northness. Variations in snow density were modelled and distributed using a multiple linear regression model. Calculated elevation, slope, aspect, solar radiation, and northness were used as independent variables to aid in snow depth and snow density estimates. Snow-covered area (SCA) was derived from aerial photographs of West Glacier Lake (WGL) watershed taken during peak snow accumulation. The goal of modelling snow depth, snow density, and SCA for this study is to distribute SWE over all snow-covered portions of the watershed in order to quantify winter precipitation inputs into a small alpine watershed.

CHAPTER 2

2.0 BACKGROUND

Recent pressure on hydrologic resources caused by increased human populations and resource development increases the need for accurate measurements of hydrologic processes occurring within a watershed. With a majority of the western mountain regions annual streamflow derived from snowmelt, it is important to further develop our understanding of the spatial variation of a snowpack processes in order to better estimate the timing and magnitude of runoff and other hydrologic processes within a watershed.

2.1 Spatial Variability

Knowledge about the physical parameters controlling snow distribution can provide valuable insight into snow accumulation and ablation processes. Snow distribution is controlled at multiple scales in which different physical processes dominate and alter the snowpack surface. Spatial variability, as snow depth or SWE, in the seasonal snowpack can be divided into two components: large-scale and small-scale variation. The difference between these two scales is dependent on the study objectives, the process scale, measurement scale, and model scale [*Blöschl, 1999*].

The process scale is related to the natural variability of the variable and is often defined as the length of spatial dependence or the correlation length. The measurement scale, is relevant to the sampling pattern, and can be characterized by a scale triplet (Figure 2.1): spacing, extent, and support [*Blöschl et al., 1991; Blöschl, 1999*]. Spacing is termed to be the distance between samples; extent is referred to the overall region of the data; and support, is defined as the size or area of the sample [*Blöschl et al., 1991; Blöschl, 1999*]. The model scale consists of a similar scale triplet, but depends on the spatial properties of the model used [*Blöschl et al., 1991; Blöschl, 1999*].

Issues of scale are inherent in snow accumulation and distribution, and a majority of all hydrologic processes. Small research areas studied in detail may exhibit extreme heterogeneity, while larger research areas studied with less detail may exhibit patterns and homogeneity [*Blöschl, 1999*]. Sampling techniques should take into account the natural variability of the measured process and account for the measurement scales and model scales in order to accurately interpret the data and model the physical process.

2.2 Factors Affecting Snow Distribution

Snow on the ground is a dynamic medium where the properties and characteristics of fallen snow change continuously as a function of energy fluxes, wind velocity, and water vapor. In addition to scale dominated processes, snow distribution is controlled through a combination of climatic and land surface processes. Snow distribution operates at multiple scales in which different processes dominate and influence snow accumulation and distribution patterns. Previous research has shown connections between certain variables and the processes that control snow distribution [*Erxleben et al., 2002; Winstral et al., 2002; Erickson et al., 2005*]. Based on these findings, the relationships between the factors of wind, elevation, slope, aspect, and solar radiation are of important variables to consider in snow distribution research.

2.2.1 Wind

In mountainous regions, the redistribution of snow by wind has often been cited as one of the predominant influences on snow accumulation and snow deposition [*Elder et al., 1991; Luce et al. 1998; Winstral et al., 2002*]. Regions of converging air flow cause wind speeds to increase, thus increasing wind scour rates and snow redistribution. Regions of diverging air flow cause winds speeds to decrease, thus decreasing wind scour rates, snow redistribution, and enabling the potential for snow deposition. Recent research has sought to parameterize the effects of wind redistribution through terrain analysis [*Marks and Winstral, 2001; Winstral et al., 2002; Winstral and Marks, 2002*].

2.2.2 Elevation

The effect of elevation on snow accumulation is thought to be one of the more significant relationships affecting snow distribution. Precipitation typically increases with elevation in mountainous regions due to orographic precipitation [*Spreen, 1947; Meiman, 1968; Barry, 1992; Roe, 2005*]. Often a linear trend can be associated between elevation and precipitation [*Gray and Male, 1981*]. This trend is generally due to the increase in the number of snowfall events and a decrease in evaporation and melt with increased elevation. The rate of increase with elevation can vary from year to year and from location to location and storm to storm. However, greater wind velocities at higher elevations produce less snowcover on ridge tops compared to basin valleys due to a greater snow redistribution potential [*Gray and Male, 1981; McClung and Schaerer, 1993*].

2.2.3 Slope

Slope is considered to be an important terrain feature due to its role in snow accumulation and redistribution patterns. Terrain slope and wind velocity are believed to affect orographic precipitation patterns and snow distribution more than elevation [*Gray and Male, 1981; Cline, 1992; Winstral et al., 2002*]. Most research that pertained to slope angle and snow redistribution has focused on the processes of moving snow from steeper slopes to less steep slopes through sloughing and avalanching [*McClung and Schaerer, 1993*]. More research has incorporated slope angle into statistical models to distribute snow depth from point observations with considerable success [*Erxleben, 2002; Winstral et al., 2002; Molotch et al., 2005*].

2.2.4 Aspect

Aspect can have fundamental effects on snow distribution processes [*Meiman, 1968; Dexter, 1986*], and snowpack energy balance components [*Barry, 1992, Deems, 2002*]. The exposure of the slope aspect to the sun can affect solar radiation, which in turn controls the snowpack temperature and stability [*McClung and Schaerer, 1993*]. Sunny, south-facing slopes tend to have warmer snow temperatures that can produce a melt region that can freeze and create an ice layer. These ice layers can play a significant role in snowpack distribution [*McClung and Schaerer, 1993*] and ablation processes [*USACE, 1998*]. Research on Niwot Ridge, Colorado, showed an increase in snow density on south-facing slopes, and an increase in snow depth and SWE on north-facing slopes [*Dexter, 1986*].

2.2.5 Solar Radiation

In alpine environments, the spatial and temporal distribution of solar radiation can significantly control the timing and magnitude of snowmelt [*Elder et al., 1991; Marks and Dozier, 1992*], and can play a significant role in the snow accumulation and redistribution patterns [*Balk and Elder, 2000; Erickson et al., 2005*]. Snow albedo is a major component of the snowpack energy balance, and is known to affect melt rates more on high-elevation south-facing slopes than lower elevation or north facing slopes [*Blöschl, 1999; Molotch et al., 2004*]. In mountainous terrain, the energy balance can vary significantly due to complex topography, such as the difference in degrees of shading and exposure of solar radiation. *Dozier* [*1980*], developed an algorithm for modelling net solar radiation in mountain terrain. This model has been used in previous snow distribution studies and has shown to be adequate for statistical models of SWE distribution in alpine regions [*Elder et al., 1995, 1998; Balk et al., 1998*].

2.3 Estimating Winter Inputs

Precipitation as rain and snow is the most commonly measured component of the hydrologic cycle. Precipitation is a major factor that controls hydrologic processes within a region and exhibits large temporal and spatial variability. Such variability can be important for modelling hydrologic variables and for accurately quantifying a water balance. Accurate measurement of precipitation in mountainous regions is particularity difficult to quantify, given that a majority falls as snow and is under collected.

2.3.1 Precipitation Gauges

Typical watershed studies measure both solid and liquid precipitation quantities with a standard precipitation gauge. Precipitation gauges, shielded and unshielded, inherently underestimate total precipitation due to local airflow, wind undercatch, wetting, and evaporation loss [e.g., *Goodison et al., 1998; Fassnacht, 2004; Roe, 2005*]. Wind-induced turbulence over the gauge orifice accounts for the greatest systematic error in precipitation measurements, this component accounts for 2–10 percent error for rain and 10-50 percent error for snow [*Groisman and Easterling*, *1994*]. Often only a few or no gauge measurements are available in the watershed of interest. Additional precipitation data from Snow Telemetry (SNOTEL), and Cooperative Observer Program (COOP) are available as an index for large scale precipitation quantity and distribution; but often not representative of the quantity and distribution within a small-scale, mountainous watershed.

In addition, most precipitation gauges are located in lower elevations based on accessibility and do not account for variable orographic influences. In rugged terrain, point measurements used to measure precipitation are often less than the ground truth due to large elevation gradients and the valley locations of most meteorological stations [*Groisman and Easterling, 1994*]. Precipitation gauge measurements need to be adjusted for wetting loss, evaporation loss, wind undercatch, and orographic influences before actual ground precipitation can be estimated [e.g. *Daly et al., 1994; Goodison et al.,* *1998*]. Even after correction methods have been applied, large uncertainties and potential data errors can still be present.

The most common and largest errors associated with precipitation gauges are those due to wind effects for both shielded and non-shielded gauges. Point measurement errors can be in the range of 5 to 15 percent for long-term data, and as high as 75 percent for individual storms [*Winter, 1981*]

2.3.2 Snow Course and SNOTEL

In the mid 1930's, the Natural Resource Conservation Service (NRCS), started the western snow course program. The NRCS program was designed to measure snowpack properties in the western mountains and to forecast water supply by watershed. Snow course teams collect SWE and snow depth data around the first of the month during the winter and spring. In the mid 1970's, the NRCS started to implement Snowpack Telemetry (SNOTEL) measurements, where SWE, precipitation, and temperature data were reported daily for each site. To date, the NRCS manages over 660 remote snow sites in different mountain regions. These data are available as an index for large scale SWE distribution and for potential snowmelt estimates; but often not representative of the quantity and distribution within a small watershed.

2.3.3 Remote Sensing

New technological advances on airborne and remotely-sensed data provide an alternative to precipitation gauge measurements. Recent progress in remotely-sensed data has shown promise for improving spatial representation of snowpack properties, and in turn provides an accurate estimate of winter accumulation. To date, several active and passive sensors are in operation for monitoring snow. The Special Sensor Microwave Imager (SSM/I) is a unique passive microwave sensor designed to measure SWE. The SSM/I sensor provides excellent representation of SWE distribution for large homogeneous areas, (25 km pixel resolution), but are limited in use for small-scale research areas. SCA can be remotely-sensed accurately, but this property is only related to the potential snow runoff volume [*Blöschl et al., 1991*]. Algorithms for estimating snowpack properties at small resolutions are still being developed by active research, (NASA Cold Land Processes Experiment (CLPX)), therefore remotely-sensed data are only feasible for large study areas unless using costly airborne data such as LiDAR (Light Detection and Ranging) [*e.g. Deems et al., 2006*].

2.3.4 Field Surveys

In a small alpine/subalpine watershed, a comprehensive understanding of net winter precipitation and distribution throughout the basin due to influences of elevation, slope, aspect, and radiation, can be attained by depth-density surveys during peak snow accumulation. Direct measurements of snow depth and snow density taken within a watershed provide accurate estimates for determining net winter precipitation and SWE distribution. Intensive field sampling has shown to provide increased knowledge on the relationship between SWE and the variables that control its distribution, as well as the scales at which they operate [*Erxleben et al., 2002; Erickson, 2004*]. Previous studies have had success using a combination of slope, aspect, elevation, solar radiation, wind redistribution, and northness as independent variables in statistical models for computing

SWE distribution across a watershed [*Erxleben et al., 2002; Winstral et al., 2002; Molotch et al., 2003, Erickson, 2004*]. In addition, intensive field measurements combined with geostatistics and binary regression tree methods have shown to provide representative estimates of water volumes stored in mountain snowpacks and SWE distribution within alpine watersheds [*Elder et al., 1995; Balk and Elder, 2000; Erxleben et al., 2002; Erickson, 2004*].

2.4 Spatial Interpolation of Point Measurements

Spatial interpolation methods use point data to estimate unknown values at specific locations. A large variety of interpolation methods exist and vary from simple to extremely complex. When selecting a model, it is important to realize that the quality of the interpolated surface is dependent on the accuracy of the original point data and how well that method reflects the underlining spatial structure [*Blöschl and Grayson, 2000*].

2.4.1 Inverse Distance Weighting

Inverse distance weighting (IDW) is one of the most simple interpolation methods and often yields satisfactory results. The basic premise of IDW is that data points are weighted by the inverse of their distance to the estimation point. This method has the effect of giving more weight to nearby data points than those farther away. IDW methods have been used to distributed point snow depth values across regional scales [*Fassnacht et al., 2003*] and at the small basin scale [*Erxleben et al., 2002; Molotch et al., 2005*].

2.4.2 Geostatistics

Geostatistical techniques were first developed in the late 1960's and early 1970's to address a crucial problem in the mining and geology industries; how to estimate the quantity of a mineral a over large region with a limited number of data. Recently, geostatistical methods have been applied throughout hydrologic sciences, especially snow hydrology. Geostatistical techniques have been used to distribute snow depth and SWE values across regional scales [*Carroll and Cressie, 1996; Molotch et al., 2005*] and at the small basin scale [*Hosang and Dettwiler, 1991; Balk and Elder, 2000; Erxleben et al., 2002; Erickson et al., 2005*].

Geostatistical methods model both the spatial trend and spatial variability of the data. Modelling both the spatial trend and spatial variability offers a stronger estimation procedure than classical statistics [*Balk et al., 1998*]. Geostatistical data usually exhibit small-scale variation that can be modelled as spatial correlation. The variogram model is used to model the spatial variability as a function of the distance between sampling points. Once a theoretical model is fit to the variogram, kriging and co-kriging interpolation methods can be performed.

2.4.3 Binary Regression Tree

Binary regression tree methods are a statistical technique developed in the 1960's that can be used to predict the response variable from a set of predictor variables [*Breiman et al., 1984*]. The independent variables can be related to the dependent variable in a non-linear hierarchical manner. The regression tree model is fit using binary recursive partitioning, where the data are split into increasingly homogeneous subsets of data [*Breiman et al., 1984*].

Early attempts were made to model the spatial distribution of snow depth in alpine regions using different topographic variables as predictors [*Elder et al., 1995; Elder et al., 1998*]. Results from these studies were able to explain a greater portion of the variance seen in field data compared to other methods used by the authors. Recently, regression tree models have been used in combination with geostatistical methods, where the large-scale trend is modelled using regression tree methods and the tree residuals are used to model the small-scale variability [*Balk and Elder, 2000; Erxleben et al., 2002; Molotch et al., 2005*].

2.5 Streamflow

Streamflow data are perhaps the most important information to the hydrologist due to its importance on determining the amount of water flowing in a river at a specific time and for quantifying the amount leaving a contributing upstream area. Streamflow has been studied extensively over the years, and a number of devices and methods have been developed to measure streamflow [*Chow, 1959; King and Brater, 1963; Henderson, 1966*]. These techniques are: 1) direct volume measurements, 2) constricting flow through weirs or flumes, and 3) current meter discharge measurements [*Winter, 1981; Dingman, 2002*].

Water level or stage height is typically measured with a staff gauge or water level recorder. The stage height is then converted to discharge either by stream gauging relationships or with precalibrated structures such as flumes and weirs. Measurement error associated with stage readings and flumes are considered to be less than 5 percent [*Winter*, 1981]. Errors associated with pygmy meter discharge measurements are +/-3.5 percent [*Herschy, 1973*].

2.6 Evapotranspiration

Evaporation is the process by which water changes from a liquid to a vapor. Transpiration is the loss of water from plant leaves by evaporation through the leaf stomata. Evaporation and transpiration combined is termed evapotranspiration. Evapotranspiration rates are dependent upon temperature, vapor pressure, wind velocity, and the nature of the surface [*Viessman and Lewis, 2003*]. Evapotranspiration is an important process within watershed studies because it can be a source of significant water loss to the atmosphere. Methods for estimating evapotranspiration from a region include budget methods, such as energy budget and water budget; comparative methods such as evaporation pans; and aerodynamic methods, such as eddy correlation, gradient, and mass transfer [*Winter, 1981*]. Previous research in mountain watersheds has documented annual evapotranspiration values between 0.1-0.8 m [*Kattelmann and Elder, 1991; Hasfurther et al., 1994; Ruess et al., 1995*]. *Antal et al.,* [1973] compared five evaporation methods to the energy balance evaporation method and showed that annual evaporation values deviate 5 percent from the energy balance method, and that monthly values deviate 10 to 15 percent from the energy balance method.

2.7 Snowpack Sublimation

Sublimation is the conversion between the solid phase and vapor phase, with no intermediate liquid stage. Sublimation of snow in wind swept alpine/subalpine regions is an important hydrological process because snowpack sublimation can account for significant water losses to the atmosphere. Methods for estimating sublimation from a snowpack are energy budget methods, snow evaporation pans, and aerodynamic profile methods, such as latent heat flux and sensible heat flux. Net sublimation losses from the seasonal snowpack have been estimated to be between 10-50% of the seasonal snow accumulation [*Hood et al., 1999; Pomeroy and Essery, 1999*].

2.8 Summary

Using the background information in this chapter, research methods were selected to perform a water budget analysis to quantify the annual inputs and outputs from a small alpine watershed.

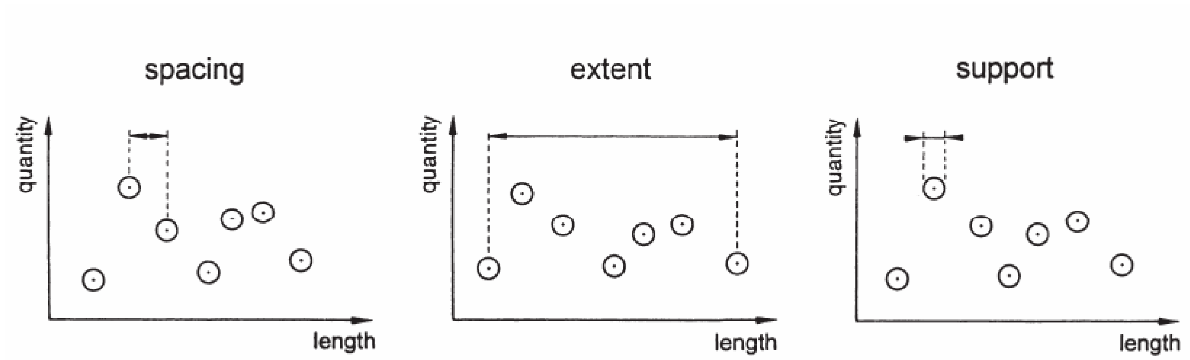

Figure 2.1. Definition of the scale triplet: spacing, extent, and support (Figure from Blöschl, 1999).

CHAPTER 3

3.0 STUDY SITE

Research for this project was conducted in West Glacier Lake (WGL) watershed within the Snowy Range Mountains, Wyoming at 41°22’30" latitude and 106°15’30" longitude (Figure 3.1). WGL watershed is part of the US Forest Service’s Glacier Lakes Ecosystem Experiments Site (GLEES) developed to conduct research on the effects of atmospheric deposition on alpine and subalpine ecosystems [*Musselman, 1994*].

GLEES is approximately 575 ha consisting of three small watersheds beneath a northeast-southwest ridge located at 3,200 to 3,500 m elevation. WGL watershed ranges in elevation from 3,277 m at West Glacier Lake outlet to 3,493 m at the top of the basin. Mean annual temperature is -1°C at the outlet and -2.5°C at the top of the basin [*Korfmacher and Hultstrand, 2006*]. Precipitation and temperature data from the GLEES Tower show that mean annual precipitation is 1.20 m, and precipitation falling below zero degrees Celsius (snow) accounts for 60 – 80 percent of the annual precipitation measured with a long-term average of 75 percent per year. Snow starts to accumulate in November and remains in the watershed until early June [*Wooldridge et al., 1996*]. This region is dominated by strong westerly winds that range between 0 m/s and 26 m/s with an average of 8 m/s [*Korfmacher and Hultstrand, 2006*]. These climatic conditions combine to create an environment where snow accumulation, snow redistribution, and snowpack sublimation can have significant impacts on the watershed hydrology.

Since 1986, meteorologic and streamflow measurements have been collected within GLEES to examine the effects of atmospheric deposition on a pristine alpine/subalpine ecosystem [*Musselman, 1994*]. Currently, there are five precipitation stations surrounding GLEES: National Atmospheric Deposition Program (NADP) WY00 and WY95, Clean Air Status and Trends Network (CASTNET), GLEES Tower, and Brooklyn Lake Snowpack Telemetry (SNOTEL). Large inter-annual and annual variability exists between measured precipitation quantities at each station. Precipitation input measurements for the GLEES are currently estimated from the WY00 and GLEES Tower, both are equipped with Belfort® rain gauges and Alter® shields [*Ellsworth, 2002*]. Streamflow outputs and inputs within GLEES are measured with four Parshall flumes: West Glacier Lake Outlet, East Glacier Lake Outlet, and Meadow Creek and Cascade Creek inlets to West Glacier Lake [*Musselman, 1994*].

WGL watershed has a unique problem in that measured streamflow out of the watershed has been estimated at 40% to 130% greater than input from precipitation gauge measurements [*Hasfurther et al., 1994; Ellsworth, 2002*]. Additional input into the watershed has been attributed to a permanent snowfield in the upper portion of the watershed [*Sommerfeld et al., 1991; Hasfurther et al., 1994*]. However, the excess output is likely a result of inaccurate estimation of water quantities using current precipitation and stream gauging methods.

Quantifying the water balance components, specifically solid precipitation, is crucial to understanding basin hydrology and hydrochemistry for the WGL watershed.

Input measurements based on alter shielded precipitation gauges may not provide accurate solid precipitation estimates in this windy alpine environment. For this reason, it is important to attain a thorough understanding of the distribution and quantity of solid precipitation stored at peak accumulation across the WGL watershed.

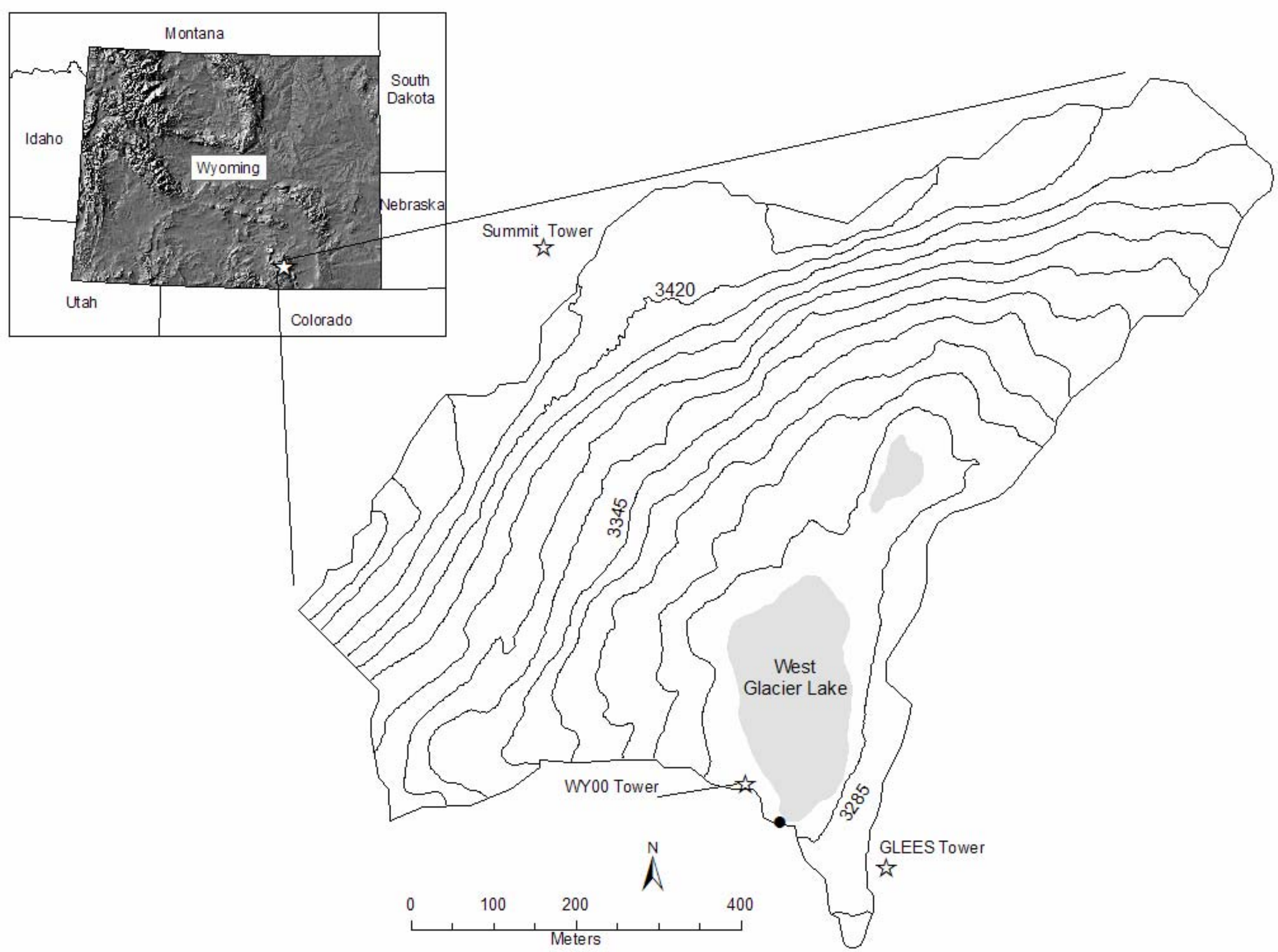

Figure 3.1 Topographic map of West Glacier Lake watershed, located in the Snowy Range of the Medicine Bow Mountains, WY. Contour interval is 15 m. Solid dot shows location of discharge measurements made with flume. Stars show location of meteorologic stations.

CHAPTER 4

4.0 METHODS

4.1 Water Balance

Development of a water balance for WGL watershed entailed measurement and estimation of multiple variables of the water balance within the basin. The most common water balance equation is the continuity equation, which states that over any time interval the difference in the volume of water entering a system, I, and leaving the system, O, must equal the change in the volume of water stored in the system, S:

$$I - O = \Delta S. \qquad \text{Equation 4.1}$$

For a small watershed, the inflow to the system is precipitation (liquid and solid). The outflow from the system would be streamflow, subsurface seepage, and losses to the atmosphere by evaporation, transpiration, and sublimation. Storage within the watershed would be soil water, groundwater, and lakes. The water balance equation was used to compare annual inputs and outputs for WGL watershed:

$$Q = P_s + P_r - E_t - E_s, \qquad \text{Equation 4.2}$$

where Q is watershed stream discharge, P_s is precipitation as snow, P_r is precipitation as rain, E_t is evapotranspiration, and E_s snowpack sublimation.

4.1.1 Precipitation

Precipitation inputs were measured in the basin for both rain and snow. Rainfall and summer snowfall data were measured with a Belfort® precipitation gauge fitted with an Alter® shield. The Belfort precipitation gauge recorded winter snowfall, but due to inherent gauge errors the snow survey estimates were considered as winter precipitation ground truth.

A major component of this research was to quantify winter precipitation and its spatial distribution. Accumulated winter precipitation was calculated from intensive snow survey data collected close to peak snowpack accumulation. Data collected during the survey were snow depth, snow density, and SCA by aerial imagery. A more in-depth description of methods used to calculate and distribute point measurement data is discussed in the subsequent sections.

4.1.2 Streamflow

Streamflow out of WGL watershed was calculated from a 0.457 m (18 inch) wide Parshall flume located at West Glacier Lake Outlet (WGLO). Daily average stream stage was measured in a stilling well with a Handar® float and pulley system. A Campbell Scientific® CR10X data-logger calculated and recorded discharge from a derived empirical stage-discharge rating equation [*USDI, 1997*]:

$$Q = \left[6.0636x^{1.522}\right] \qquad \text{Equation 4.3}$$

where Q (cfs) is discharge, and x (ft) is stage height.

In addition, streamflow measurements were collected at WGLO during the summer of 2004 and 2005. Stream velocity was measured with a Pygmy® meter at the inlet to the Parshall flume. Field data were used to create a stage-discharge relationship, and used to evaluate the accuracy of the precalibrated Parshall flume stage-discharge relationship.

4.1.3 Evapotranspiration

Water losses by evapotranspiration were calculated using two methods: (1) the difference between runoff and precipitation; and (2) calculating estimates for evaporation and evapotranspiration. The mass transfer method was used to calculate lake evaporation, and the Blaney-Criddle method was used to calculate evapotranspiration losses. The area of West Glacier Lake was assumed to remain constant at six percent of the watershed area. The percentage of ground cover in WGL watershed was assumed to be thirty-five percent of WGL watershed, as per [*Hasfurther et al., 1994*]. Evaporation and evapotranspiration from WGL watershed was calculated from June 1 to September 30 using procedures in *Hasfurther et al*., [1994]. In addition, potential evapotranspiration (PET) was calculated using the Thornthwaite method for an additional comparison. Calculations used meteorological data collected within the GLEES.

4.1.4 Snowpack Sublimation

Sublimation losses from the snowpack were calculated from a mass transfer equation, as per [*Dingman, 2002 and Fassnacht, 2004*]. The latent-heat flux, Q_E, is equal to the product of the latent-heat of vaporization (or sublimation), L_V, and the rate of mass transfer, E:

$$Q_E = L_V \times E \qquad \text{Equation 4.4}$$

Sublimation losses from the snowpack were calculated by rearranging equation 4.4 and solving for the mass transfer term. The mass transfer of water vapor from the snowpack to the atmosphere through sublimation was calculated as:

$$E = \frac{0.623\rho_a}{P} \frac{k^2 U_a (e_a - e_s)}{\left[\ln\left(\frac{z_a}{z_0}\right)\right]^2} 3600 \qquad \text{Equation 4.5}$$

where E is the sublimation rate (mm/h), ρ_a is the density of air (kg/m^3), P is air pressure (mb), k is von Karmen constant (0.4), U_a is measured wind speed (m/s) at height z_a (m), z_0 is the surface roughness height (m), e_a is vapor pressure (mb) at height z_a (m), and e_s is surface vapor pressure (mb).

4.1.5 Permanent Snowfield

A survey of the permanent snowfield in the upper portion of the watershed was conducted on October 28, 2004 during maximum snowfield ablation. The snowfield area and snow cornice were quantified using a Leica® Total Station. Surveyed points were used for calculating the snowfield area and for modelling the snowfield topography. The snowfield was too dense to measure with a Federal Sampler thus density was not measured. The snowfield density was assumed to be 80% based on density of snow to ice transformation measurements [*Singh and Singh, 2001*]. The bed surface below the snowfield was unknown, an assumption was made that the bed surface was linear between the known top and bottom points. Thee two assumptions were the best that could be done with the resources in hand. These data were used to estimate the water volume stored within the permanent snowfield.

4.2 Field Measurements of SWE

SWE at a point is calculated as the product of snow depth and snow density for snow-covered areas. Snow depth and snow density both vary with physiographic characteristics such as elevation, solar radiation, slope, aspect, and vegetation. Sample snow depth and density locations were collected representative of the range of elevation, slope, and aspect within the WGL watershed. In mountainous environments, snow depth is highly variable when compared to the average depth integrated snow density [*Elder et al., 1991*]. Therefore, fewer density measurements are needed to capture the variability. Ground observations of snow depth and snow density were collected near maximum snow accumulation on April 20 and 23 of 2005. Global positioning systems (GPS) were used to record the location of each depth and density measurement.

4.2.1 Snow Depth

Snow depths were measured using aluminum probe poles on an approximate 50 m measurement grid. At each sample location, five depth measurements were collected (a center plus four in each cardinal direction 2-meters away from center). The five measurements were recorded to the nearest 0.01 m and averaged to minimize local variation in snow depth at that point. The five points provide a better representation of the 5 m grid that is used to represent snow depth at that location.

4.2.2 Snow Density

Snowpits were excavated within the watershed with different elevations, slopes, and aspects in order to account for density variations. Snow density was measured with a 1-L stainless steel cutter and an electronic digital scale with 1g resolution. Density profiles were collected at 0.10 m increments, and then integrated over total depth to obtain one density value for each snowpit.

4.2.3 Snow-Covered Area

Snow-covered area (SCA) was derived from aerial photographs of the GLEES taken on April 16, 2005 close to peak accumulation. Photographs were rectified using ArcGIS 9.0, a geographic information system (GIS), to ground control points in the watershed. The rectified photographs were used to create a digital SCA layer with an approximate resolution of 1-m^2. A supervised classification scheme in ArcGIS 9.0 was used to classify each pixel as snow or no snow. Each pixel was given a binary value of zero (0% snow cover) or one (100% snow cover). The final binary SCA layer was resampled from 1-m to 5-m grid resolution to match the digital elevation model (DEM). The final SCA layer was classified as 100% snow if 50% or more of the pixel was classified as snow covered; otherwise the pixel was classified as snow free.

4.3 Analytical Methods

Physical parameters that control snow distribution can provide insight into snow accumulation and ablation processes, and can be utilized by modelling efforts [*Erxleben et al., 2002*]. Independent variables were used to aid in statistical modelling of snow depth and snow density.

4.3.1 Independent Variables

The physical parameters elevation, slope, aspect, solar radiation, northness, and vegetation have been shown to influence snow distribution. Each variable except vegetation was considered as independent variables in snow depth and snow density models to improve interpolated estimates. Vegetation was not used as a predictor due to the limited influence/lack of vegetation within WGL watershed.

Elevation, Slope, Aspect, and Northness:

Elevation (Figure 4.1) for each pixel within WGL watershed was derived from a 5-m digital elevation model (DEM). Slope (Figure 4.2) was derived from the 5-m DEM using the spatial analyst function in ArcGIS 9.0®. An output grid contained a slope value for each pixel within the watershed. Aspect (Figure 4.3) was derived using the same procedure stated above. An output grid provided an aspect value (N, NE, E, SE, S, SW, W, or NW, and another layer in degrees) for each pixel within the watershed. Northness (Figure 4.4) was calculated as the product of the cosine of the aspect and the sine of the slope. Summary statistics for each parameter are listed in Table 4.1.

Solar Radiation:

An index of daily incoming direct solar radiation was modelled for each pixel in WGL watershed. Solar Analyst, an ArcView® GIS extension, computes direct, diffuse, global radiation, and direct radiation duration, sunmaps and skymaps, and viewsheds was used for the modelling [*Fu and Rich, 2000*]. The required inputs for Solar Analyst were elevation, slope, and aspect grids.

Using Solar Analyst, solar radiation was calculated for the basin for the 15th of each month from December to April. The average monthly value for the five dates was used as an index of direct solar radiation during the accumulation season. Previous research has calculated a solar radiation index using similar methods [*Elder et al., 1998; Erxleben, 2002; Molotch et al. 2003*]. The final 5-m solar radiation index map is displayed in Figure 4.5 and summary statistics are listed in Table 4.2.

4.4 Snow Density Modelling Methods

In order to accurately estimate SWE, representative variations of snow density distribution must be accounted for. *Elder et al.*, [1991] stated that a near isothermal snowpack exhibits less spatial variability in snow density when compared to snow depth. Therefore, fewer snow density samples are required to explain the density variation. Previous research has shown that linear regression and multiple linear regression models are adequate for modelling snow density variations [*Elder and Dozier, 1990; Elder et al., 1998*].

4.4.1 Snow Density

Using the SPLUS® statistical and mathematical software, the calculated snowpit densities were used to predict density distribution across WGL watershed. Multiple linear regression models were applied to point snow densities along with different combinations of the derived independent variables slope, aspect, elevation, solar radiation, and northness. A regression model that contained all significant terms with the lowest residual standard error and highest coefficient of determination (R^2) was chosen to model and distribute snow density.

4.5 Snow Depth Modelling Methods

4.5.1 Snow Depth

Snow depth data were distributed using three main interpolation techniques at a 5-m grid resolution: inverse distance weighting (IDW), geostatistical methods, and binary regression tree methods. Geostatistical models used were ordinary kriging, co-kriging, modified residual kriging, and a combination of regression tree and kriging. A total of nine spatial interpolation models were selected: IDW, binary regression tree, kriging, a combined method of binary regression tree and kriging, modified residual kriging, co-kriging with elevation, co-kriging with slope, co-kriging radiation, and co-kriging with northness.

Data analysis and spatial modelling methods were done using SPLUS. Commands for IDW, ordinary kriging, co-kriging, and residual kriging are from the spatial library developed by *Venables and Ripley,* [1994] and expanded by *Reich and Davis,* [2004]. Binary regression analysis was performed in SPLUS using the "tree" function. The final interpolated snow depth layers were exported to an ASCII grid file and imported to an ArcGIS grid format. Final snow depth maps for WGL watershed were created using ArcGIS 9.0.

4.5.2 Inverse distance weighting

Inverse distance weighting (IDW) was selected because it is a simple distance weighted estimate of the value at an unknown location. IDW is based on the assumption that neighboring points are inversely proportional to the distance separating sample points. In addition, weights can be made inversely proportional to any power of the distance [*Isaaks and Srivastava, 1989*]:

$$\hat{z}(x_0) = \frac{\sum_{i=1}^{n} \frac{z(x_i)}{d_i^p}}{\sum_{i=1}^{n} \frac{1}{d_i^p}}, \qquad \text{Equation 4.3}$$

where $\hat{z}(x_0)$ is the interpolated value, n is the total number of sample points, $z(x_i)$ is the ith data value, d_i denotes the separation distance between interpolated value and data value, and P denotes the weighting power. The number of nearest neighbors and the weighting power were optimized to yield the lowest root mean square error (RMSE) [*Fassnacht et al., 2003*]. The optimal weighting power between 1 and 4 with 2 to 12 nearest neighbors was selected as IDW parameters for interpolating snow depth.

4.5.3 Geostatistical Methods

Geostatistical methods were selected because they model both the spatial trend and spatial correlation of a regionalized variable. Modelling both the spatial trend and spatial correlation offers a stronger estimation procedure than classical statistics that assume variables are spatially independent and random [*Balk et al., 1998*]. The regionalized variable can be broken into a deterministic/spatial trend component and a stochastic/spatial correlation component (*Erickson, 2004*):

$$z(x) = m(x) + \varepsilon(x), \qquad \text{Equation 4.4}$$

where $z(x)$ is the regionalized variable at location x, $m(x)$ is the deterministic trend component, and $\varepsilon(x)$ is the stochastic residual component.

Spatial trend was modelled using both linear regression analyses such as ordinary least squares (OLS) and binary regression trees. The residual difference between the trend predictions and the actual values are the stochastic component of the regionalized variable. Often these residuals are spatially-correlated, and can be used to improve the predictive ability of the regionalized variable. Scaling issues are always a concern in hydrologic applications. For this study, large-scale is referred to the extent of the watershed (trend component), and small-scale is equivalent to the 5-m grid resolution of the DEM (stochastic component).

Geostatistical methods such as kriging and co-kriging consist of three steps: (1) examination of the spatial correlation using variograms or cross-variograms; (2) fitting a theoretical model (spherical, Gaussian, or exponential) to the variogram or cross-variogram relationship; and (3) use the model to calculate weights for neighboring points and to compute the interpolated values using kriging or co-kriging methods.

4.5.3.1 Kriging

The empirical variogram was calculated to provide a description of how the data are related/correlated with distance. The semi-variogram function, $\gamma(h)$ is defined as half the average squared difference between pair of points separated by a distance h [*Kaluzny et al., 1998*] The semi-variogram was calculated as:

$$\gamma(h) = \frac{1}{2m(h)} \sum_{i=1}^{m(h)} \left[Z(x_i) - Z(x_i + h) \right]^2, \qquad \text{Equation 4.5}$$

where $\gamma(h)$ is the semi-variance function, $m(h)$ is the number of data pairs separated by distance h, $Z(x_i)$ is the sample value of the variable z at location x_i, and $Z(x_i + h)$ is the sample value of the variable z at location $x_i + h$ [*Webster and Oliver, 2001*].

Spherical, Gaussian, and exponential models were fit to the semi-variogram data to obtain the weights used for kriging and co-kriging. Initial values for the range, sill, and nugget effect parameters were selected from the empirical variogram. The model with the lowest RMSE and lowest Akaike information criterion (AIC) was selected to interpolate snow depth. The AIC was used to estimate the difference between the unknown true model and the experiment model. The model with the lowest AIC value was selected to model snow depth data because it modelled the spatial structure of the true data best.

Once a theoretical model was fit, kriging (universal kriging) interpolation methods were performed. Kriging uses the random spatial correlation function in order to predict unknown nearby unsampled locations [*Kalunzy et al., 1998*]. Weights were chosen to ensure the average error for the model is zero, and that the modelled error variance was minimized [*Isaaks and Srivastava, 1989*]. Ordinary kriging estimates were determined by:

$$\hat{Z}(x_0) = \sum_{i=1}^{n} \lambda_i Z(x_i), \qquad \text{Equation 4.6}$$

where $\hat{Z}(x_0)$ is the estimate of the variable at location x_0, $Z(x_i)$ is the value of the variable Z at location x_i, λ_i is the weight assigned to $Z(x_i)$, and n is the number of nearest neighbors [*Webster and Oliver, 2001*]. The sum of the weights, λ_i must be equal to 1 to ensure an unbiased estimate.

4.5.3.2 Co-Kriging

Snow depth has been shown to vary with independent variables such as elevation, solar radiation, slope, aspect, and northness. Multivariate cross-correlation between these variables and the depended variable snow depth may exist. If cross-correlation existed, co-kriging was used to try and improve the predictive ability of the dependent variable and minimize the variance of the estimation error. Cross-variograms were created between snow depth and each independent variable:

$$\gamma_{zw}(h) = \frac{1}{2m(h)} \sum_{i,j=1}^{m(h)} \left[Z(x_i) - Z(x_i + h) \right] \left[w(x_j) + w(x_j + h) \right], \qquad \text{Equation 4.7}$$

where $\gamma_{zw}(h)$ is the cross-variance function for dependent variable z and the secondary variable w separated by distance *h*, and $w(x_j)$ is the sample value of the variable w at location x_j, and $w(x_j + h)$ is the sample value of the variable w at location $x_j + h$ [*Webster and Oliver, 2001*].

Once empirical cross-variograms were calculated, co-kriging models were created using either the Spherical, Gaussian, or an exponential model to fit the cross-variogram. The theoretical model with the lowest RMSE and lowest AIC was selected to interpolate snow depth data. Co-kriging estimates were determined by:

$$\hat{Z}(x_0) = \sum_{i=1}^{n} \lambda_i^Z Z(x_i) + \sum_{j=1}^{m} \sum_{i=1}^{n} \lambda_j^w w(x_j), \qquad \text{Equation 4.8}$$

where $\hat{Z}(x_0)$ is the estimate of the dependent variable at location x_0, $Z(x_i)$ is the value of the variable Z at location x_i, $\lambda_{i\,i}^{Z}$ is the weight assigned to $Z(x_i)$, n is the number of nearest neighbors, λ_j^w are the weights for the secondary data w for the m data values, and $w(x_j)$ is the sample variable w at the location w_j. The sum of the weights, $\lambda_{i_i}^Z$ must be equal to 1, and the sum of the weights, λ_j^w must be equal to 0 [*Webster and Oliver, 2001*].

4.5.4 Binary Regression Tree

Binary regression tree methods were selected due to the ease of calculation and interpretation and due to previous success in snow distribution studies. Binary regression tree models were used to predict dependent variables from a group of independent variables in a non-linear hierarchical manner through a series of binary decisions [*Breiman et al.*, 1984]. Snow depth data are often related to independent variables in a non-linear and hierarchical manner, thus binary regression trees provide an alternative to linear and non-additive models [*Erxleben et al., 2002; Molotch et al., 2005*]. Increasing homogenous subsets of data were binned together through binary recursive partitioning. Detailed explanation of binary regression tree fitting, pruning, and cross-validation can be found in *Breiman et al*., [1984], *Elder et al*., [1995], and *Balk and Elder* [2000]. The tree model with the lowest deviance and highest coefficient of determination (R^2) using a combination of elevation, solar radiation, slope, aspect, and northness as independent values was chosen to model large-scale variability. Spatially correlated residuals were kriged to account for the small scale variability. Again, large-scale referred to the overall coverage of the watershed, and small-scale was equivalent to the 5-m grid size of the DEM.

4.5.5 Evaluation of Snow Depth Models:

In order to determine which spatial interpolation method provided the most accurate estimate of snow depth, cross-validation procedures were used to compare the value estimated (without using the observed value or “jack-knifing”) to the observed snow depth value. Residuals from cross-validation procedures were used to evaluate the performance of each model based on the following goodness-of-prediction estimates: the root mean square error (*RMSE*), the mean absolute error (*MAE*), and the coefficient of determination (R^2).

The *RMSE* is the square root of the mean square error. The smallest *RMSE* was used to determine which model had the most accurate local or small-scale estimates [*Erxleben et al., 2002*]. The *RMSE* was calculated as:

$$RMSE = \sqrt{\frac{1}{n}\sum_{i=1}^{n}\left[z(x_i) - \hat{z}(x_i)\right]^2} \,, \qquad \text{Equation 4.10}$$

where $z(x_i)$ is the observed value at location *i*, $\hat{z}(x_i)$ is the predicted value at location *i*, and *n* is the number of samples.

The *MAE* is the mean absolute error of all observed data. The smallest MAE was used to determine which model had the most accurate large-scale estimates [*Erxleben et al., 2002*]. The *MAE* was calculated as:

$$MAE = \frac{1}{n}\sum_{i=1}^{n}\left[\left|z(x_i) - \hat{z}(x_i)\right|\right], \qquad \text{Equation 4.11}$$

where $z(x_i)$ is the observed value at location *i*, $\hat{z}(x_i)$ is the predicted value at location *i*, and *n* is the number of samples.

The R^2 was used to assess the overall goodness of fit for each model. The R^2 was calculated as [*Reich and Davis, 2004*]:

$$R^2 = 1 - \frac{\sum_{i=1}^{n}(\varepsilon_i - \bar{\varepsilon})^2}{\sum_{i=1}^{n}(z_i - \bar{z})^2}, \qquad \text{Equation 4.12}$$

where ε_i is the residual error at location *i*, $\bar{\varepsilon}$ is the mean of the residuals, z_i is the observed value at location *i*, and $\bar{z}$ is the mean of all observed data.

4.6 SWE Estimates

The goal of modelling snow depth, snow density, and SCA for this study was to distribute SWE over all snow-covered portions of the watershed in order to quantify winter precipitation. In order to accurately assess winter water storage in WGL watershed, the two components of SWE, snow depth and snow density were distributed over all snow-covered portions of the basin. Net winter precipitation was derived by modelling SWE for each 5-m pixel within WGL watershed. Each final layer of SWE distribution was calculated as the product of the interpolated snow depth surface, the modelled snow density, and SCA:

$$SWE = d_s \times (\rho_s/\rho_w) \times SCA, \qquad \text{Equation 4.9}$$

where *SWE* (cm) is snow water equivalent at a point, d_s (cm) is the modelled snow depth, ρ_s is the modelled snow density (kg/m^3), ρ_w is the density of water (1,000 kg/m^3), and

SCA is the snow covered area at that point. The best snow depth layer from each interpolation method was used to derive SWE distribution and quantity within the watershed. Each spatially distributed SWE layer was used to calculate total winter water volume and used as an estimate of potential water available for snowmelt runoff. Potential water volume available for snowmelt runoff was calculated by:

$$V_w = \sum_{i=1}^{n}(SWE_i \times A_i), \qquad \text{Equation 4.10}$$

where V_w (m^3) is the total water volume stored in the watershed at peak accumulation, SWE_i (m) is snow water equivalent at a point, A_p is the area represented by the point.

Table 4.1. Maximum, minimum, mean, standard deviation, and coefficient of variation for elevation (m), slope (°), aspect (°), and northness maps for WGL watershed.

	Max	Min	Mean	St. Dev	CV
Elevation	3493	3277	3385	62.64	0.018
Slope	59.1	0	29.5	17.31	0.587
Aspect	360	0	180	104.21	0.578
Northness	0.999	-0.999	-0.004	0.485	-121.25

Table 4.2. Maximum, minimum, mean, standard deviation, and coefficient of variation for direct solar radiation (W/m^2) and solar index (W/m^2) maps for WGL watershed.

Radiation	Max	Min	Mean	St. Dev	CV
December	177	0	92.72	31.93	0.344
January	191	0	105.06	33.46	0.318
February	234	0	152.14	35.69	0.235
March	273	4	211.73	31.79	0.150
April	306	69	274.15	20.89	0.076
Index	229	15	167.14	30.30	0.181

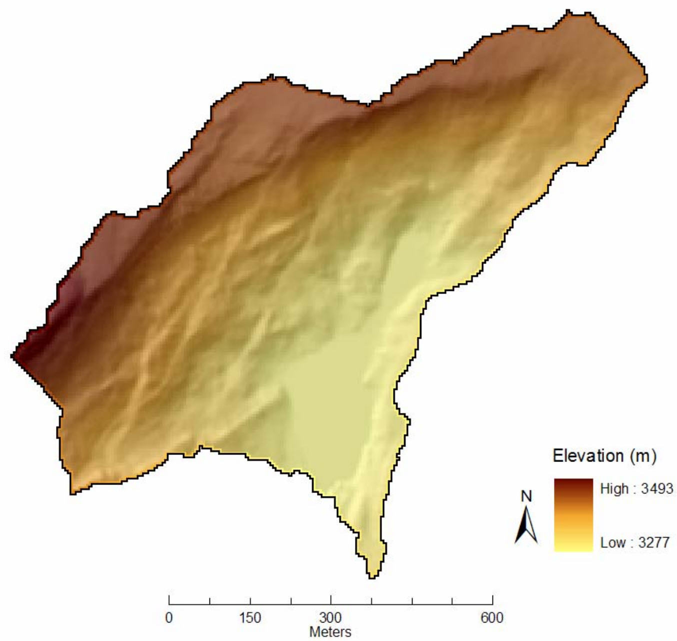

Figure 4.1. Elevation map of WGL watershed generated from a 5-m DEM.

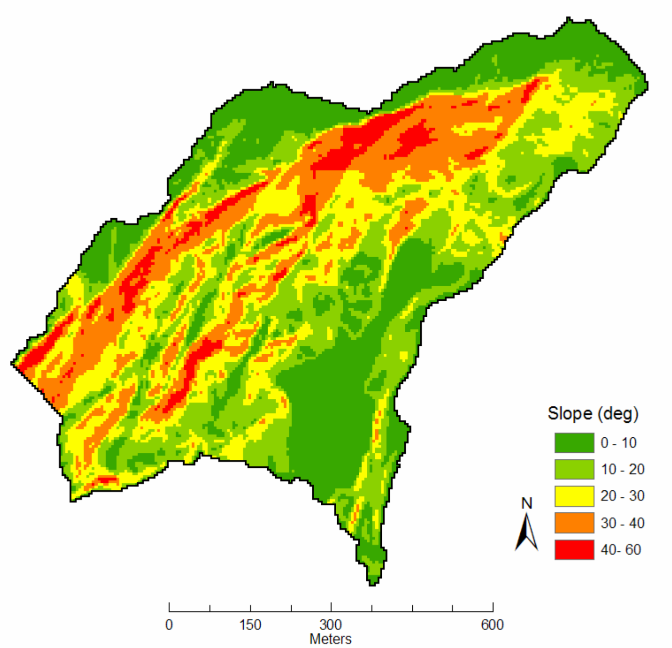

Figure 4.2. Slope map of WGL watershed generated from a 5-m DEM.

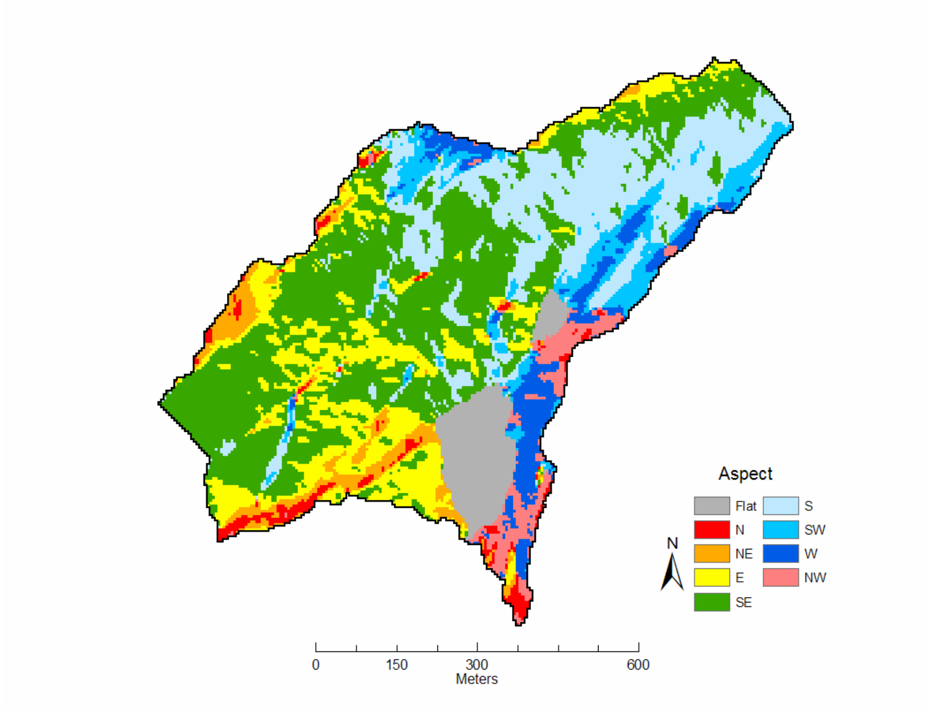

Figure 4.3. Aspect map of WGL watershed generated from a 5-m DEM.

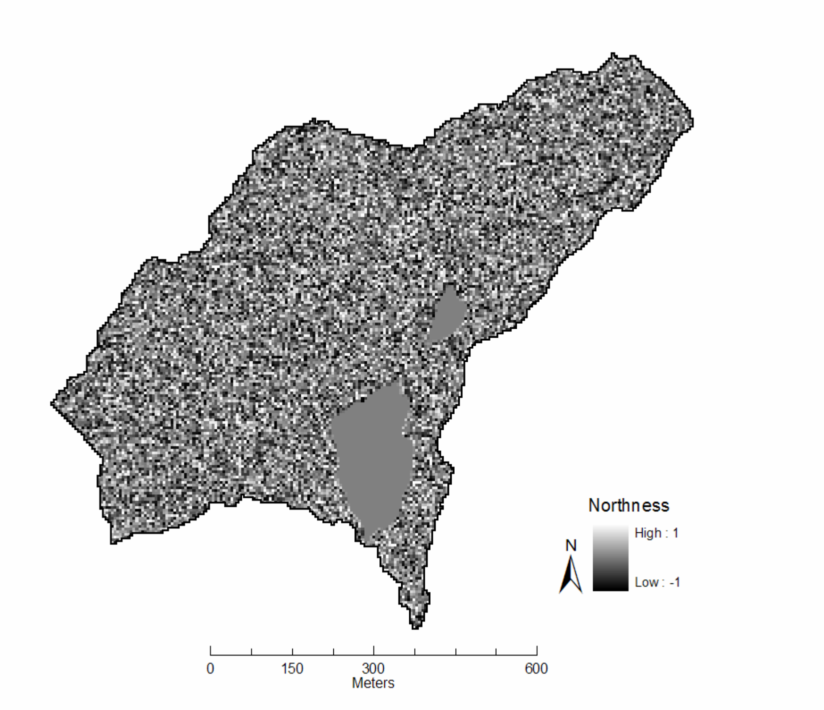

Figure 4.4. Northness map of WGL watershed generated from a 5-m DEM.

Northness = COS(aspect) * SIN(slope)

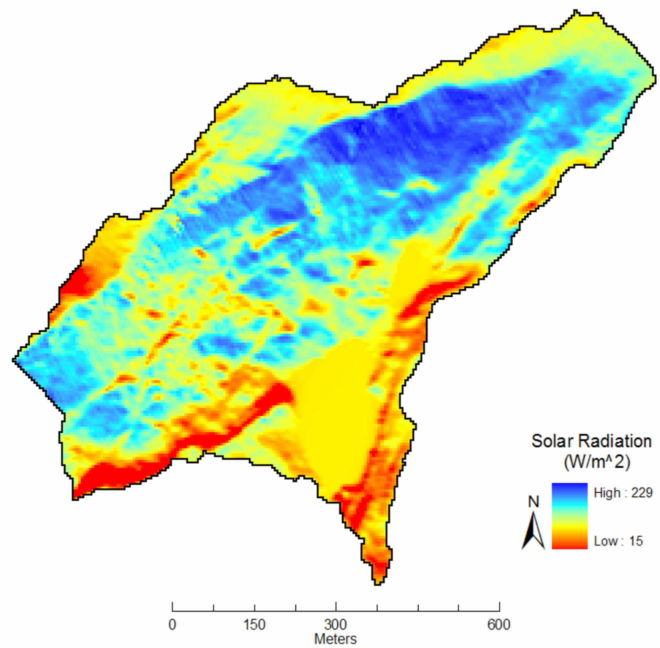

Figure 4.5. Solar radiation index map generated from a 5-m DEM**.**

CHAPTER 5

5.0 RESULTS

Measurement and estimation of water balance variables were analyzed for WGL watershed. The water balance components consisted of precipitation as rain, precipitation as snow, streamflow, sublimation, and evapotranspiration. SWE estimates based on the methods used to model snow depth, snow density, and SCA were used to evaluate the accuracy of winter precipitation inputs and streamflow outputs. The results of these procedures are discussed below.

5.1 Precipitation

The GLEES meteorologic tower measured 953 mm of precipitation for water year 2005. For the winter period, October 1 through May 13, 783 mm of precipitation was recorded; and during the summer period, May 14 through September 30, the remaining 170 mm of precipitation was recorded. The winter period was defined as the period when precipitation fell below the freezing point of 0°C. Summer period was defined as the period when precipitation fell above the freezing point. Daily precipitation gauge data for water year 2005 (Figure 5.1) and monthly summary statistics were calculated (Table 5.1). Winter precipitation that fell after the survey between April 21 and May 13 was 203 mm. This value was corrected for gauge undercatch using the relationship determined from SWE estimates and precipitation gauge estimates. The correction yielded 340 mm. The 340 mm of additional precipitation was added to the SWE estimates derived from the interpolation methods. Summer precipitation inputs were 170 mm. Winter precipitation used in the water balance calculations is discussed in the SWE section.

5.2 Streamflow

Streamflow out of the WGL watershed was calculated from records of average daily stream stage. Pygmy meter measurements based on 2004 and 2005 data resulted in a rating curve significantly different than the factory formula Equation 4.3 (Figure 5.2). The new stage-discharge relationship is a second order polynomial with an R^2 of 0.95. Discharge was calculated from the new relationship as:

$$Q = 3.9704x^2 - 0.5357x, \qquad \text{Equation 5.1}$$

where Q (cfs) is discharge, and x (ft) is stage height. The new stage-discharge relationship calculated 52% less runoff than the original Parshall flume equation (Figure 5.3). The new relationship calculated 1,000 mm (558,175 m^3) of runoff, compared to 2,072 mm (1,156,259 m^3) using the precalibrated Parshall flume relationship.

The hydrograph for water year 2005 (Figure 5.3 and 5.4) illustrates the snowmelt hydrograph of WGL watershed. Streamflow from WGL watershed began on May 12, and contained bi-modal peaks. The first peak occurred early in the melt season on May 24 with a daily average discharge of 9,162 m^3/d (16 mm). The second peak, the maximum, occurred later in the melt season on June 23 with a daily average discharge of

17,282 m^3/d (31 mm). From this date, the hydrograph recessed for the remainder of the water year and ended with a low flow of 780 m^3/d (1.4 mm).

5.3 Evaporation and Evapotranspiration

Water losses due to evaporation and evapotranspiration from WGL watershed were calculated from the GLEES meteorological tower data. Lake evaporation was calculated by the mass transfer method, yielding a total of 285 mm of lake evaporation from June 15 through September 30. The area-weighted lake evaporation value resulted in 17 mm of lake evaporation. Evapotranspiration from WGL watershed was calculated by the Blaney-Criddle method, yielding a total of 416 mm from May through September. The area-weighted evapotranspiration value was 146 mm. Combining lake evaporation with evapotranspiration yielded a total water loss of 163 mm.

The Thornthwaite method was used to calculate potential evapotranspiration (PET) for an additional comparison. Total PET for WGL watershed was calculated to be 347 mm, a difference of -184 mm from the combined methods. Monthly evaporation and evapotranspiration summary statistics were calculated (Table 5.2). Evapotranspiration losses calculated as the difference between runoff and precipitation is discussed in the Water Balance section.

5.4 Snowpack Sublimation

Winter water losses due to sublimation were calculated from hourly meteorological data collected from the GLEES meteorological tower. Monthly estimates of snowpack sublimation losses were derived from hourly data (Figure 5.5). Monthly summary statistics are shown in Table 5.3. Total sublimation losses accounted for 251 mm, with an average loss of 36 mm per month during the snow accumulation season. A maximum sublimation loss of 60 mm occurred during the month of December, and a second peak of 46 mm occurred during the month of February.

5.5 Permanent Snowfield

A total of 196 survey points were used to calculate the dimensions of the permanent snowfield. The snowfield was calculated to be 13,824 m^2, or less than 2.4% of the watershed area. The average height of the snow cornice was 5.3 m. Using an assumed snow density of 80% and a linear bed slope yielded 25,408 m^3 (42 mm) of water stored within the snowfield or approximately 1 mm over the watershed.

5.6 Snow Depth

A total of 538 snow depth measurements were used for modelling snow depth distribution (Figure 5.6). Summary statistics for the 538 snow depth measurements and non-zero snow depth measurements were calculated (Table 5.4). The average spatial density between snow depth sample locations was 32 m. Of the 538 snow depth measurements, 419 were a single depth measurement and 119 were an average value of five points, one center point and four additional points in each cardinal direction. This yielded a total of 1014 snow depth measurements collected during intensive snow survey.

Single snow depth measurements were made below the snow cornice and on steep avalanche prone slopes. Regression analysis between the average snow depth vs. the center point yielded a significant relationship. The individual snow depth measurements were able to explain 96% of the observed variance in the average snow depth values ($R^2 = 0.96$, $n = 119$, $p = 0.00$). The center snow depth point values followed the same frequency distribution as the average snow depth values.

In addition, three regions were selected to perform intensive snow depth transects to capture the small-scale snow depth variability. At the three intensive transects, snow depth measurements were collected every meter over a 15 m distance. Two snow depth measurements exceeded the length of the snow probes carried by the surveyor. In these cases, the probed depth was recorded along with a comment indicating that snow depth was greater than the measurement.

5.7 Snow Depth Models

Spatial interpolation methods used to distributed snow depth measurements, and to estimate snow depth distribution included inverse distance weighting, binary regression tree, kriging, binary regression tree and kriging, modified residual kriging, co-kriging with elevation, co-kriging with slope, co-kriging radiation, and co-kriging with northness. All methods were evaluated using cross-validation procedures. The residuals were analyzed and used to evaluate the accuracy of each snow depth measurement and the overall model results. The results of each model are presented below.

5.7.1 Inverse Distance Weighting

Spatial interpolation of the snow depth data using IDW for two to eight nearest neighbors provided reasonable results. IDW achieved R^2 values ranging from 0.29 to 0.66. IDW with three nearest neighbors resulted in an R^2 of 0.54 and had the lowest model deviance. The MAE of the residuals is 66.98, and the RMSE is 89.24. A map of the snow depth estimates using IDW with three nearest neighbors is displayed in Figure 5.7. The modelled minimum, maximum, and mean snow depth estimates are 9, 436, and 179 centimeters, respectively.

5.7.2 Binary Regression Tree

A regression tree was grown to estimate snow depth in SPLUS. Using the predictor variables, elevation, slope, aspect, solar radiation, and northness, a tree was grown to its maximum at 65 terminal nodes. Cross-validation procedures indicated that a tree size between 12 to 15 terminal nodes would be optimal (Figure 5.8). Through the process of pruning, a tree of 15 terminal nodes was selected to model snow depth distribution (Figure 5. 9). The 15-node tree used the variables elevation, slope, solar radiation, and northness. Aspect was not used to build the final tree because including it did not yield better results. The tree was able to explain 33.2% of the observed variability in snow depth. A map of snow depth estimates using a 15-node regression tree is displayed in Figure 5.10. The MAE of the 15-node tree is 63.57, and the RMSE is 79.73. The modelled minimum, maximum, and mean snow depth estimates are 46, 268, and 170 centimeters, respectively.

5.7.3 Kriging

To examine the spatial variability of snow depth, a semi-variogram was calculated for WGL watershed. Snow depth variograms were constructed over a variety of distances ranging from 50 m to 1400 m. Cross-validation procedures indicated that a distance of 100 m would provide the best results (Figure 5.11). The weighted Gaussian model had the lowest AIC value and was used to model the experimental semi-variogram. The nugget of the Gaussian variogram model is 479, the sill is 9612, and the range is 33.7 m.

Spatial interpolation of the snow depth data using ordinary kriging for two to twelve nearest neighbors provided exceptional results. Ordinary kriging achieved R^2 values ranging from 0.51 to 0.68. Ordinary kriging with two nearest neighbors resulted in the highest R^2 and lowest model deviance. The ordinary kriging model explained 68% of the observed snow depth variance, the MAE of the residuals is 70.51, and the RMSE is 94.93. A map of the snow depth estimates using ordinary kriging with two nearest neighbors is displayed in Figure 5.12. The modelled minimum, maximum, and mean snow depth estimates are 0, 502, and 236 centimeters, respectively.

5.7.4 Binary Regression Tree and Residual Kriging

For this method, in order to accurately represent snow depth distribution, the large-scale variability and small-scale variability were modelled. The large-scale variability was modelled using binary regression tree results discussed earlier. In order to model the small-scale variability, the residuals from the 15-node regression tree were tested for spatial autocorrelation with Moran's I statistic. The snow depth residuals were positively spatially correlated (Moran's I = 0.018, $p = 0.002$) and used for kriging.

A model variogram was constructed with distances ranging from 50 m to 1400 m. Cross-validation procedures indicated that a distance of 125 m would provide the best results. An experimental variogram with a weighted Gaussian model was calculated for the residuals of the 15-node regression tree (Figure 5.13). The nugget of the Gaussian variogram model is 129, the sill is 7854, and the range is 27.2 m.

Spatial interpolation of the snow depth data using binary regression tree plus residual kriging for two to twelve nearest neighbors provided reasonable results. The R^2 values ranged from 0.36 to 0.61. Residual kriging of regression tree residuals with two nearest neighbors resulted in the highest R^2 and lowest model deviance. The model explained 61% of the observed snow depth variance, the MAE of the residuals is 66.51, and the RMSE is 90.82. A map of the snow depth estimates using residual kriging with two nearest neighbors is displayed in Figure 5.14. The modelled minimum, maximum, and mean snow depth estimates are 0, 703, and 264 centimeters, respectively.

5.7.5 Modified Residual Kriging

An elevation trend surface model was created to model the large scale variability. A linear trend surface model explained 2% of the variability in observed snow depths. The residuals from the trend surface model were tested for spatial autocorrelation. The snow depth residuals were positively spatially correlated (Moran's I = 0.109, $p = 0.0006$) and were used to krig the small-scale variability.

A model variogram was constructed with distances ranging from 50 m to 1400 m. Cross-validation procedures indicated that a distance of 100 m would provide the best results. An experimental variogram with a weighted Gaussian model was calculated for the snow depth residuals (Figure 5.15). The nugget of the Gaussian variogram model is 480, the sill is 9617, and the range is 33.8 m.

Interpolation of the snow depth data using modified residual kriging for two to twelve nearest neighbors provided exceptional results. Modified residual kriging achieved R^2 values ranging from 0.49 to 0.67. Two nearest neighbors resulted in the highest R^2 and lowest model deviance. The modified residual kriging model explained 67% of the observed snow depth variance, the MAE of the residuals is 70.53, and the RMSE is 94.94. A map of the snow depth estimates using modified residual kriging with two nearest neighbors is displayed in Figure 5.16. The modelled minimum, maximum, and mean snow depth estimates are 0, 500, and 235 centimeters, respectively.

5.7.6 Co-kriging With Elevation

Spatial correlation between snow depth and elevation were tested to see if co-kriging methods were possible. The results indicated that snow depth and elevation exhibited a non-significant weak negative cross-correlation (r = -0.0023, p = 0.00). Co-kriging methods were performed, even with the poor cross-correlation.

The Gaussian snow depth variogram model discussed previously was scaled by the maximum snow depth and was used to model snow depth in co-kriging models (Figure 5.17). A model variogram was constructed for elevation with a distance of 800 m. An experimental variogram with a weighted Gaussian model was calculated for the elevation data (Figure 5.18). The nugget of the elevation Gaussian variogram model is 0, the sill is 0.0004, and the range is 448.5 m. A Gaussian cross-variogram model was constructed between snow depth and elevation with a distance of 1000 m (Figure 5.19).

Interpolation of the snow depth data using co-kriging with elevation for two to eight nearest neighbors provided poor results. Co-kriging achieved R^2 values ranging from -0.271 to 0.18. Three nearest neighbors resulted in the highest R^2 and lowest model deviance. The co-kriging model explained 18% of the observed snow depth variance, the MAE of the residuals is 78.27, and the RMSE is 107.14. A map of the snow depth estimates using co-kriging with elevation and three nearest neighbors is displayed in Figure 5.20. The modelled minimum, maximum, and mean snow depth estimates are 0, 599, and 252 centimeters, respectively.

5.7.7 Co-kriging With Slope

Spatial correlation between snow depth and slope were tested to determine if co-kriging methods were possible. The results indicated that snow depth and slope exhibit a positive cross-correlation (r = 0.35, p = 0.00), and were used for co-kriging.

The Gaussian snow depth variogram model discussed previously was used to model snow depth (Figure 5.17). A model variogram was constructed for slope with a distance of 600 m. An experimental variogram with a weighted spherical model was calculated for the slope data (Figure 5.21). The nugget of the slope spherical variogram model is 0.017, the sill is 0.054, and the range is 255 m. A cross-variogram was constructed between snow depth and slope with a distance of 300 m. A spherical cross-variogram model was calculated for snow depth and slope (Figure5.22).

Interpolation of the snow depth data using co-kriging with slope for two to twelve nearest neighbors provided exceptional results. Co-kriging achieved R^2 values that ranged from 0.72 to 0.94. Four nearest neighbors resulted in the highest R^2 and lowest model deviance. The co-kriging with slope model explained 94% of the observed snow depth variance, the MAE of the residuals is 10.21, and the RMSE is 24.48. A map of the snow depth estimates using co-kriging with slope and four nearest neighbors are displayed in Figure 5.23. The modelled minimum, maximum, and mean snow depth estimates are 0, 596, and 227 centimeters, respectively.

5.7.8 Co-kriging With Solar Radiation

Spatial correlation between snow depth and radiation were tested to see if co-kriging methods were possible. The results indicate that snow depth and radiation exhibit a positive cross-correlation ($r = 0.19$, $p = 0.003$), and were used for co-kriging.

The Gaussian snow depth variogram model discussed previously was used to model snow depth (Figure 5.17). A model variogram was constructed for solar radiation with a distance of 1100 m. An experimental variogram with a weighted spherical model was calculated for the radiation data (Figure 5.24). The nugget of the radiation spherical variogram model is 0.008, the sill is 0.024, and the range is 828 m. A cross-variogram was constructed between snow depth and radiation with a distance of 1000 m. A spherical cross-variogram model was calculated for snow depth and radiation (Figure 5.25).

Interpolation of the snow depth data using co-kriging with radiation for two to twelve nearest neighbors provided exceptional results. Co-kriging achieved R^2 values that ranged from 0.89 to 0.94. Two nearest neighbors resulted in the highest R^2 and lowest model deviance. The co-kriging with radiation model explained 94% of the observed snow depth variance, the MAE of the residuals is 5.25, and the RMSE is 8.58. A map of the snow depth estimates using co-kriging with radiation and three nearest neighbors is displayed in Figure 5.26. The modelled minimum, maximum, and mean snow depth estimates are 0, 550, and 241 centimeters, respectively.

5.7.9 Co-kriging With Northness

Spatial correlation between snow depth and northness were tested to determine if co-kriging methods were possible. The results indicate that snow depth and northness exhibit a slight positive cross-correlation ($r = 0.029$, $p = 0.003$), and were used for co-kriging.

The Gaussian snow depth variogram model discussed previously was used to model snow depth (Figure 5.17). A model variogram was constructed for northness with a distance of 1000 m. An experimental variogram with a weighted spherical model was calculated for the northness data (Figure 5.27). The nugget of the northness spherical variogram model is 0.13, the sill is 0.164, and the range is 1,135 m. A cross-variogram was constructed between snow depth and radiation with a distance of 1,000 m. A spherical cross-variogram model was calculated for snow depth and northness (Figure 5.28).

Interpolation of the snow depth data using co-kriging with northness for two to twelve nearest neighbors provided great results. Co-kriging achieved R^2 values that ranged from 0.89 to 0.93. Two nearest neighbors resulted in the highest R^2 and lowest model deviance. The co-kriging with northness model explained 93% of the observed snow depth variance, the MAE of the residuals is 6.59, and the RMSE is 10.67. A map of the snow depth estimates using co-kriging with northness and two nearest neighbors are displayed in Figure 5.29. The modelled minimum, maximum, and mean snow depth estimates are 0, 511, and 222 centimeters, respectively.

5.7.10 Summary of Snow Depth Spatial Modelling

Cross-validation procedures were used to examine the validity of the snow depth interpolation models. The nine spatial snow depth models explained 18% to 94% of the observed variance in the measured snow depths (Table 5.5). Based on the cross-validation procedures, co-kriging with solar radiation was determined to be the most accurate method for estimating snow depth across WGL watershed. Co-kriging with radiation explained 94% of the variance in observed snow depth measurements. The co-variable solar radiation, improved the models predicative ability 26% from 68% for the kriging model alone. Gaussian and spherical variogram and cross-variogram models were used for co-kriging snow depth through WGL watershed. The Gaussian model was used to model snow depth. The spherical model had the lowest AIC value and was selected to model solar radiation. A spherical cross-variogram model was calculated for snow depth and radiation.

5.8 Snow Density

Seven snowpits were excavated and density profiles were colleted at each site during the intensive snow survey (Figure 5.30). The weighted mean density for each snowpit was used to distribute snow density over WGL watershed. A simple multiple linear regression model was applied to the snowpit data. Independent variables used in the regression were elevation, slope, solar radiation, and northness. The density equation derived from the regression was:

$$\rho = 2849.35 - 0.8315x_1 + 2.3639x_2 + 174.8386x_3 \qquad \text{Equation 5.2}$$

where ρ is density (kg/m^3), x_1 is elevation (m), x_2 is direct solar radiation (W/m^2), and x_3 is northness. All independent variables were significant at $p < 0.05$, elevation at $p = 0.012$, direct solar radiation at $p = 0.015$, and northness at $p = 0.001$. An upper limit of 474 (kg/m^3) and a lower limit of 339 (kg/m^3) was set for the snow density model. The multiple linear regression model was able to explain 93% of the observed variance in the field measurements of density ($n = 7$, $p = 0.028$). Figure 5.31 shows the distributed snow density over WGL watershed, and summary statistics for the weighted averages of the snowpit densities and the distributed model snow densities are shown in Table 5.6.

5.9 SCA

Ten classes were used in the supervised classification scheme to determine snow-cover versus snow free regions. This procedure did not distinguish between forested and shadowed snow-covered regions from wind-scoured snow free regions. Therefore, forested and shadowed regions that were snow-covered and classified as no snow were reclassified as snow-covered. The final SCA layer (Figure 5.32), shows the distribution of snow-covered versus snow free regions. The peak SCA for WGL watershed was calculated to be 94% of the watershed area.

5.10 SWE

All interpolation models show relatively high SWE accumulations just below the ridge line and relatively low SWE accumulations along the upper basin boundaries and across West Glacier Lake (Figures 5.33-5.41). The effects of wind scour on ridge tops and redistribution onto the lee side of the ridge can be seen in the modelled snow depth and SWE. The modelled SWE (solar radiation) distribution resulted in a maximum SWE depth estimate of 240 cm, a mean of 113 cm, and a minimum of 0 cm. All models produced similar estimates of SWE for WGL watershed (Table 5.5). A maximum SWE volume of 1,074 mm was estimated from co-kriging with slope model, a minimum estimate of 1,052 mm was from the co-kriging with elevation model, and the average SWE for the nine interpolation models was 1,060 mm.

5.11 Water Balance

Calculated inputs and outputs were applied to a simple water balance. Summer 2005 precipitation collected by the Belfort precipitation gauge was 170 mm. Total winter inputs in WGL watershed were calculated as peak SWE (1,060 mm) plus snowpack sublimation loss (251 mm) which yielded a total 1,311 mm of winter precipitation. Total net input from precipitation as snow (1,311 mm) and rain (170 mm) was 1,481 mm. Annual runoff calculated from the Parshall flume was 1,000 mm. Snowpack sublimation calculated from mass transfer equations yielded 251 mm of water lost from the snowpack. The difference between the inputs and outputs yielded an evapotranspiration estimate of 230 mm.

5.12 Error Analysis

Errors associated with measuring and estimating hydrologic variables in an alpine watershed can have a significant impact on water balance calculations. The degree of error associated with each individual water balance variable was estimated (Table 5.7). The error associated with snowfall was determined from co-kriging with solar radiation cross-validation statistics. The largest error for the model was the RMSE (8.58 cm), this value resulted in about 10% small-scale error; and the lowest error was the MAE (5.25 cm), this value resulted in about 5% large-scale error. The larger 10% error (106 mm) was used for error analysis. A rainfall error of 10% (17 mm) was selected to represent the average long-term error that *Winter* [1981] associated with point precipitation gauge estimates. A 20% error (50 mm) for snowpack sublimation was selected to represent sublimation error presented by *Kattelmann and Elder* [1991] in the Sierra Nevada. A 5% streamflow error (50 mm) was selected to represent the stage discharge relationship and flume measurement errors cited in *Winter* [1981] and *Dingman* [2002].

The estimated residual evapotranspiration error (173 mm) was calculated by combining the individual error components. Snowpack sublimation was not included because this component did not directly affect the evapotranspiration term. In water year 2005, the uncertainty was estimated to be 173 mm or 12% of the total precipitation. Snowfall accounted for the largest part of the total error. If the smaller 5% error (53 mm) term were used instead of 10% error, then the snowfall error term would had a similar error quantity as streamflow and sublimation.

Table 5.1. Minimum and maximum daily precipitation (mm) for each month; and monthly total precipitation (mm) for water year 2005.

	Oct	Nov	Dec	Jan	Feb	Mar	Apr	May	Jun	Jul	Aug	Sep	
Min	0	0	0	0	0	0	0	0	0	0	0	0	-
Max	48	12	31	18	16	16	41	50	27	5	13	23	-
Total	95	59	123	89	68	115	114	139	75	12	23	41	953

Table 5.2. Calculated monthly evaporation rates (mm) for West Glacier Lake watershed water year 2005. Lake evaporation (mass-transfer) plus evapotranspiration (Blaney-Criddle) are equal to total evaporation and compared to calculated potential evapotranspiration (Thornthwaite)

	May	Jun	Jul	Aug	Sep	Total	Area Corrected
Mass Transfer	-	50	100	66	69	285	17
Blaney-Criddle	60	69	98	96	93	416	146
SUM	*60*	*119*	*198*	*162*	*162*	*701*	*163*
Thornthwaite	27	65	109	85	61	347	
Difference	33	54	89	77	101		-187

Table 5.3. Minimum and maximum daily snowpack sublimation losses (mm) for each month; and monthly total snowpack sublimation losses (mm) for water year 2005.

	Oct	Nov	Dec	Jan	Feb	Mar	Apr	May	Jun	Jul	Aug	Sep	
Min	0	0	0	0	0	0	0	0	0	0	0	0	-
Max	2	5	7	5	6	4	7	0	0	0	0	0	-
Total	15	28	60	38	46	38	26	0	0	0	0	0	251

Table 5.4. Summary statistics for measured snow depth and non-zero snow depth field measurements including standard deviation (Std. Dev), coefficient of variation (*cv*), and number of samples (*n*).

Summary Statistics	All Depths	Non-zero Depths
Minimum	0	1
Maximum	500	500
Mean	182	187
Std. Dev	98	95
cv	0.54	0.51
n	538	524

Table 5.5. Cross-validation summary statistics for snow depth (cm) interpolation models include the mean absolute error (MAE), root mean square error (RMSE), coefficient of determination (R^2), and modelled SWE (mm) inputs to WGL watershed.

Model	MAE	RMSE	R^2	SWE
IDW	66.98	89.24	0.54	1,063
Kriging	70.51	94.93	0.68	1,058
Regression Tree	63.57	79.73	0.33	1,060
Tree and Residual Kriging	66.51	90.82	0.61	1,057
Modified Residual Kriging	70.53	94.94	0.67	1,054
Co-kriging, Solar Radiation	5.25	8.58	0.94	1,060
Co-kriging, Slope	10.21	24.48	0.94	1,074
Co-kriging, Northness	6.59	10.67	0.92	1,063
Co-kriging, Elevation	78.27	107.14	0.18	1,052

Table 5.6. Summary statistics for measured and snow density (kg m^{-3}) and modelled snow density (kg m^{-3}) including standard deviation (Std. Dev), coefficient of variation (*cv*), and number of samples (*n*).

Summary Statistics	Snow Pits	Modelled
Minimum	339	339
Maximum	474	474
Mean	417	429
Std. Dev	48	53
cv	0.11	0.12
n	7	7

Table 5.7. Estimated lower and upper error limits for water balance components.

Components	Amount (mm)	Error (%)	Range (mm)	Lower (mm)	Upper (mm)
Snowfall	1,060	10	106	954	1,166
Rainfall	170	10	17	153	187
Sublimation	251	20	50	201	301
Streamflow	1,000	5	50	950	1,050
Evapotranspiration*	230	-	173	57	403

* Estimated by combining errors in individual components (sublimation not included).

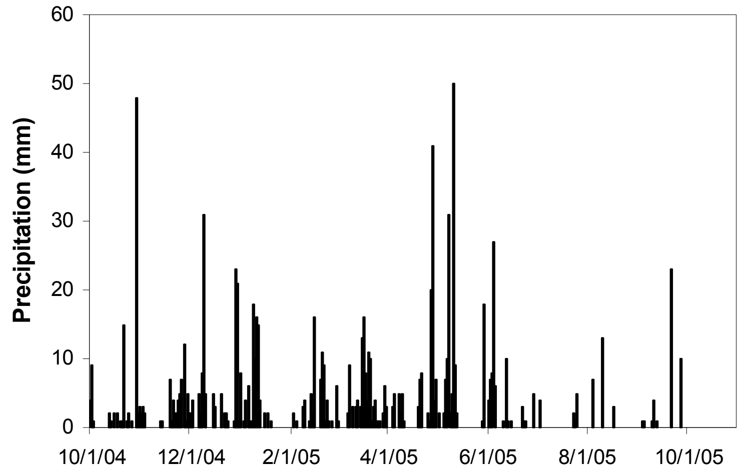

Figure 5.1. Daily precipitation data for West Glacier Lake watershed, water year 2005.

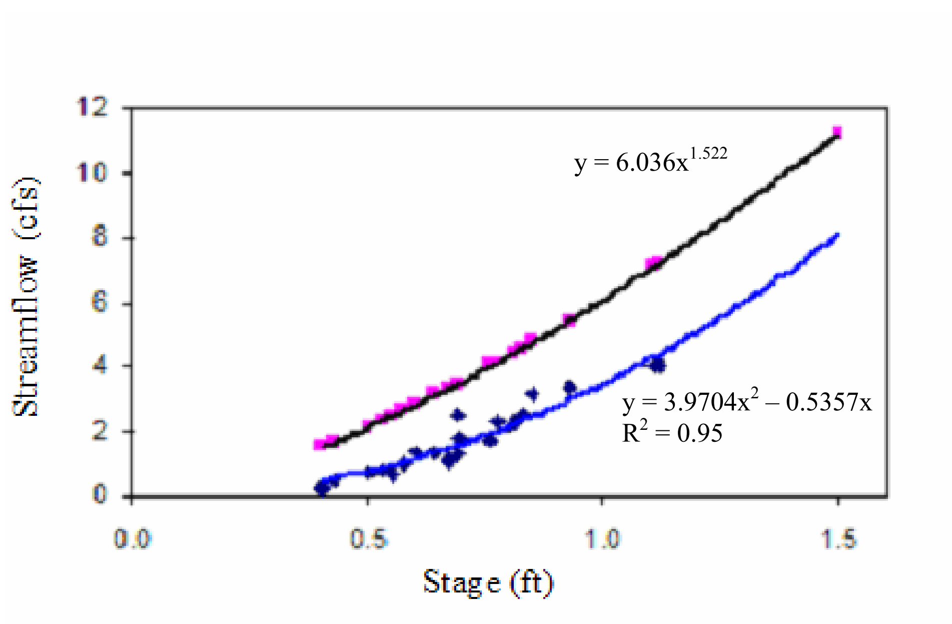

Figure 5.2. New stage-discharge relationship (bottom) derived from field measurements compared to precalibrated flume stage-discharge relationship (top).

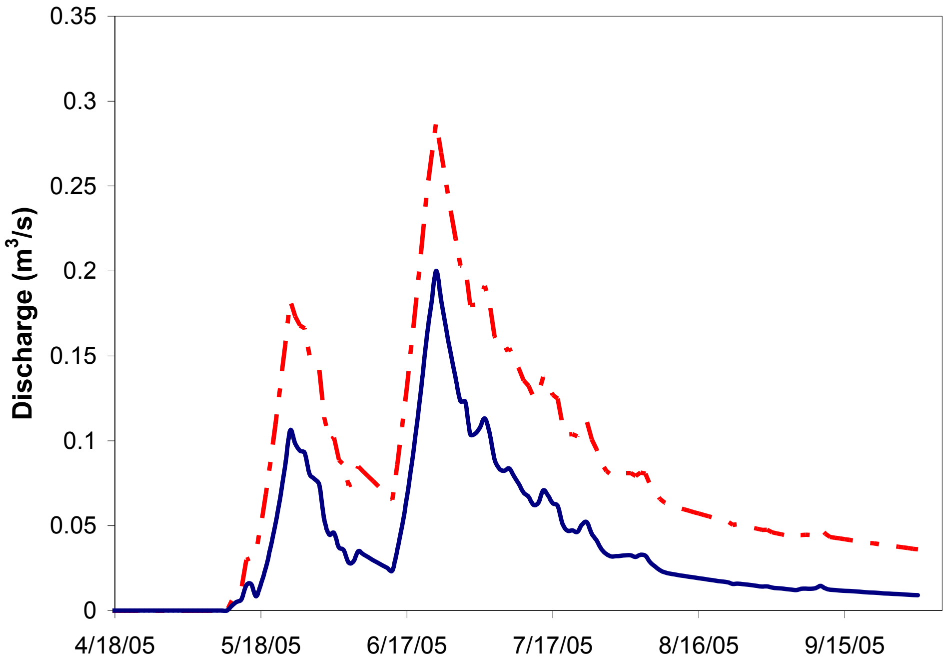

Figure 5.3. Uncorrected hydrograph (dashed line) and corrected hydrograph (solid line) for West Glacier Lake watershed water year 2005. Streamflow was dominated by a bi-modal snowmelt period in the early spring and summer.

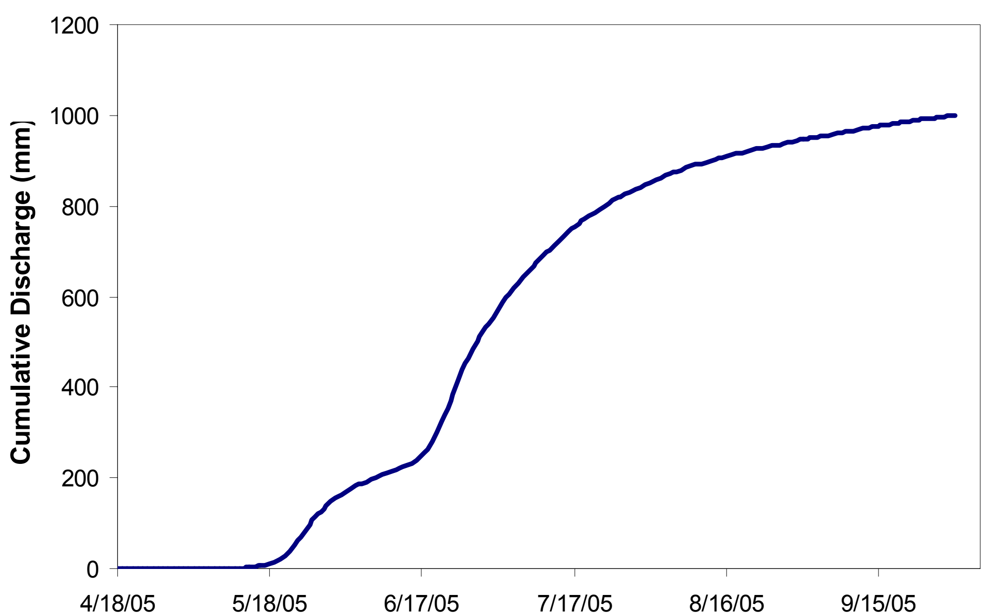

Figure 5.4. Cumulative streamflow from West Glacier Lake watershed for water year 2005. The bi-modal peak is event in the cumulative discharge.

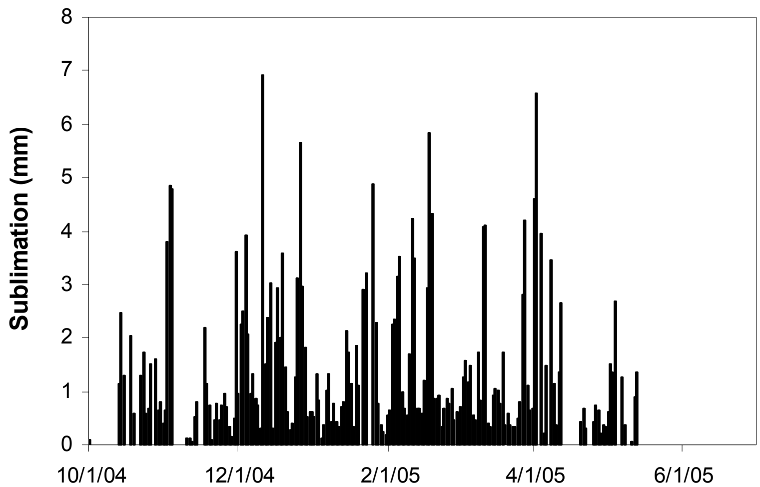

Figure 5.5. Daily snowpack sublimation data for West Glacier Lake watershed, water year 2005.

Figure 5.6. Snow depth sample locations for West Glacier Lake watershed, water year 2005 (n =538). Contour interval is 15 meters.

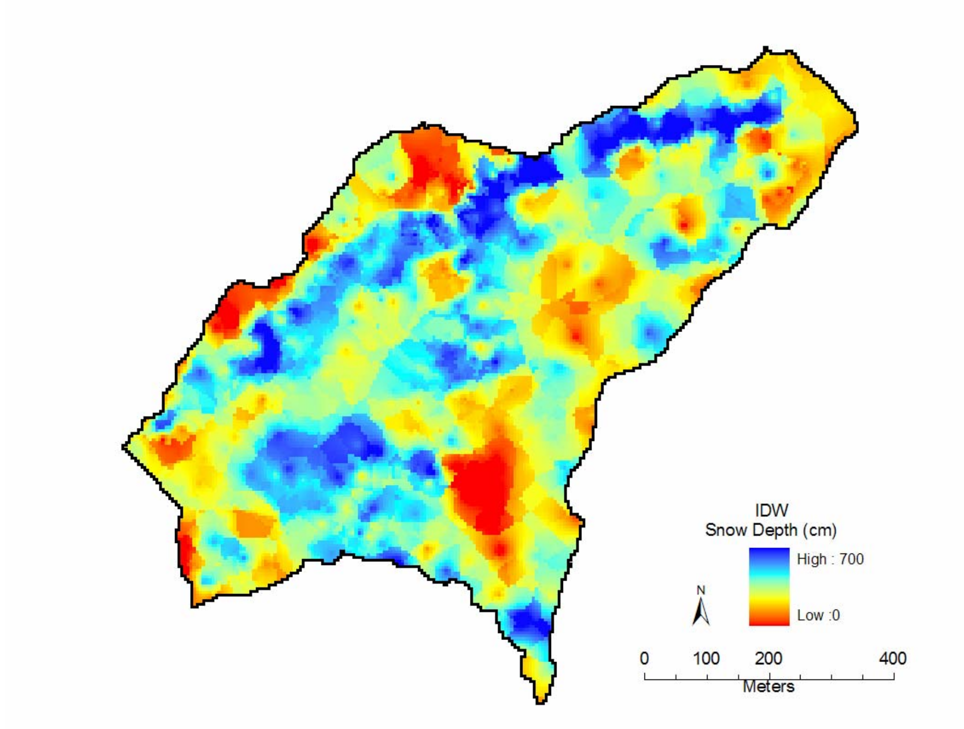

Figure 5.7. Distributed snow depth estimates from inverse distance weighting (IDW) for April, 2005 using 6 nearest neighbors. Red colors indicate shallower snow depths; blue colors are deeper snow depths.

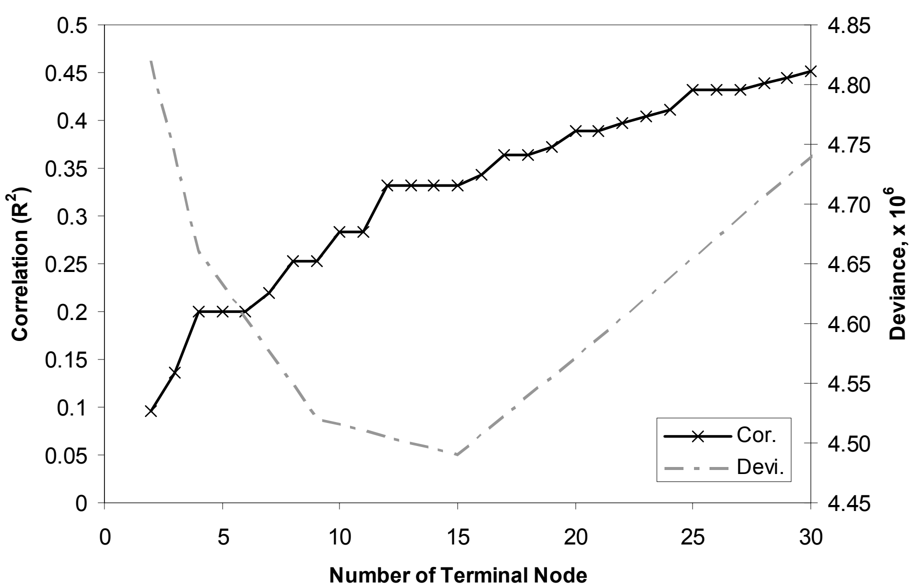

Figure 5.8. Cross validation for binary regression tree model.

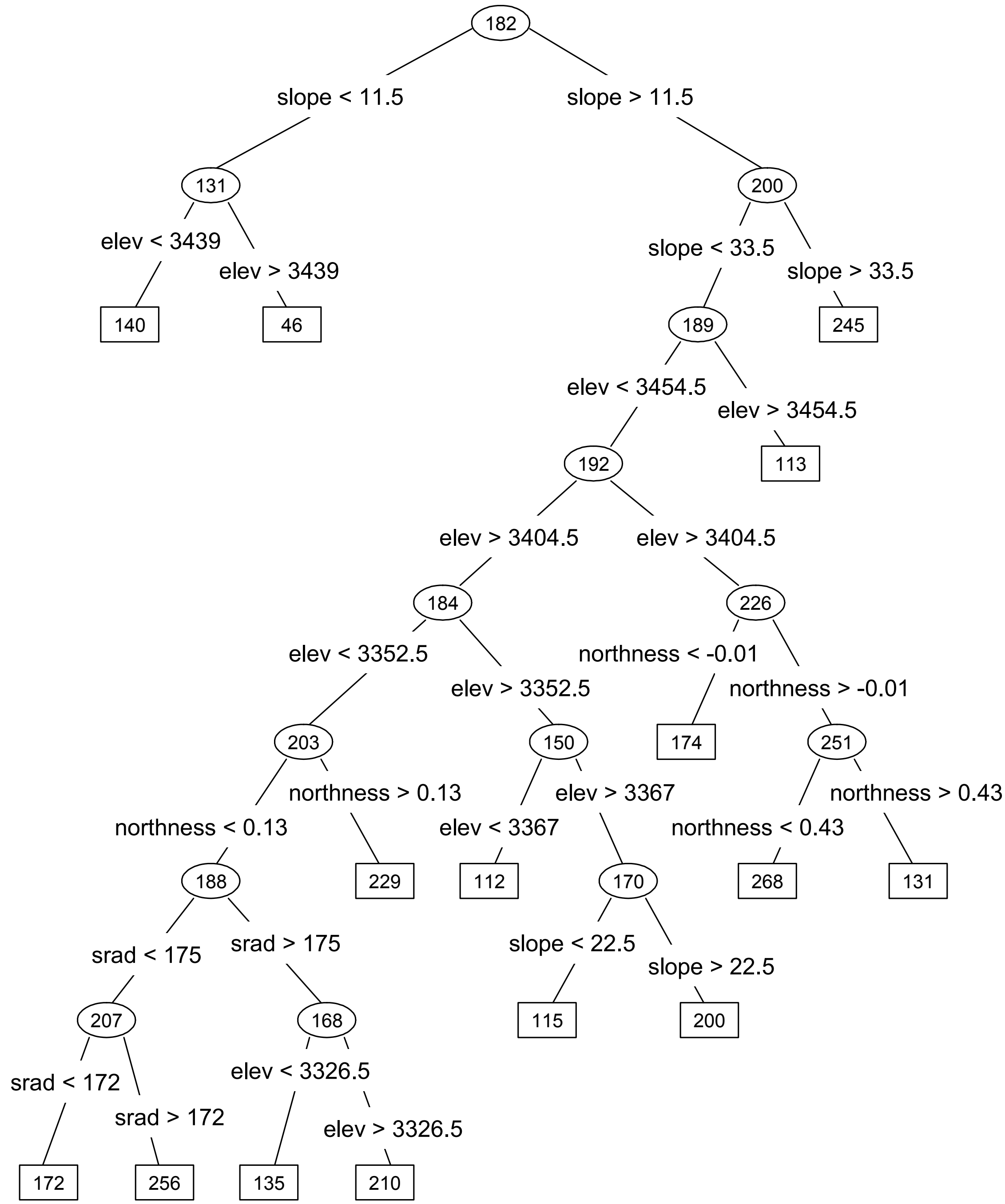

Figure 5.9. 15-node regression tree for West Glacier Lake watershed snow depth (cm). The root node is an ellipse located at the top of the figure, and terminal nodes are represented by the rectangles. The mean snow depth value at that node is located within the ellipses and rectangles.

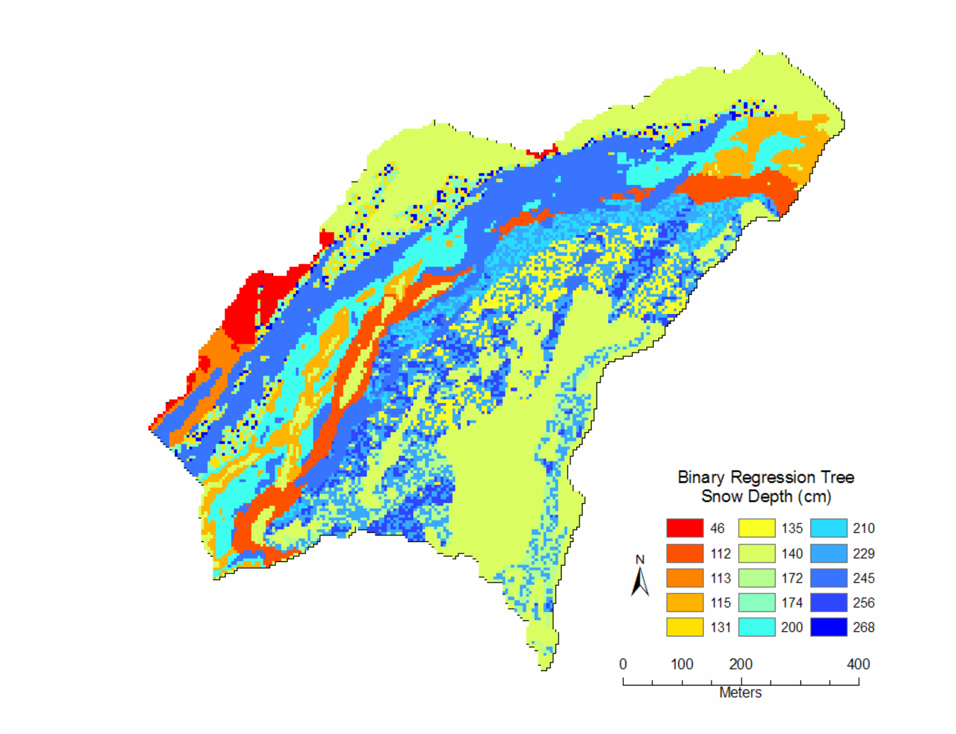

Figure 5.10. Distributed snow depth estimates from binary regression tree for April, 2005 using 15-terminal nodes. Red colors indicate shallower snow depths; blue colors are deeper snow depths.

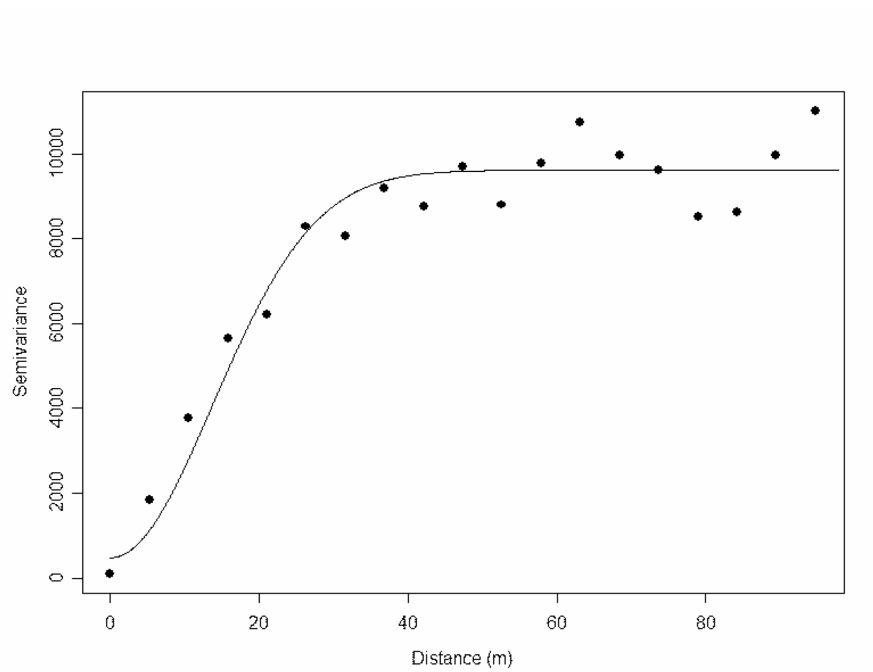

Figure 5.11. Snow depth experimental variogram and Gaussian model for West Glacier Lake watershed.

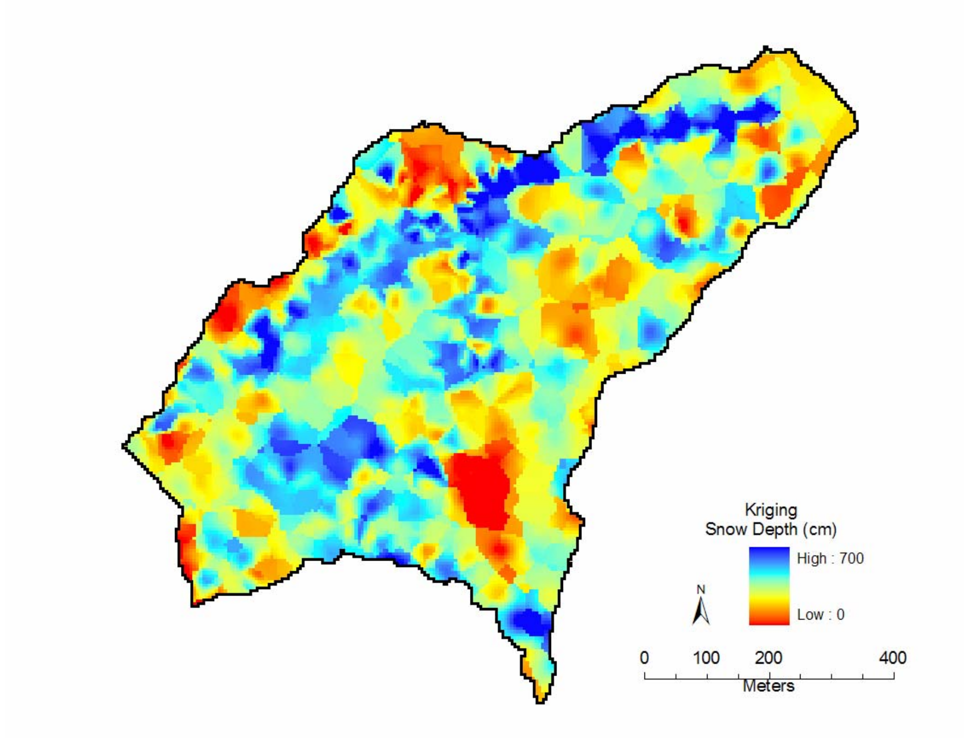

Figure 5.12. Distributed snow depth estimates from kriging for April, 2005 using 2 nearest neighbors. Red colors indicate shallower snow depths; blue colors are deeper snow depths.

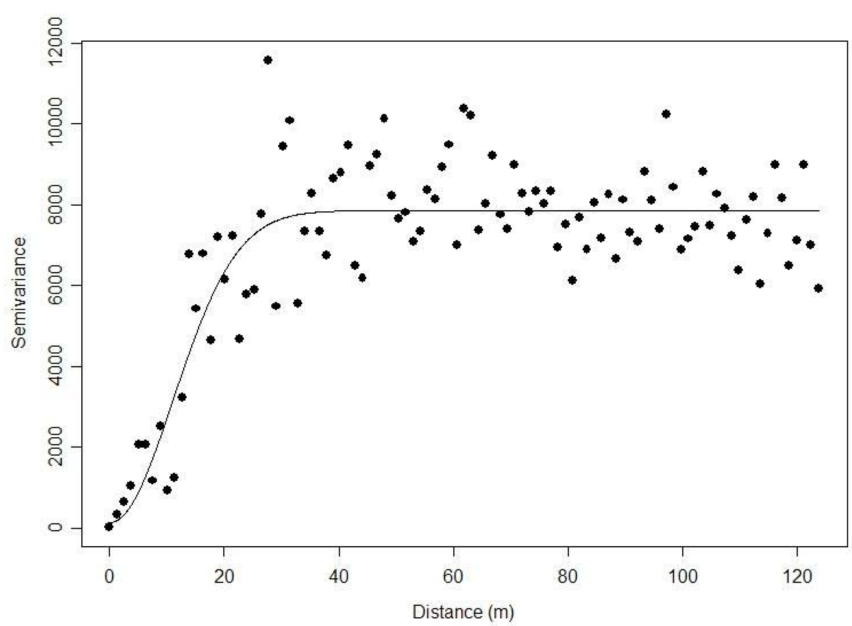

Figure 5.13. Regression tree residual snow depth experimental variogram and Gaussian model for West Glacier Lake watershed.

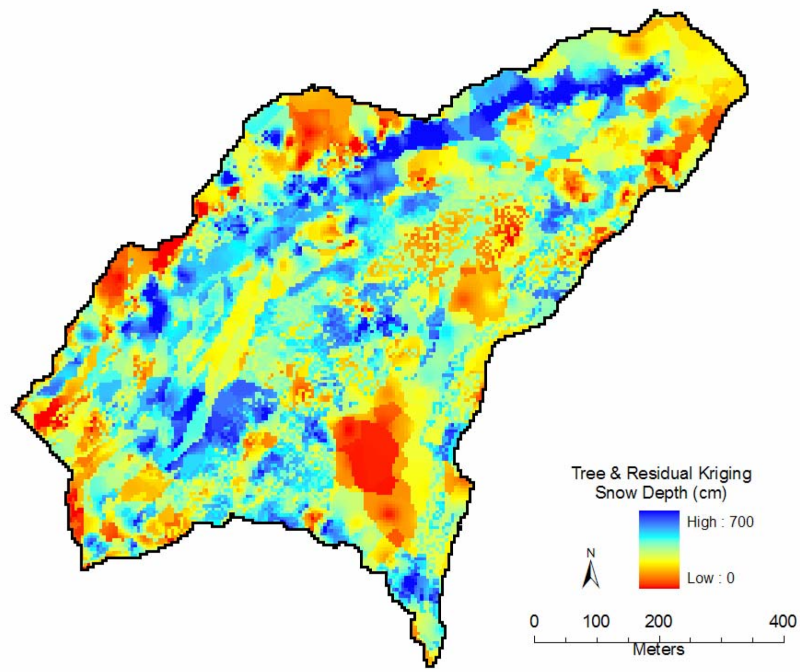

Figure 5.14. Distributed snow depth estimates from residual kriging of regression tree for April, 2005 using 2 nearest neighbors. Red colors indicate shallower snow depths; blue colors are deeper snow depths.

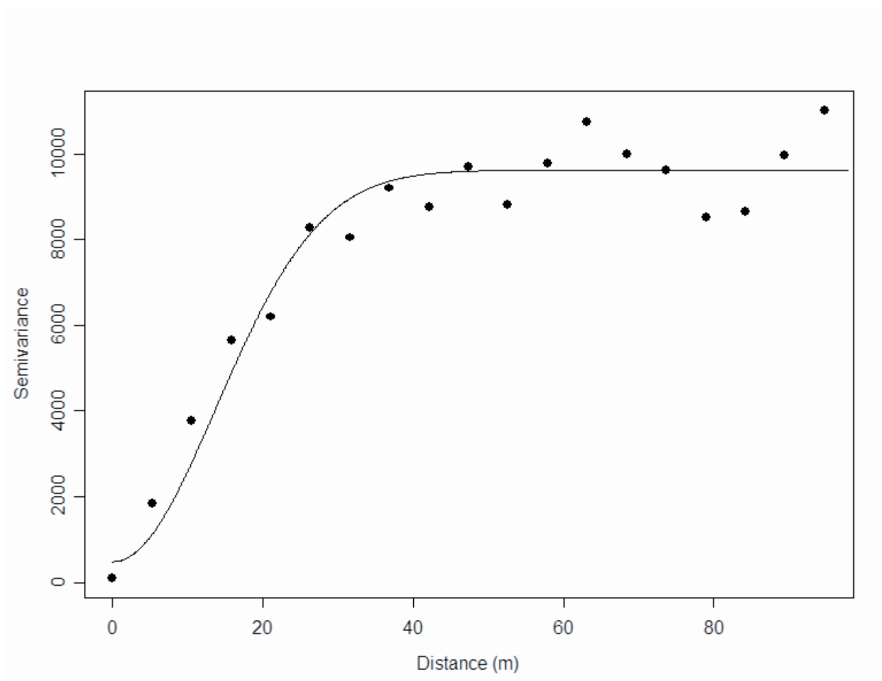

Figure 5.15. Modified residual snow depth experimental variogram and Gaussian model for West Glacier Lake watershed.

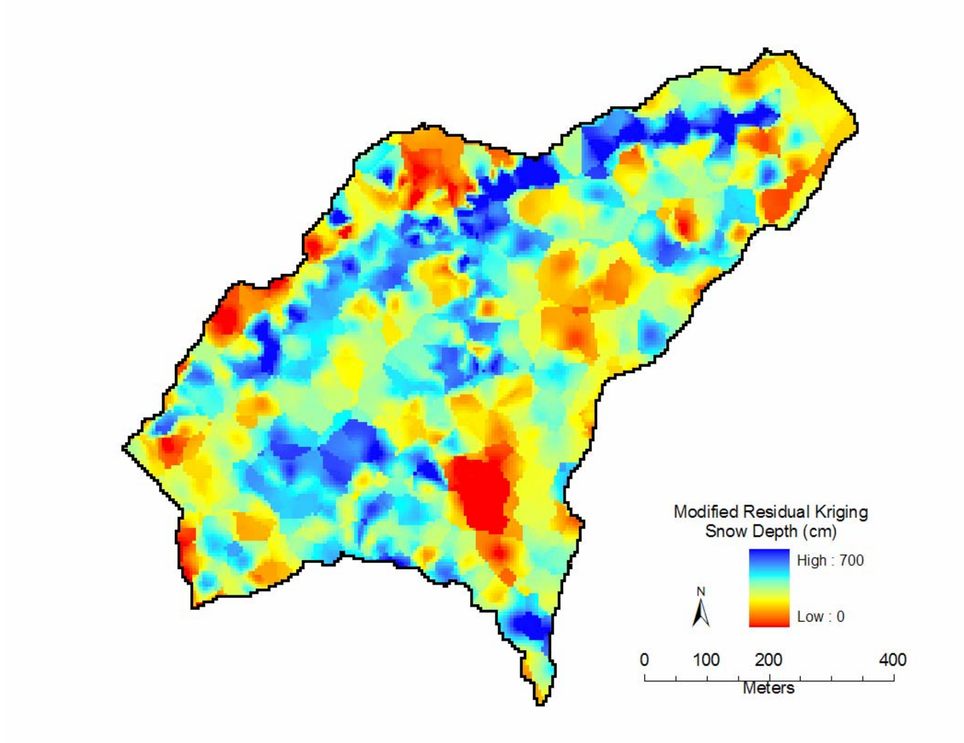

Figure 5.16. Distributed snow depth estimates modified residual kriging for April, 2005 using 2 nearest neighbors. Red colors indicate shallower snow depths; blue colors are deeper snow depths.

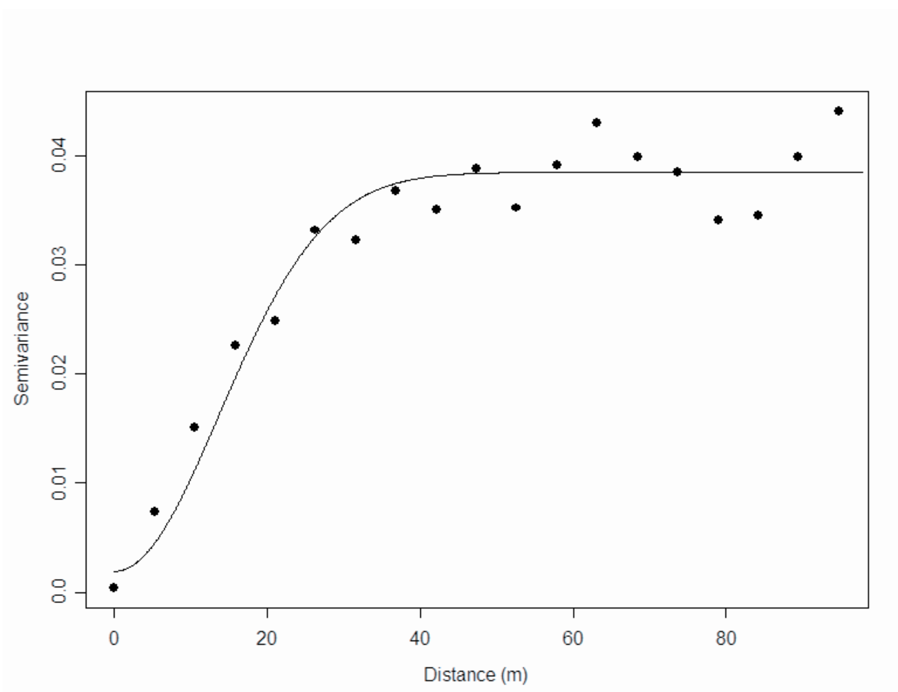

Figure 5.17. Scaled snow depth experimental variogram and Gaussian model for West Glacier Lake watershed.

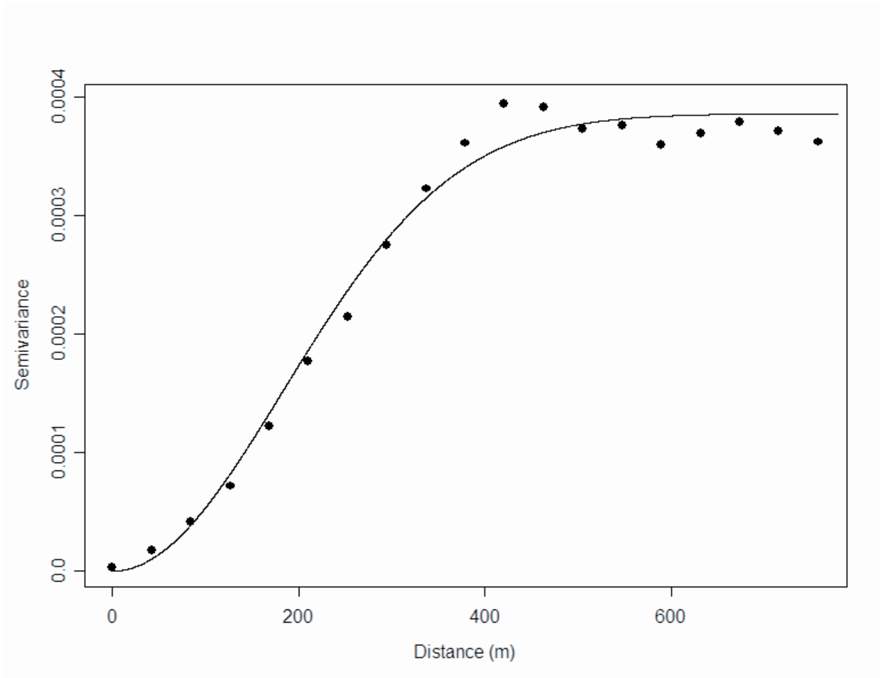

Figure 5.18. Scaled elevation experimental variogram and Gaussian model for West Glacier Lake watershed.

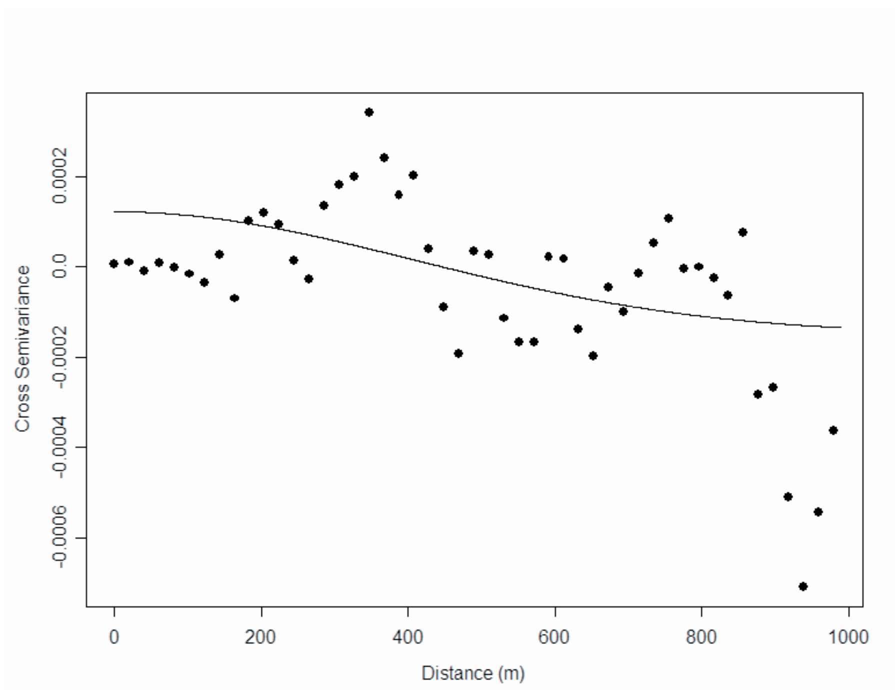

Figure 5.19. Snow depth and elevation experimental cross variogram and Gaussian model for West Glacier Lake watershed.

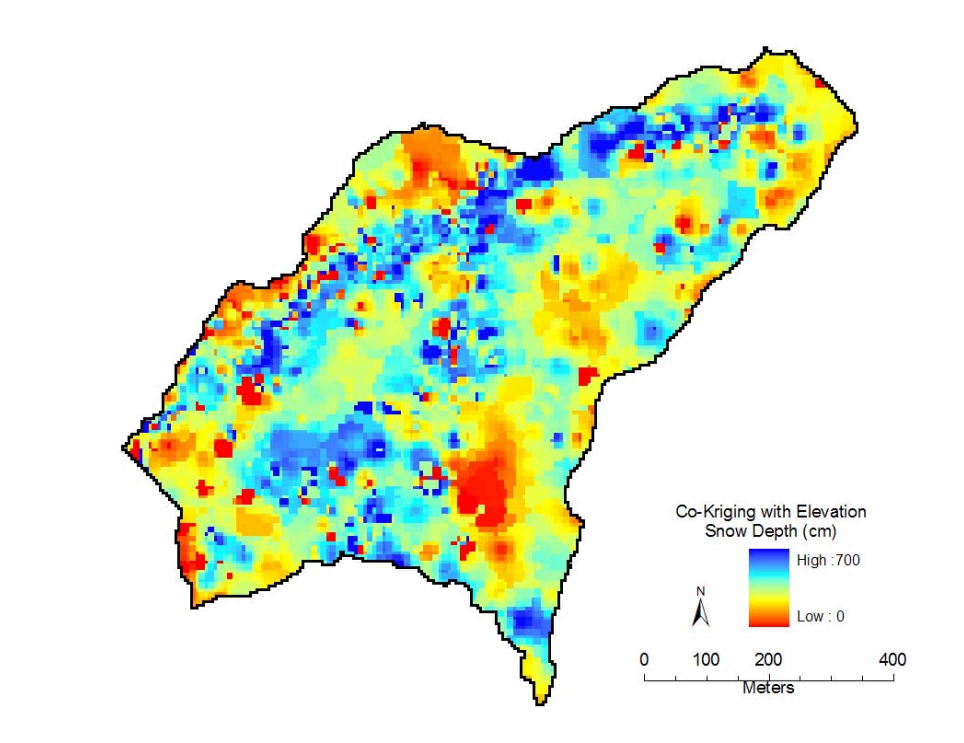

Figure 5.20. Distributed snow depth estimates from co-kriging with elevation for April, 2005 using 3 nearest neighbors. Red colors indicate shallower snow depths; blue colors are deeper snow depths.

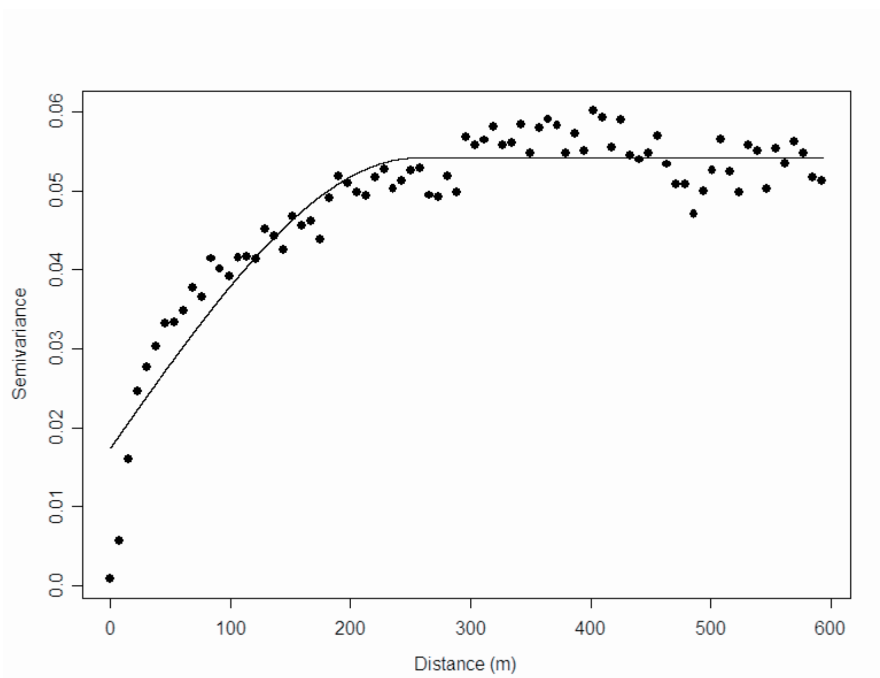

Figure 5.21. Scaled slope experimental variogram and spherical model for West Glacier Lake watershed.

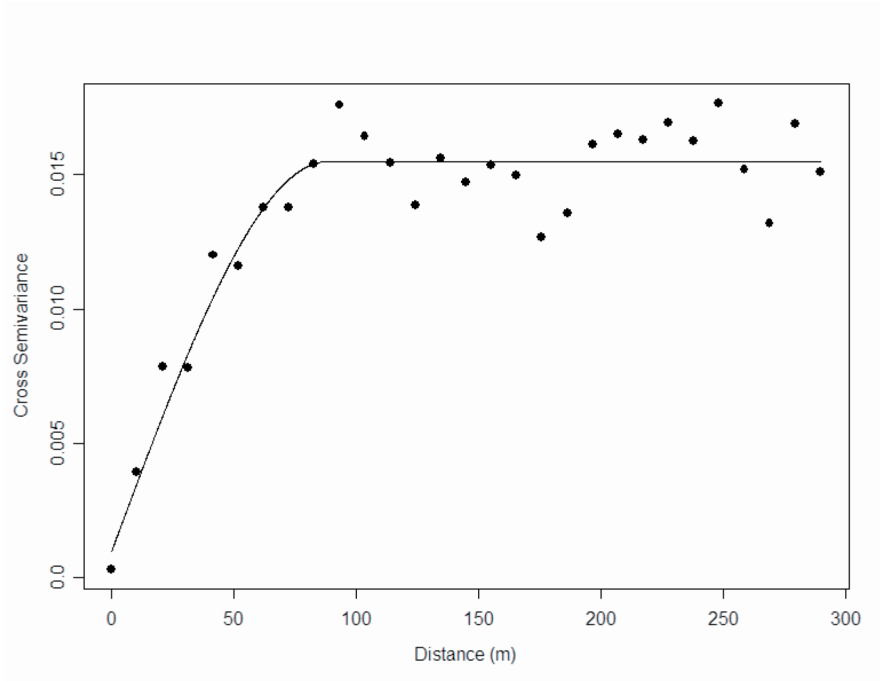

Figure 5.22. Snow depth and slope experimental cross variogram and spherical model for West Glacier Lake watershed.

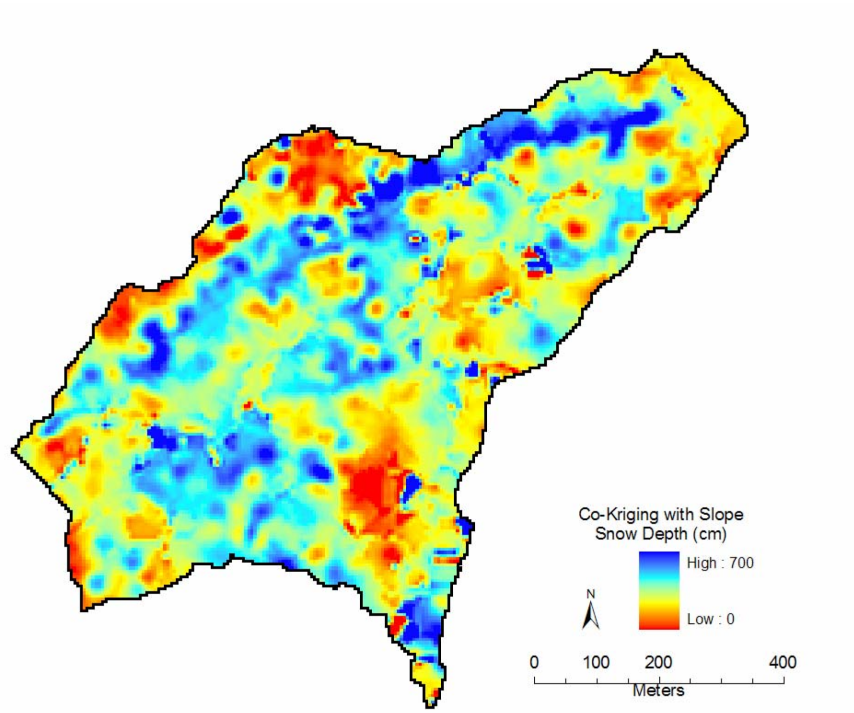

Figure 5.23. Distributed snow depth estimates from co-kriging with slope for April, 2005 using 3 nearest neighbors. Red colors indicate shallower snow depths; blue colors are deeper snow depths.

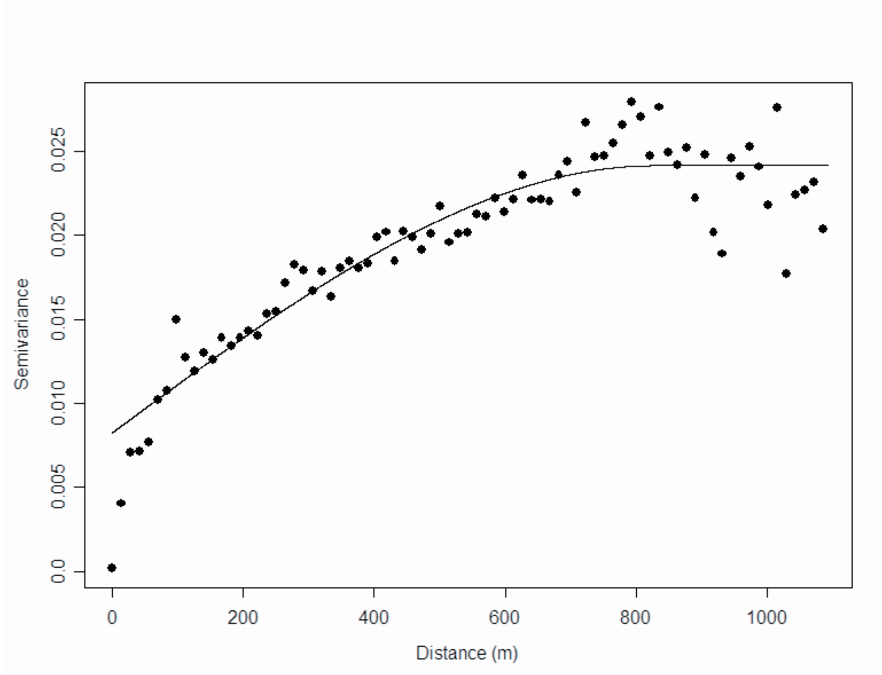

Figure 5.24. Solar radiation experimental variogram and spherical model for West Glacier Lake watershed.

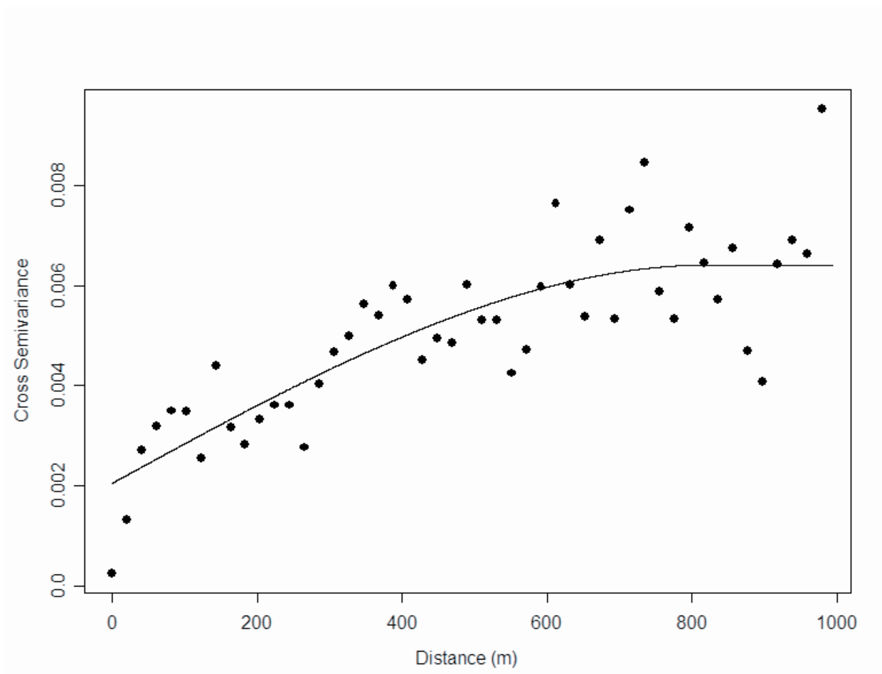

Figure 5.25. Snow depth and solar radiation experimental cross variogram and spherical model for West Glacier Lake watershed.

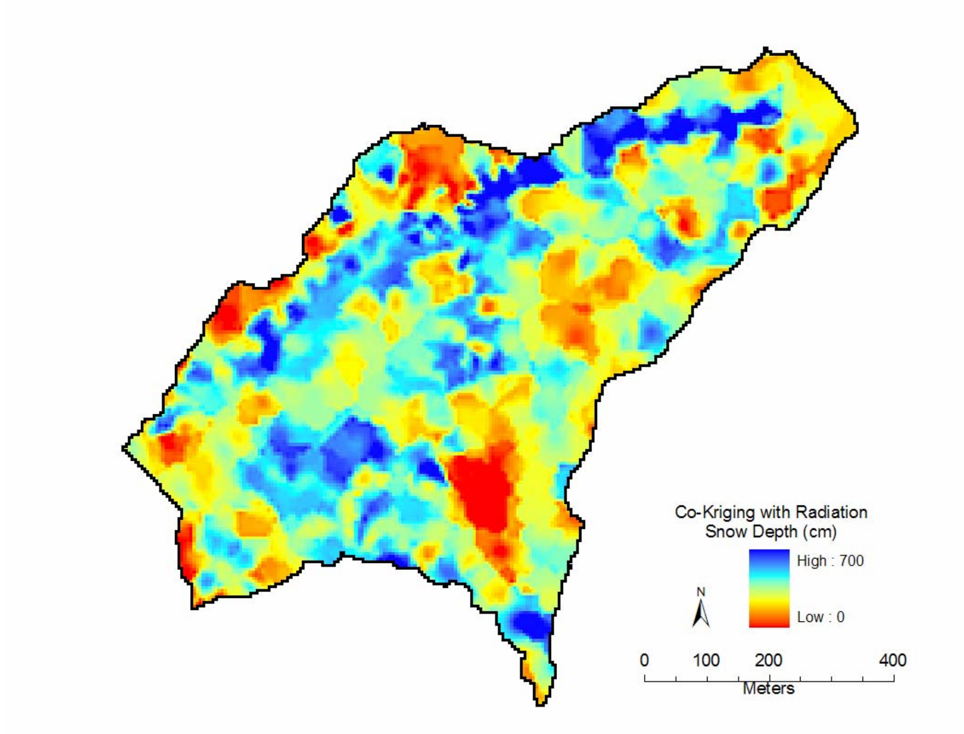

Figure 5.26. Distributed snow depth estimates from co-kriging with solar radiation for April, 2005 using 3 nearest neighbors. Red colors indicate shallower snow depths; blue colors are deeper snow depths.

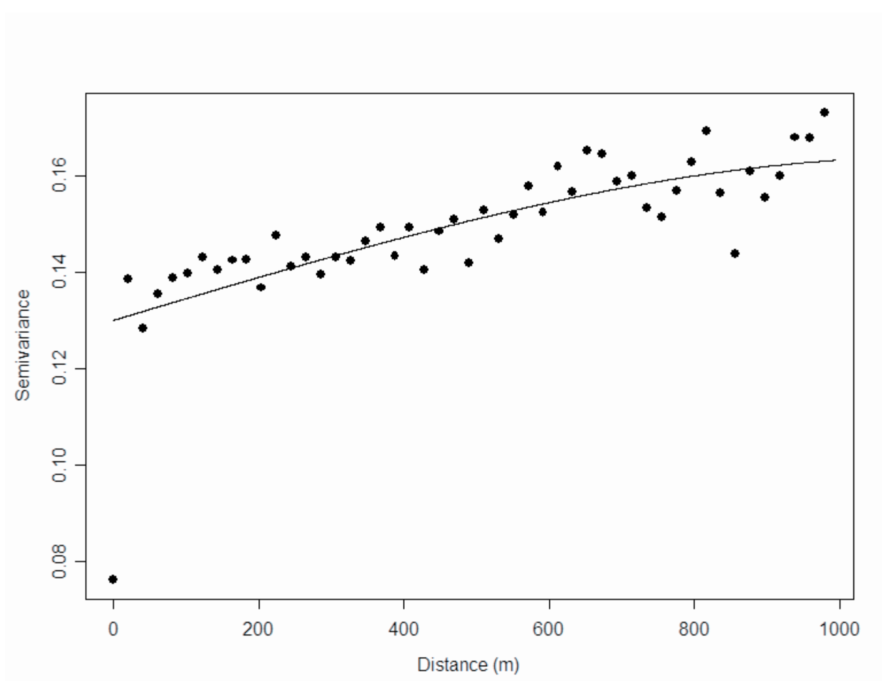

Figure 5.27. Scaled northness experimental variogram and spherical model for West Glacier Lake watershed.

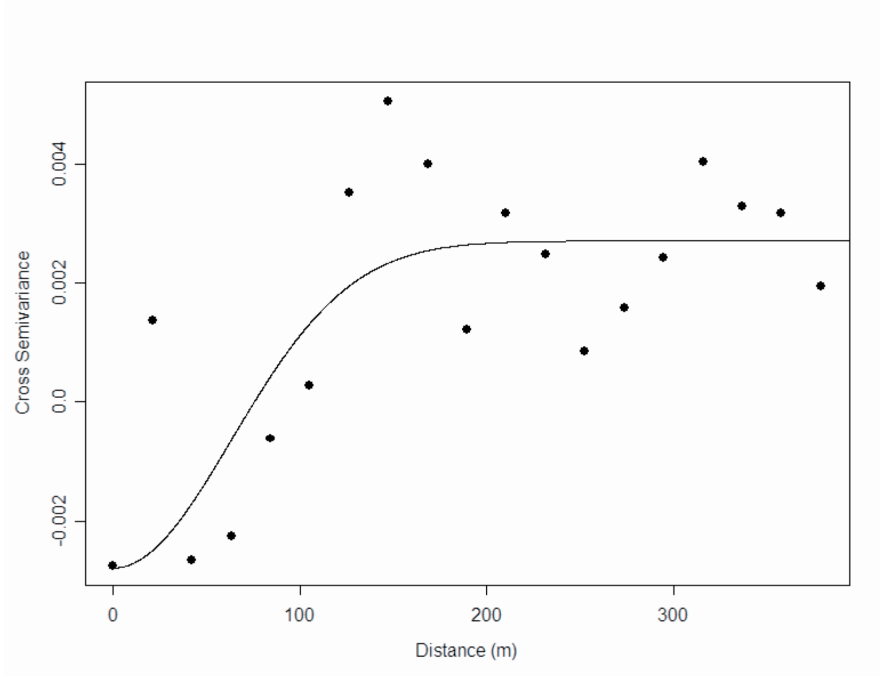

Figure 5.28. Snow depth and northness experimental cross variogram and Gaussian model for West Glacier Lake watershed.

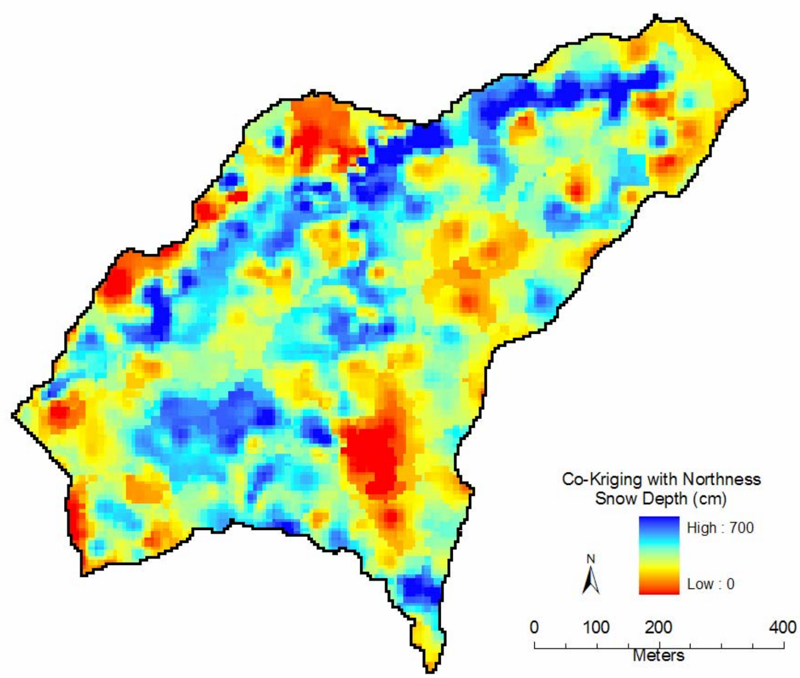

Figure 5.29. Distributed snow depth estimates from co-kriging with northness for April, 2005 using 3 nearest neighbors. Red colors indicate shallower snow depths; blue colors are deeper snow depths.

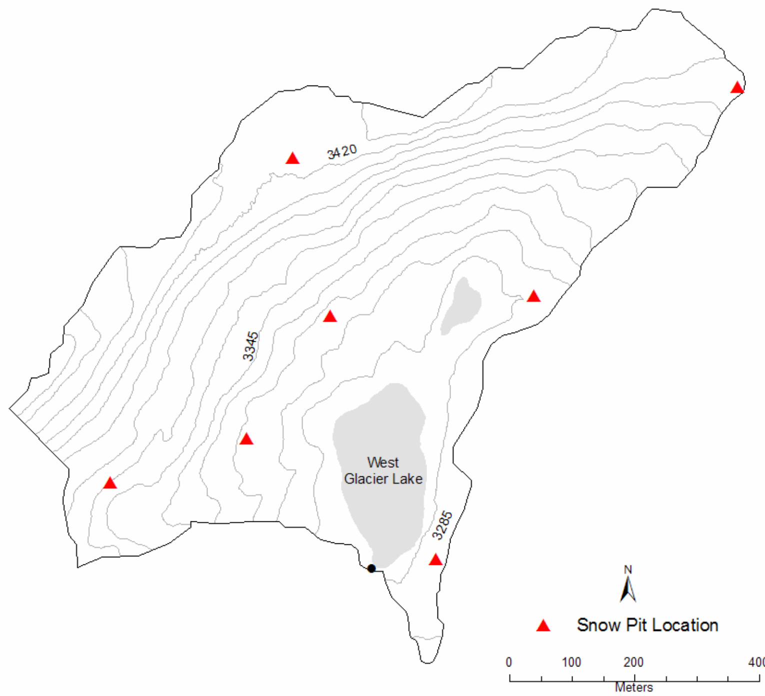

Figure 5.30. Snow pit and snow density locations for West Glacier Lake watershed, water year 2005 (n = 7). Contour interval is 15 meters.

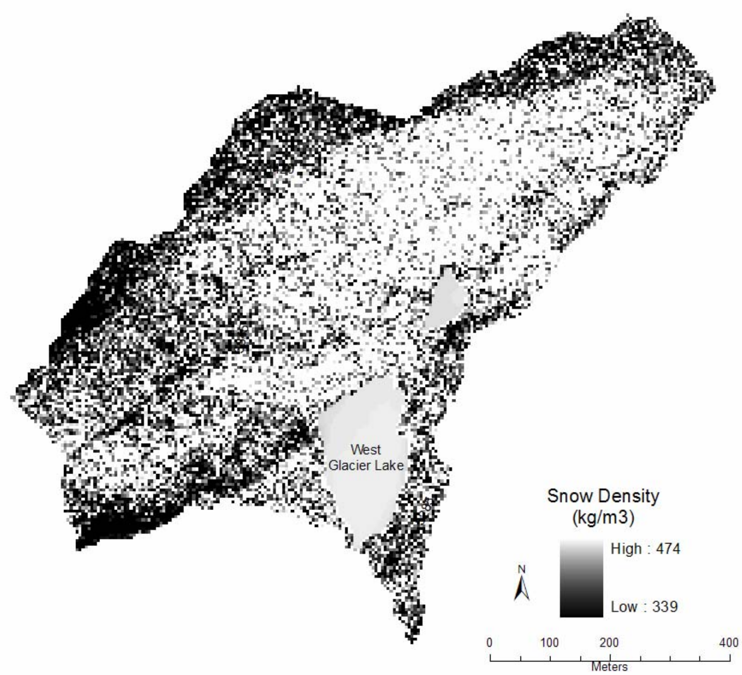

Figure 5.31. Snow density distributed over West Glacier Lake watershed by regression analysis. Dark colors indicate lower densities; bright areas are higher densities.

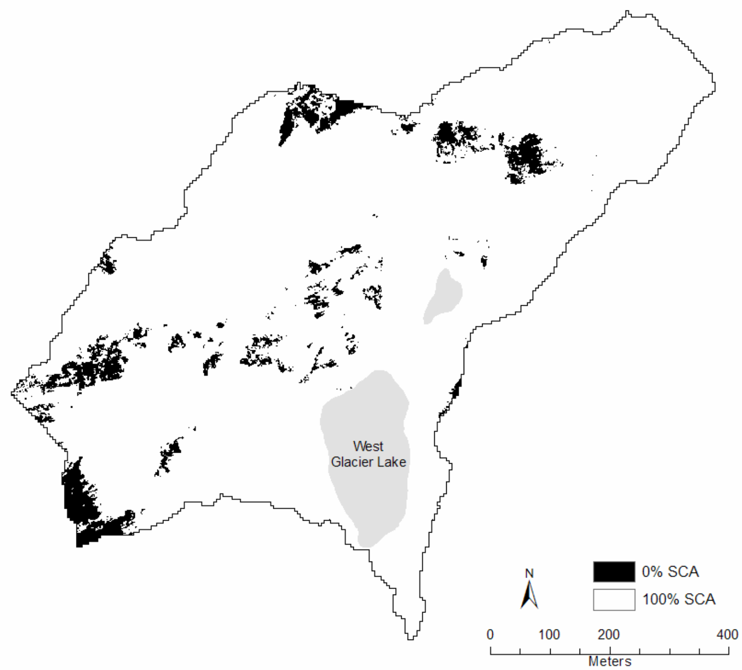

Figure 5.32. Snow-Covered Area (SCA) across West Glacier Lake watershed, water year 2005.

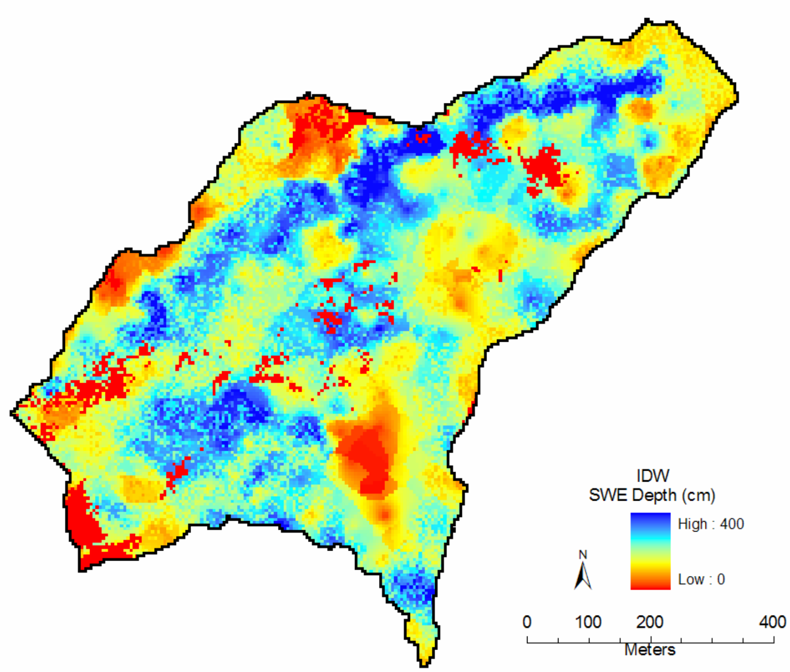

Figure 5.33. Distributed SWE estimates from IDW snow depth model, snow density model, and SCA model for April, 2005. Red colors indicate low SWE depths, and blue colors are deeper SWE depths.

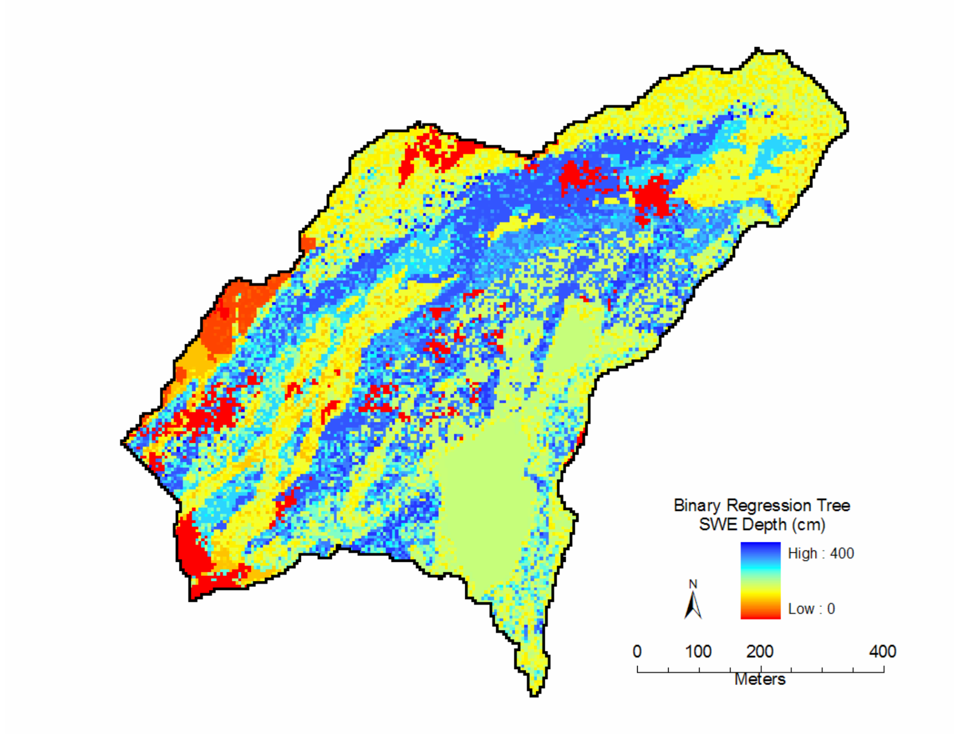

Figure 5.34. Distributed SWE estimates from regression tree snow depth model, snow density model, and SCA model for April, 2005. Red colors indicate low SWE depths, and blue colors are deeper SWE depths.

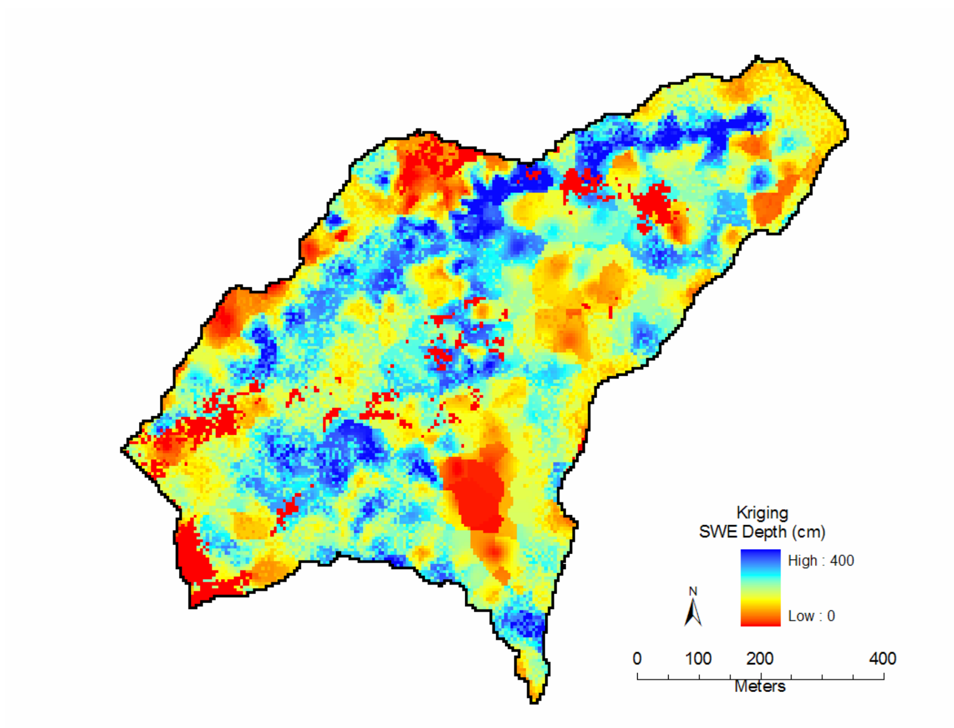

Figure 5.35. Distributed SWE estimates from kriging snow depth model, snow density model, and SCA model for April, 2005. Red colors indicate low SWE depths, and blue colors are deeper SWE depths.

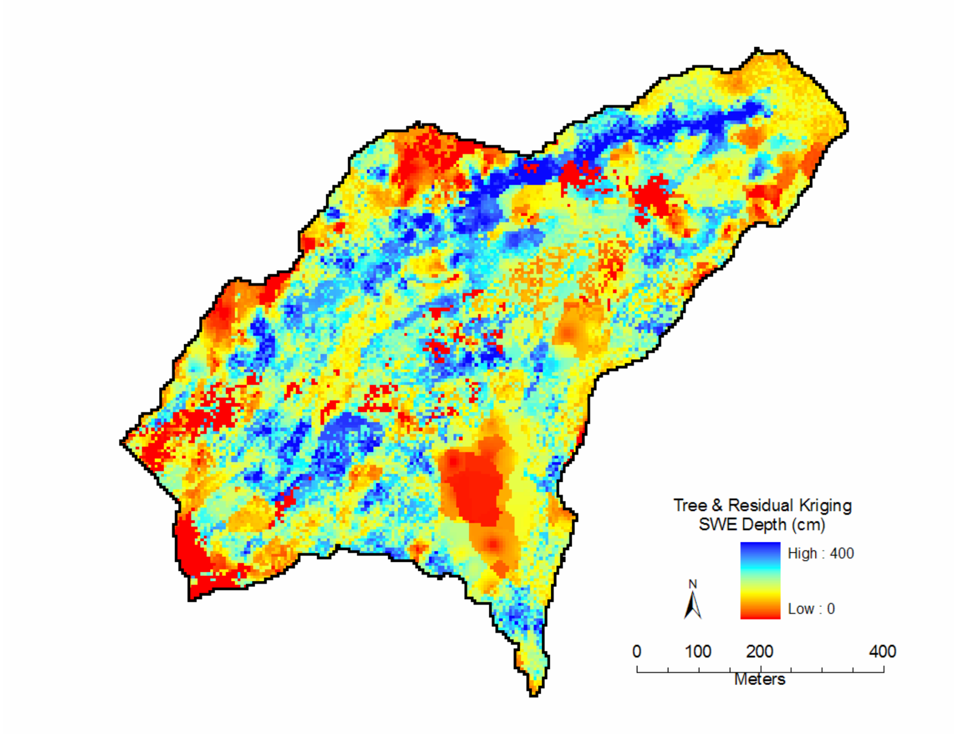

Figure 5.36. Distributed SWE estimates from tree & residual kriging snow depth model, snow density model, and SCA model for April, 2005. Red colors indicate low SWE depths, and blue colors are deeper SWE depths.

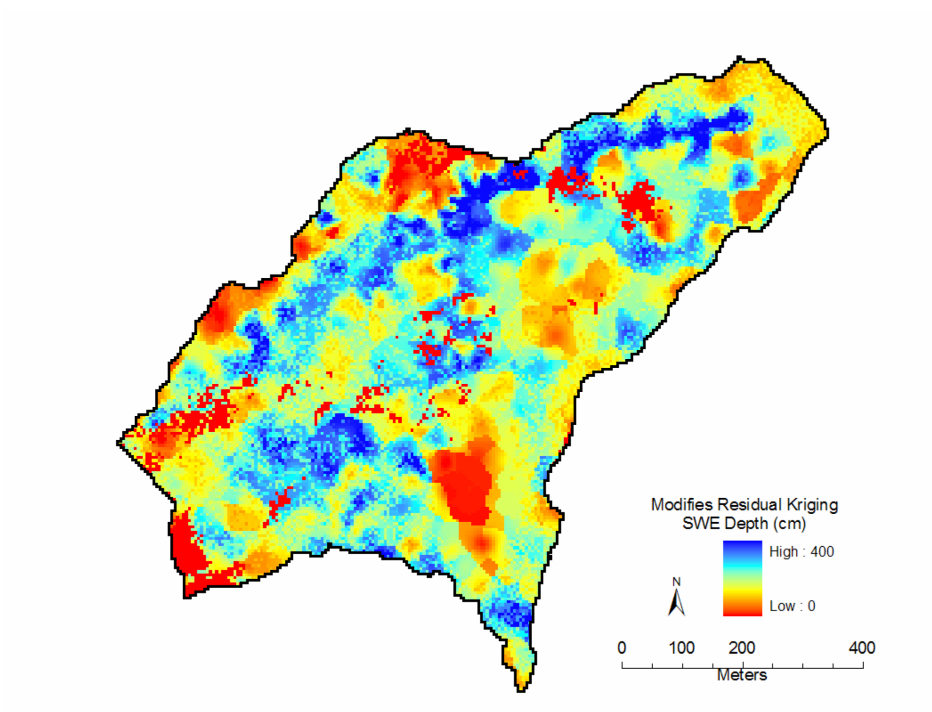

Figure 5.37. Distributed SWE estimates from modified residual kriging snow depth model, snow density model, and SCA model for April, 2005. Red colors indicate low SWE depths, and blue colors are deeper SWE depths.

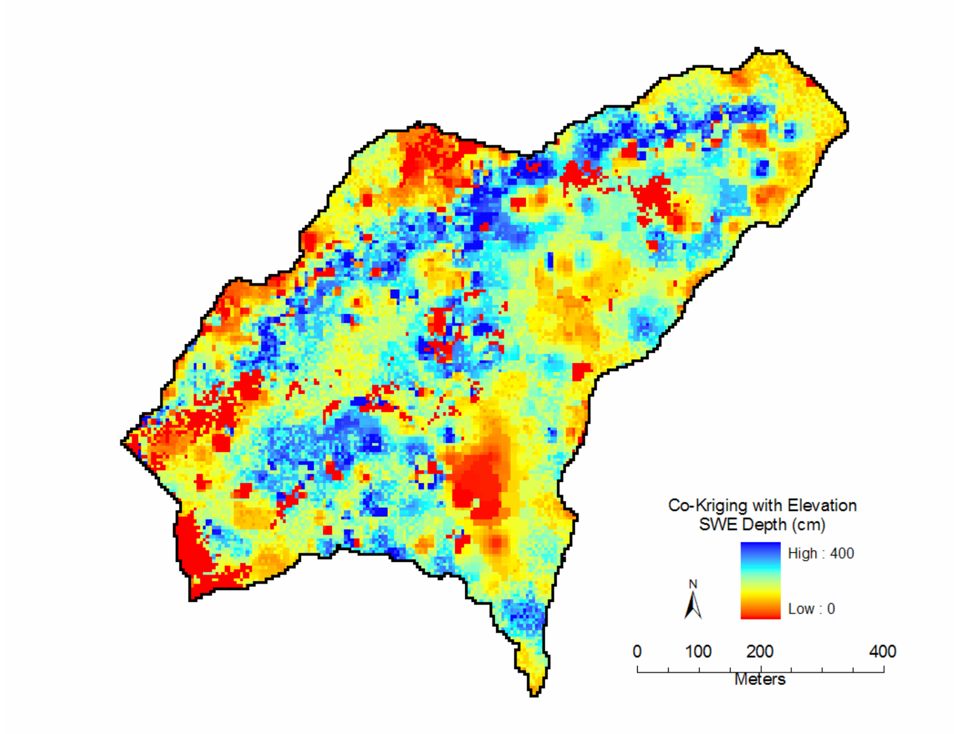

Figure 5.38. Distributed SWE estimates from co-kriging with elevation snow depth model, snow density model, and SCA model for April, 2005. Red colors indicate low SWE depths, and blue colors are deeper SWE depths.

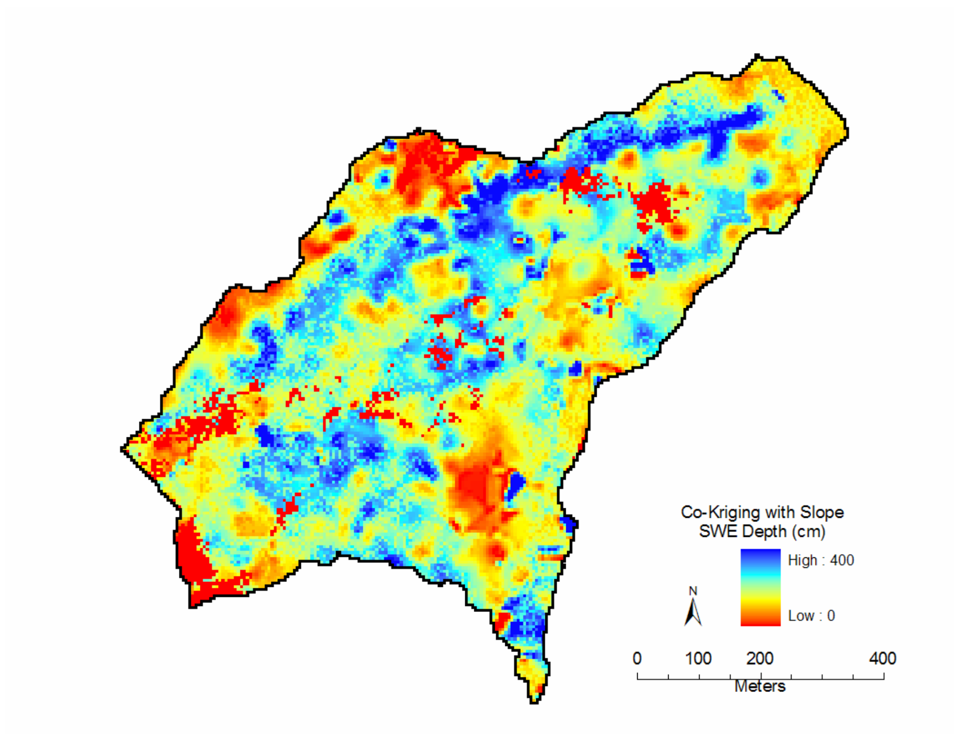

Figure 5.39. Distributed SWE estimates from co-kriging with slope snow depth model, snow density model, and SCA model for April, 2005. Red colors indicate low SWE depths, and blue colors are deeper SWE depths.

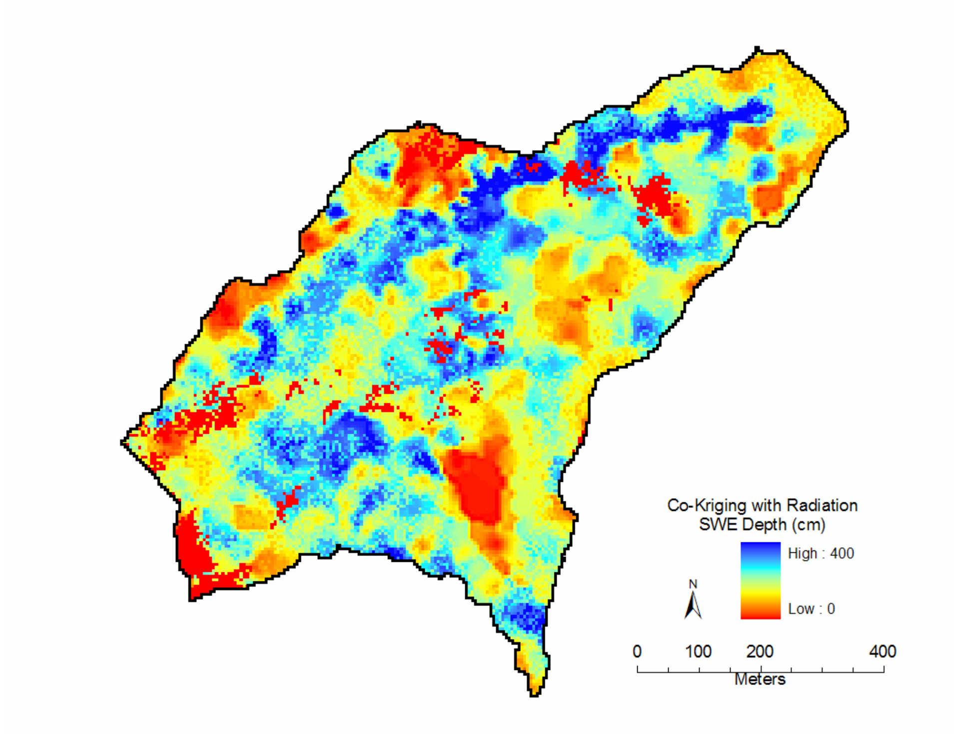

Figure 5.40. Distributed SWE estimates from co-kriging with radiation snow depth model, snow density model, and SCA model for April, 2005. Red colors indicate low SWE depths, and blue colors are deeper SWE depths.

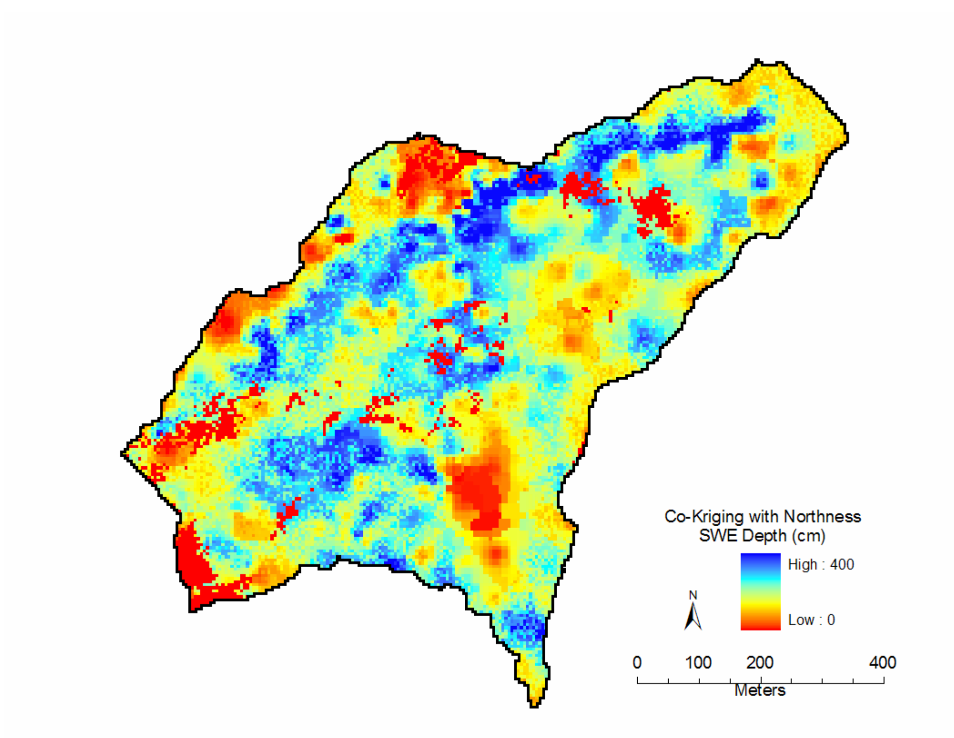

Figure 5.41. Distributed SWE estimates from co-kriging with northness snow depth model, snow density model, and SCA model for April, 2005. Red colors indicate low SWE depths, and blue colors are deeper SWE depths.

CHAPTER 6

6.0 DISCUSSION

Water balance variables for WGL watershed were calculated and used to quantify water year 2005 inputs and outputs. Discussion on the methods used and results for WGL watershed water balance are discussed in the following sections.

6.1 Precipitation

In windy, snow-dominated regions, precipitation gauges are prone to underestimate winter precipitation and snow accumulation. Precipitation collected at the GLEES gauge recorded 953 mm for water year 2005; this was 20 percent less than the measured annual mean of 1.20 m. Calculated annual inputs from the snow survey and summer precipitation were 55% greater than the annual GLEES precipitation gauge measurements.

Wind correction estimates based on daily precipitation totals were calculated using a catch ratio (CR) versus wind speed relationship based on the National Weather Service (NWS) 8" Alter shield for snow and mixed precipitation [*Goodison et al., 1998*]. The applied wind corrections resulted in an annual precipitation estimate of 2,005 mm for water year 2005. This value is 35% greater than the quantified summer and winter precipitation inputs. The excess wind corrected precipitation could be a result of 1) empirically fit equations (r^2 = 0.72, *n* = 107 for snow, r^2 = 0.59, *n* = 75 for mixed precipitation) and/or 2) that the measured wind speed (15 m "above forest canopy") was adjusted to the gauge orifice height (3 m) using a logarithmic wind profile equation [*Goodison et al., 1998*]. Quantifying the water balance using the wind corrected precipitation would have resulted in an evapotranspiration estimate of 754 mm, which is greater than the range of error associated with the evapotranspiration estimate in Table 5.7.

6.2 Streamflow

Parshall flumes are designed to measure streamflow within 5% accuracy. Flume accuracy is extremely dependent on site characteristics and proper installation. A proper location for flume placement is dependent on the approach characteristics, channel characteristics, and the amount of potential erosion/scour [*USDI, 1997*]. For accurate flow measurements, the flume must be correctly set, placed at the proper elevation and must be properly leveled.

West Glacier Lake Parshall flume was installed in 1986 at the outlet of West Glacier Lake. Many years of freeze thaw cycles, pressure from deep seasonal snowpacks and annual deterioration has caused the flume to shift and settle from its original placement. Flume displacement led to the belief that the predetermined rating curves might be incorrect, and that the flume needed to be recalibrated to confirm the applicability of the rating curve and/or to determine a new relationship.

Streamflow measurements during water year 2004 and 2005 at West Glacier Lake outlet resulted in a new stage-discharge relationship that was significantly different from the factory relationship. The new relationship reduced annual streamflow outputs by

200%, allowing the annual water balance to close with a sufficient estimate of evapotranspiration.

6.3 Evapotranspiration

Potential evapotranspiration (PET) calculated using the Thornthwaite method and Blaney-Criddle method resulted in 347 mm and 416 mm, respectively. The estimated evapotranspiration value of 230 mm is 30% to 45% lower than Thornthwaite and Blaney-Criddle PET estimates. The PET estimate may be greater than the actual evapotranspiration in this water limited environment and due to limited vegetation within WGL watershed. Even in this water limited environment, there is an abundant source of water from West Glacier Lake, approximately 5.5% of the watershed area.

The annual evapotranspiration estimate determined from lake evaporation (17 mm) and evapotranspiration (146 mm), as per Hasfurther *et al*., [1994] yielded 163 mm. The combined mass transfer and Blaney-Criddle estimate is less than the 230 mm residual evapotranspiration estimate. Both values are comparable to previous evapotranspiration quantities reported from research in alpine regions of the Sierra Nevada [*Kattelmann and Elder, 1991*] and from the WGL watershed [*Hasfurther et al., 1994; Ruess et al., 1995; Ellsworth, 2002*].

6.4 Snowpack Sublimation

The mass transfer method, also known as the bulk aerodynamic method, is based on the assumption that the snow surface temperature effectively follows the air temperature. This allows the measurements of temperature and wind speed to be collected at one height. However, this assumption is often inaccurate below 0°C, and can lead to an over-estimation of sublimation [*Bernier and Edwards, 1989*]. Bulk transfer methods also assume the snow surface is saturated with respect to ice or water, i.e. 100% relative humidity [*Box and Steffen, 2001*].

Aerodynamic profile methods measure temperature and wind speed at multiple heights above the surface. This technique has been shown to underestimate the magnitude of the latent heat flux by 36% in the Colorado Rocky Mountains [*Hood et al., 1999*] and to be within a few percent on the Greenland ice sheet [*Box and Steffen, 2001*] when compared to the more accurate eddy correlation method. *Box and Steffen* [*2001*], reported annual sublimation losses from the bulk aerodynamic method to be 23% of precipitation, this is 11% more than the aerodynamic profile method calculated. These results suggest that the 251 mm of snowpack sublimation calculated from the mass transfer method may be an overestimate.

The bulk aerodynamic method also requires an estimate of the surface roughness height parameter (z_o) in order to define the wind speed profile. The surface roughness parameter is an important component for quantifying snowpack sublimation losses. Surface roughness was assumed to be 1 x 10^{-3} m; previous research has used roughness parameters of 5 x 10^{-2} m [*Fassnacht, 2004*] and 5 x 10^{-4} m [*Box and Steffen, 2001*].

6.5 Permanent Snowfield

The permanent snowfield covers less than 2.5% of the watershed area, and was previously believed to account for the 40% to 130% excess streamflow [*Sommerfeld et al., 1991; Hasfurther et al., 1994*]. The estimated water volume stored within the snowfield is 25,408 m^3 (42 mm), which is about 0.1% of water year 2005 total streamflow. The small contributions from the permanent snowfield to streamflow led to the determination that the previously used rating equation for the Parshall flume was incorrect. WGL water balance was closed without consideration of snowmelt contributions from the permanent snowfield.

6.6 Snowpack Conditions

The 2005 water year precipitation was below average for the Medicine Bow region. The Natural Resources Conservation Service (NRCS), Brooklyn Lake SNOTEL site is less than 2 km from WGL watershed and reported April 1 and May 1 SWE values at 72% and 66% of the long term average. The snowpack conditions on April 20 and 23, during the snow survey, were 75% of the 18 year daily averages from the Brooklyn Lake SNOTEL site. Brooklyn Lake SNOTEL site had a peak SWE on 5/13/05 of 516 mm; an increase of 82 mm from the snow survey (Figure 6.1 and 6.2). Average monthly temperature for water year 2005 was similar to the fifteen year monthly average values, except for January, February, and July which were slightly warmer than the average records (Figure 6.3).

6.7 Spatial Snow Depth Modelling

The complex topography of WGL watershed played a dominate role in snow distribution. In the winter months, WGL watershed is subject to strong westerly winds that average 8 m/s. The strong winds aided by rugged topography create patterns of snow drifted and wind scoured regions. Modelling the spatial distribution of snow depth and

SWE in this alpine region is complex due to variability in snow properties. Using interpolation techniques in a snow dominated and wind-swept terrain provides a more accurate estimate of water inputs than precipitation gauge estimates. Spatial interpolation techniques and geostatistical methods have been used to estimate snow depth and SWE distribution in complex terrain with considerable results [*Balk and Elder, 2000; Molotch et al., 2005; Erickson et al., 2005*].

Using the independent variables slope, aspect, elevation, solar radiation, and northness, the spatial interpolation models were able to explain 18%-94% of the observed variance in snow depths in WGL watershed. If the lowest snow depth model is removed (co-kriging with elevation), then the spatial models explained 33%-94% of the observed snow depth variance. The success of previous snow distribution studies in mountain watersheds have focused on binary regression tree residual kriging and co-kriging methods for capturing snow distribution [*Balk and Elder, 2000; Molotch et al., 2005*]. The results presented in this study are not consistent with other snow distribution studies, in that the combined binary regression tree and residual kriging technique was not the most accurate interpolation method. The most accurate models in this study entailed using cross-correlated co-variables as auxiliary data to aid in the prediction of snow depth. The co-variable solar radiation, northness, and slope provided the most accurate results. The co-variable elevation produced the worst results; this could be due to the weak spatial cross-correlation between snow depth and elevation.

Co-kriging with solar radiation produced the best model results. Using the fifteenth of each month to quantify and calibrate the solar radiation index during the accumulation period was based on previous snow studies. Measured solar radiation, from the GLEES Tower, for the fifteenth were slightly greater than the monthly solar radiation values for November, January, March, and April and were less than the monthly solar radiation values for December and February. The measured monthly average solar radiation during the accumulation period was 158 W/m^2, the average of the fifteenth of each month was 175 W/m^2, and the modelled solar radiation index average was 167 W/m^2. Using the fifteenth as an index might have slightly over estimated solar radiation inputs when compared to the measured, but this method allowed for an effective and efficient estimate of the distributed solar radiation inputs into WGL watershed.

Another, but less intensive snow survey was performed on May 2, 2006. The 2006 water year was above average for a most of the accumulation period and then dropped below average due to limited snowfall in April. The Brooklyn Lake SNOTEL site reported April 1 and May 1 SWE values at 108% and 88%, respectively. A total of 395 snow depth measurements were collected and used to model snow depth distribution. Cross-validation procedures were used to examine the validity of the 2006 snow depth interpolation models. Results suggest that the spatial snow depth models produced similar results to the 2005 snow depth dataset.

6.8 Spatial Snow Density Modelling

Point values of measured snow density were interpolated within WGL watershed using the derived independent variables. Point snow density values were conservative when compared to snow depth values having an average range of 135 kg/m^3. Elevation, solar radiation, and northness variables were used to predict snow density distribution. These variables directly or indirectly influence snow density and the snowpack energy balance. Elevation indirectly affects snow density through temperature differences (energy balance). Solar radiation increases energy inputs and increases snow metamorphism, which ultimately increases snow density. *Molotch et al*. [2005], reported northness can be used a surrogate to solar radiation, which affects snow density through metamorphism processes. Distributed snow density values ultimately provide more detailed information and are more accurate than using a simple basin average density for calculating SWE.

6.9 SCA

SCA is an important component of SWE distribution and snowmelt runoff volume studies. SCA decreases rapidly at the onset of melt, within the first one hundred to two hundred degree days SCA is reduced 30 to 50 percent within the GLEES (Figure 6.4). Aerial imagery was used to derive SCA for WGL watershed; each pixel within the watershed was assigned a binary value of one (snow covered) or zero (snow free). Elder *et al.* [1998], used algorithms for estimating SCA from multispectral analysis. Their results showed that SCA estimated from a 50% binary threshold over estimated SCA by 3.9% when calculated and compared to the subpixel method (fractional percent of each pixel). WGL watershed SCA was calculated to be 94% with a 50% binary threshold. Applying the 3.9% correction *Elder et al*., [1998] reported would reduce SCA to 90%, a decrease of 51 mm from the calculated 1,311 mm of winter precipitation.

6.10 SWE

Knowledge on the spatial distribution of SWE is crucial for accurate prediction of the magnitude and timing of snowmelt runoff. Using different spatial interpolation techniques can result in different spatial snow depth patterns, which can ultimately influence snowmelt rates. The nine spatial models used in this study represented the observed snow distribution exceptionally well, and all models estimated total SWE in WGL watershed to be within +/- 2 percent of the best snow depth model. These SWE results are similar to previous snow distribution studies, in that total SWE calculated from different interpolation models was not significantly different from the best model [*Balk and Elder, 2000; Erxleben et al., 2002; and Molotch et al. 2005*]. Spatially distributed SWE values should produce better results in any snowmelt modelling effort when compared to using basin-wide mean values for snow depth, snow density, and SCA.

6.11 Water Balance

Development of a water balance for WGL watershed provided insight on the dominant hydrologic process. Precipitation as snow dominated the water balance, accounting for 85% of the precipitation. Total winter inputs in WGL watershed were calculated as peak SWE (1,060 mm) plus snowpack sublimation loss (251 mm) which yielded a total 1,311 mm of winter precipitation. Sublimation losses from the snowpack accounted for 19% of total winter precipitation, and are comparable to snowpack sublimation loss in the Colorado Rocky Mountains by *Hood et al*., [1999] (15%) and in the Sierra Nevada by *Kattelmann and Elder* [1991] (18%). Calculated SWE was 67% greater than collected winter precipitation gauge estimates (783 mm). Summer rainfall accounted for 15% of the precipitation and was less than snowpack sublimation losses. This suggests that snowpack sublimation losses should not dismissed as a negotiable variable in alpine water balance studies. The difference between the inputs and outputs yielded an evapotranspiration estimate of 230 mm.

These results suggest that precipitation gauge estimates were unrepresentative of actual precipitation inputs, and that depth-density field surveys combined with spatially distributed snow depth models provided better estimates of precipitation inputs.

Other sources of error that were not considered in this water balance were East Glacier Lake water inputs, snow blowing in and out of the watershed, groundwater flow and subsurface seepage. Geophysical data collected between West and East Glacier Lake has previously been analyzed and determined to be minimal (less than 1 mm/day) contribution, but still can add to water inputs [*Harry, 2006*]. Blowing snow in and out of the watershed was treated as precipitation since it was quantified in the snow survey. Groundwater flow and subsurface seepage was assumed not to change or add to the water balance. Quantifying groundwater flow and subsurface seepage into and out of WGL watershed would be valuable, but equipment were not in hand to collect the necessary data.

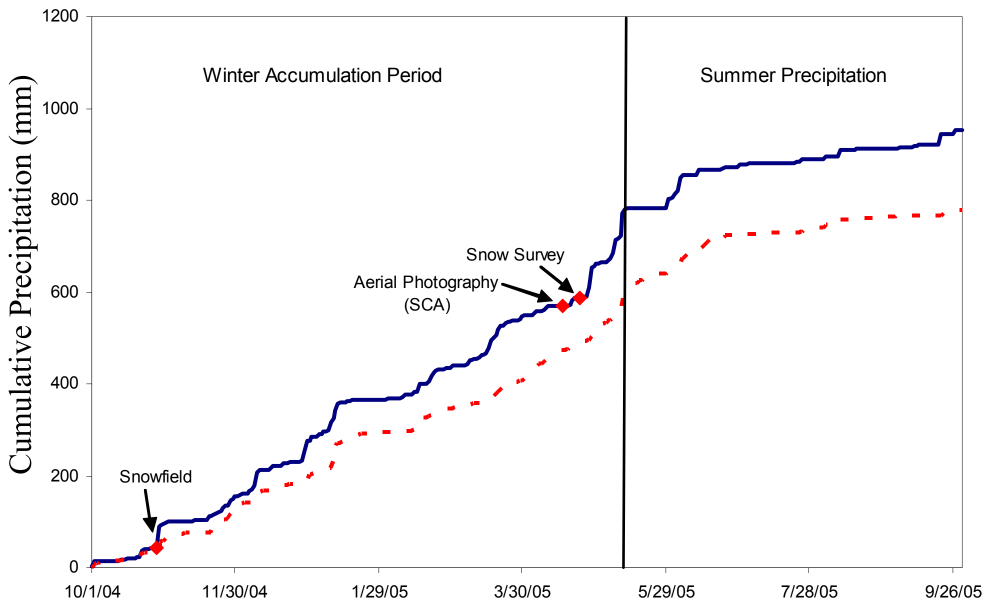

Figure 6.1. Cumulative precipitation from GLEES Tower (solid line) and Brooklyn Lake SNOTEL (dashed line) for water year 2005. Points represent the date of field collection for the snowfield survey, snow survey, and aerial photography.

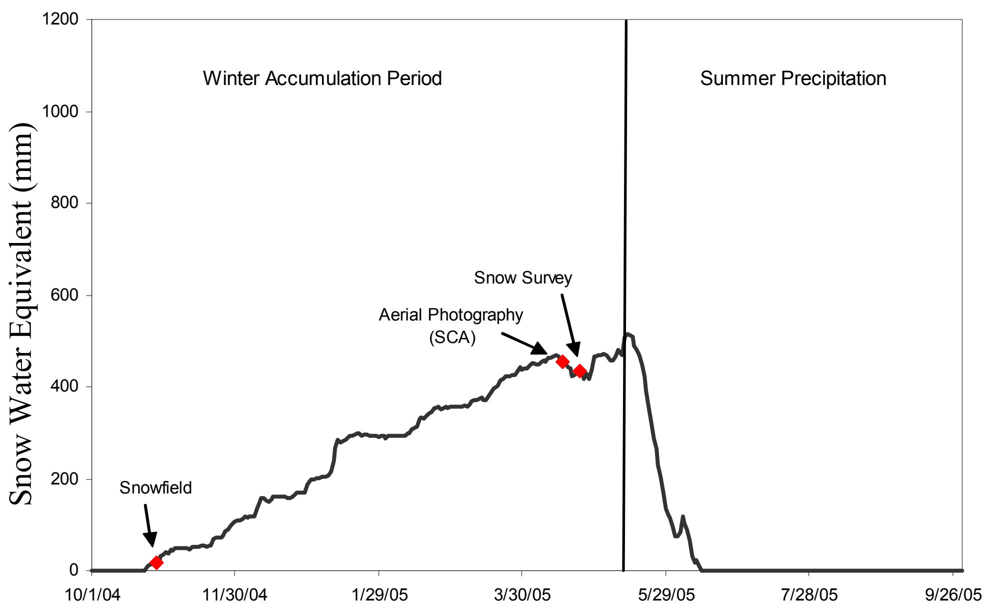

Figure 6.2. Brooklyn Lake SNOTEL snow water equivalent for water year 2005. Points represent the date of field collection for the snowfield, snow survey, and aerial photography.

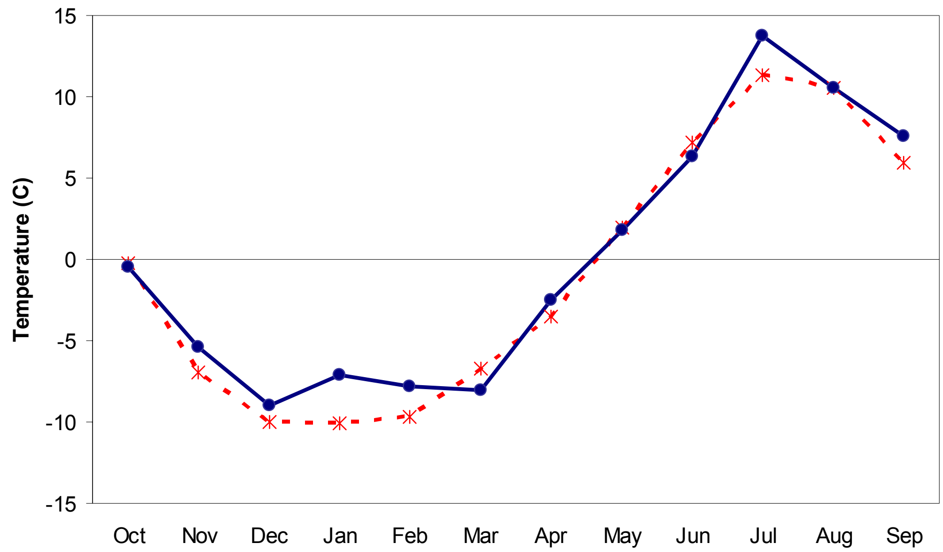

Figure 6.3. Annual average monthly temperature (dashed line) and water year 2005 average monthly temperature (solid line) measured from the GLEES Tower.

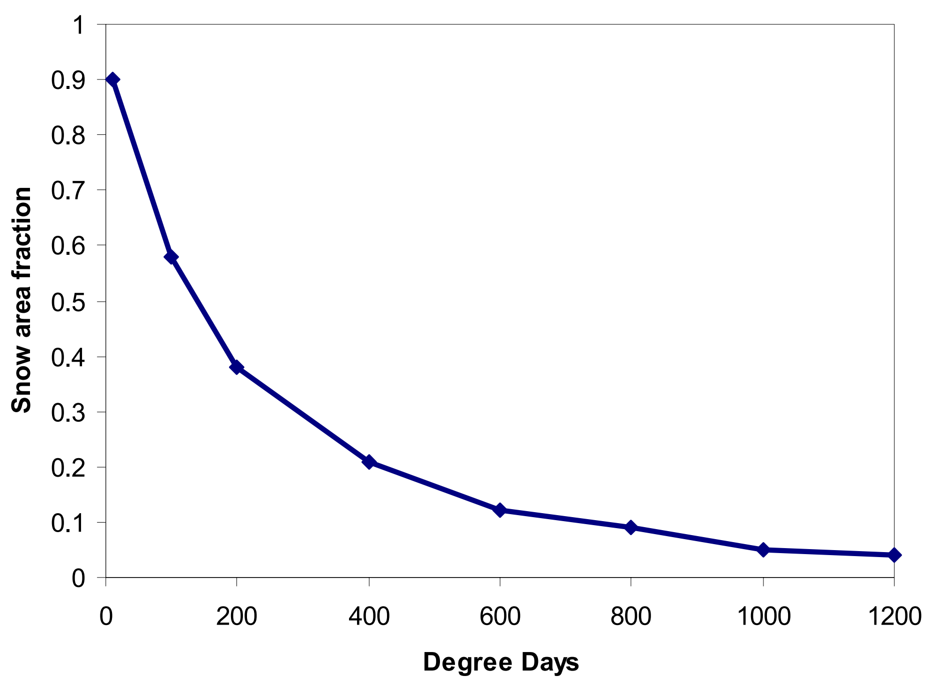

Figure 6.4. Average 1987-91 snow covered area recession curve versus degree days for GLEES. This figure was created from data presented in [*Sommerfeld, 1994*].

CHAPTER 7

7.0 CONCLUSION

This study explored the spatial distribution of SWE by examining the relationships with independent variables and was used to quantify WGL watershed's annual inputs and outputs of water. This research showed that intensive snow survey data combined with spatial interpolation techniques provide a more accurate representation of winter precipitation inputs into WGL watershed than precipitation gauge estimates.

The nine spatial models explained 18% to 94% of the observed snow depth variance, but SWE estimates were within +/- 2 percent of the best snow depth model. The distributed snow depth model results are slightly higher but still comparable to previous snow distribution studies. The intensive snow survey was able to capture the large-scale and small-scale snow depth variability. The estimated SWE inputs were 67% greater than precipitation gauge estimates. Spatially distributed SWE estimates combined with summer precipitation were able to close WGL water balance without consideration of snowmelt contributions, albeit small, from the permanent snowfield.

Intensive field measurements and spatial interpolation techniques were able to provide a representative estimate of winter precipitation into WGL watershed, supporting the hypothesis. The overall objective to quantify the annual water balance was attained and provided insight on the hydrologic variables of WGL watershed.

CHAPTER 8

8.0 LITERATURE CITED

Antal, E., S. Baranyi, and E. Toth, 1973. Comparison of calculation methods for evaporation using lake Balaton as an example, in *Hydrology of Lakes,* Helsinki Symposium*, IAHS Publ* no. 109, 220-224.

Balk, B., K. Elder, and J. Baron, 1998. Using geostatistical methods to estimate snow water equivalence distribution in a mountain watershed, in Proceedings of the *Western Snow Conference*, 66th Annual Meeting, Snowbird, Utah, April, 100-111.

Balk B., and K. Elder, 2000. Combining binary regression tree and geostatistical methods to estimate snow distribution in a mountain watershed, *Water Resources Research*, 36 (1), 13-26.

Barry, R.G., 1992. *Mountain weather and climate*, Second edition, Routledge, New York, 402 pp.

Bernier, P and G.C. Edwards, 1989. Differences between air and snow surface temperatures during snow evaporation, in *Proceedings of the Eastern Snow Conference*, 46, 117-120.

Blösch, G., R. Kirnbauer, and D. Gutknecht, 1991. Distributed Snowmelt Simulations in an Alpine Catchment 1. Model Validation on the basis of Snow Cover Patterns, *Water Resources Research*, 27 (12), 3171-3179.

Blösch, G., 1999. Scaling Issues in Snow Hydrology, *Hydrological Processes*, 13, 2149-2175.

Blösch, G., R. Grayson, 2000. Spatial Observations and Interpolation, in *Spatial Patterns in Catchment Hydrology: Observations and Modelling*, Cambridge University Press, New York, NY, 395 pp.

Box, J.E. and K. Steffen, 2001. Sublimation on the Greenland ice sheet from automated weather station observations, *Journal of Geophysical Research*, 106, 28 pp.

Breiman, L, J. Friedman, R. Olsen, and C. Stone, 1984. *Classification and Regression Trees*, Wadsworth and Brooks, Pacific Grove, Ca, 358 pp.

Carroll, S.S., and N. Cressie, 1996. A comparison of geostatistical methodologies used to estimate snow water equivalent, *Water Resources Bulletin*, 32 (2), 267-278.

Cline, D.W., 1992. Modelling the redistribution of snow in alpine areas using geographic information processing techniques, in *Proceedings of the Eastern Snow Conference*, 49, 13-24.

Chow, V.T., 1959. *Open Channel Hydraulics*, McGraw-Hill, New York, New York, 680 pp.

Daly, C., R.P. Neilson, and D.L. Phillips, 1994. A statistical-topographic model for mapping climatological precipitation over mountainous terrain, *Journal of Applied Meteorology*, 33: 140-158.

Deems, J.S., 2002. *Topographic effects on the spatial and temporal patterns of snow temperature gradients in a mountain snowpack*. Master of Science Thesis, Department of Earth Sciences, Montana State University, 85 pp.

Deems, J.S., S.R. Fassnacht, and K.J. Elder, 2006. Fractal distribution of snow depth from LiDAR data, *Journal of Hydrometeorology*, 7(2), 285-297.

Dexter, L.R., 1986. *Aspect and elevation effects on the structure of the seasonal snowcover in Colorado.* Ph.D. dissertation, University of Colorado, 228 pp.

Dingman, S.L., 2002. *Physical Hydrology*. Second edition, Prentice Hall, Upper Saddle River, New Jersey, 646 pp.

Doesken, N.J., and A. Judson, 1996. *The Snow Booklet: A Guide to the Science, Climatology, and Measurement of Snow in the United States*, Department of Atmospheric Science, Colorado State University, Fort Collins, 86 pp.

Dozier, J., 1980. A clear-sky spectral solar radiation model for snow-covered mountainous terrain, *Water Resources Research*, 16 (4), 709-718.

Elder, K., and J. Dozier, 1990. Improving methods for measurement and estimation of snow storage in alpine watersheds, in *Hydrology in Mountain Regions. I - Hydrological Measurements, Water Cycle, IAHS Publ*. no. 193, 147-157.

Elder, K., J. Dozier, and J. Michaelsen, 1991. Snow accumulation and distribution in an alpine watershed, *Water Resources Research*, 27, 1541-1552.

Elder, K., J. Michaelsen, and J. Dozier, 1995. Small basin modelling of snow water equivalent using binary regression tree methods, in *Biogeochemistry of Seasonal Snow-Covered Catchments, IAHS Publ.* No. 228, 129-139.

Elder, K., W. Rosenthal, and R. Davis, 1998. Estimating the spatial distribution of snow water equivalent in a montane watershed, *Hydrological Processes*, 12, 1793-1808.

Ellsworth, A.C., 2002. *Inorganic Nitrogen retention within a high-elevation watershed in the Snowy Range of Wyoming*. Master of Science thesis, Department of Earth Resources, Colorado State University, 79 pp.

Erickson, T.A., 2004. *Development and Application of Geostatistical Methods to Modelling Spatial Variation in Snowpack Properties, Front Range, Colorado*. Ph.D. dissertation, Department of Geography, University of Colorado, 190 pp.

Erickson, T.A., M.W. Williams, and A Winstral, 2005. Persistence of topographic controls on the spatial distribution of snow in rugged mountain terrain, Colorado, United States, *Water Resources Research*, 41 (4), 1-17, doi:10.1029/2003WR002973.

Erxleben, J., K. Elder, and R. Davis, 2002. Comparison of spatial interpolation methods for estimating snow distribution in the Colorado Rocky Mountains, *Hydrological Processes*, 16, 3627-3649.

Fassnacht, S.R., K.A. Dressler, and R.C. Bales, 2003. Snow water equivalent interpolation for the Colorado River Basin from snow telemetry (SNOTEL) data, *Water Resources Research*, 39 (8), 1208-1218.

Fassnacht, S.R., 2004. Estimating Alter-shielded gauge snowfall undercatch, snowpack sublimation, and blowing snow transport at six sites in the coterminous USA, *Hydrological Processes*, 18, 3481-3492.

Fu, P., and P.M. Rich, 2000. *The Solar Analyst 1.0 User Manual*, Helios Environmental Modeling Institute, LLC (HEMI).

Goodison, B.E., P.Y.T Louie, and D. Yang, 1998. *WMO solid precipitation measurement intercomparison final report*, WMO Instruments and Observing Methods Report No. 67, WMO/TD No. 872.

Gray, D.M., and D.M. Male, 1981. *Handbook of Snow: Principles Processes, Management and Use*. Blackburn Press, Caldwell, New Jersey, 776 pp.

Groisman, P.Y., and D.R. Easterling, 1994. Variability and trends of total precipitation and snowfall over the United States and Canada, *Journal of Climate*, 7, 184-205.

Harry, D., 2006. *Personal communication*, Associate Professor of Geophysics, Department of Geosciences, Colorado State University.

Hasfurther, V.C., G.L. Kerr, G. Parks, and J. Wetstein, 1994. Chapter 9 "*Hydrology*" in *The Glacier Lakes Ecosystem Experiments Site*, R.C. Musselman (editor), General Technical Report RM-249.

Henderson, F.M., 1966. *Open Channel Flow*, MacMillan, New York, New York, 544 pp.

Herschy, R.W., 1973. The magnitude of errors at flow measurement stations: Hydrometry, Proceedings of the Koblenz Symposium, 1970, UNESCO, *World Meteorological Organization, International Association of Hydrological Sciences*, 1:109-131.

Hood, E., M. Williams, D. Cline, 1999. Sublimation from a seasonal snowpack at a continental, mid-latitude alpine site, *Hydrological Processes*, 13, 1781-1797.

Hosang, J., and K. Dettwiler, 1991. Evaluation of a water equivalent of snow cover map in a small catchment area using a geostatistical approach, *Hydrological Processes*, 5 283-290.

Isaaks, E.H, and R.M. Srivastava, 1989. *An introduction to applied geostatistics*, Oxford University Press: New York, 592 pp.

Johnson, G. L., and C. L. Hanson, 1995. Topographic and Atmospheric Influences on Precipitation Variability over a Mountainous Watershed, *Journal of Applied Meteorology*, 34, 68-87.

Kaluzny S.P., S.C. Vega, T.P. Cardoso, and A.A. Shelly, 1998. *S+ Spatial Stats: User's Manual for Windows and Unix*, Springer Press, New York, 327 pp.

Kattelmann, R. and K. Elder, 1991. Hydrologic characteristics and water balance of an alpine basin in the Sierra Nevada, *Water Resources Research*, 27(7), 1553-1562.

King, H.W. and E.F. Brater, 1963. *Handbook of Hydraulics*, Fifth edition, McGraw-Hill, New York, New York, 582 pp.

Korfmacher, J.L. and D.M. Hultstrand, 2006. Glacier Lakes Ecosystem Experiments Site hourly meteorology tower data. Fort Collins, CO: U.S. Department of Agriculture, Forest Service, Rocky Mountain Research Station.

Luce, C. H., D.G. Tarboton, and K.R. Cooley, 1998. The influence of the spatial distribution of snow on basin-averaged snowmelt, *Hydrological Processes*, 12, 1671-1683.

Marks, D., and J. Dozier 1992. Climate and energy exchange at the snow surface in the alpine region of the Sierra Nevada, *Water Resources Research*, 28 (11), 3043-3054.

Marks, D., and A. Winstral, 2001. Comparison of Snow Deposition, in Snow Cover Energy Balance, and Snowmelt at Two Sites in a Semiarid Mountain Basin, *Journal of Hydrometeorology*, 2 (3), 213-227.

McClung, D. and P. Schaerer, 1993. *The Avalanche Handbook,* The Mountaineers, Seattle, WA, 272 pp.

Meiman, J.R., 1968. Snow accumulation related to elevation, aspect and forest canopy, in *Snow Hydrology, Proceedings of Workshop Seminar*, Ottawa, Ontario, 35-47.

Molotch, N.P., R. C. Bales, M.T. Colee, and J. Dozier, 2003. Optimization of binary regression tree models for estimating the spatial distribution of snow water equivalent in an alpine basin, *71st Annual Meeting Western Snow Conference*, Scottsdale, Arizona, 3-15.

Molotch, N.P., T.H. Painter, R.C. Bales, and J. Dozier, 2004. Incorporating remotely sensed snow albedo into spatially distributed snowmelt modeling, *Geophysical Research Letter*, 31, 18 pp.

Molotch, N.P., M.T. Colee, R.C. Bales, and J. Dozier, 2005. Estimating the spatial distribution of snow water equivalent in an alpine basin using binary regression tree models: the impact of digital elevation data and independent variable selection, *Hydrological Processes*, 19 (7), 1459-1479. DOI: 10:1002/hyp.5586.

Musselman, R.C., 1994. The Glacier Lakes Ecosystem Experiments Site, *Rocky Mountain Forest and Range Experiment Station, General Technical Report RM-249*, 94 pp.

Pomeroy, J.W. and R.L.H. Essery, 1999. Turbulent fluxes during blowing snow: field tests of model sublimation predictions, *Hydrological Processes*, 13, 2963-2975.

Reich R.M., and R. Davis, 2004. *Quantitative spatial analysis: Course Reader NR/ST 523*, Colorado State University, Fort Collins, CO.

Roe, G.H, 2005. Orographic Precipitation, *Annual Review, Earth Planet Science,* 33, 645-671.

Ruess, J.O., F.A. Vertucci, R.C. Musselman, and R.A. Sommerfeld, 1995. Chemical fluxes and sensitivity to acidification of two high-elevation catchments in southern Wyoming, *Journal of Hydrology*, 173: 165-189.

Singh, P., and V.P. Singh, 2001. *Snow and Glacier Hydrology*, in Water Science and Technology Library, 37, Kluwer Academics Publishers, The Netherlands, 741 pp.

Sommerfeld, R.A., R.C. Musselman, G.L. Wooldridge, and M.A. Conrad, 1991. The performance of a simple degree-day estimate of snow accumulation to an alpine watershed, in *Snow, Hydrology and Forests in High Alpine Areas, IAHS-AIHS Publ*. no. 205: 221-228.

Sommerfeld, R.A., 1994. Chapter 10 Snow, in The Glacier Lakes Ecosystem Experiments Site, *Rocky Mountain Forest and Range Experiment Station, General Technical Report RM-249*, 94 pp.

Spreen, W.C., 1947. Determination of the effect of topography on precipitation, *Trans. Am. Geophysical Union.*, 28, 285-290.

U.S. Army Corps of Engineers (USACE), 1998. *Engineering and Design: Runoff from snowmelt*, *Department of the Army*, Washington, D.C., EM 1110-2-1406.

U.S. Department of the Interior (USDI), 1997. *Water Measurement Manual*. Third edition, Bureau of Reclamation, A Water Resources Technical Report.

Venables, W.N., and B.D. Ripley, 1994. *Modern applied statistics with S-plus*, Springer-Verlag, New York, 501 pp.

Viessman, W., and G.L. Lewis, 2003. *Introduction to Hydrology*, Fifth edition, Prentice Hall, Upper Saddle River, New Jersey, 612 pp.

Webster, R., and M.A. Oliver, 2001. *Geostatistics for Environmental Scientists*, John Wiley and Sons, New York, NY 271 pp.

Winstral, A., K. Elder, and R.E. Davis, 2002. Spatial Snow Modeling of Wind-Redistributed Snow Using Terrain-Based Parameters, *Journal of Hydrometeorology*, 3, 524-538.

Winstral, A., and D. Marks, 2002. Simulating wind fields and snow redistribution using terrain-based parameters to model snow accumulation and melt over a semi-arid mountain catchment, *Hydrological Processes*, 16, 3585-3603.

Winter, T.C., 1981. Uncertainties in estimating the water balance of lakes, *Water Resources Bulletin*, 17(1), 82-115.

Wooldridge, G.L., R.C. Musselman, R.A. Sommerfeld, D.G. Fow, and B.H. Connell, 1996. Mean wind patterns and snow depth in an alpine-subalpine ecosystem as measured by damage to coniferous trees, *Journal of Applied Ecology* 33, 100-1088.

APPENDIX A:

Snow depth and snow density measurements and the associated values of the independent variables at snow depth measurement locations.

Snow depth measurements were collected using aluminum probe poles and global positioning systems (GPS) were used to record the location of each depth measurement. The independent variables associated with the snow depth location were derived from a 5-m digital elevation model (DEM). Snow density values at each location are the average depth integrated snow density values recorded from the 0.10 m measurements.

n	Easting (m)	Northing (m)	Snow Depth (cm)	Aspect (degree)	Aspect	Elevation (m)	Slope (degree)	Solar Radiation (W/m^2)	Northness
1	394323	4581633	267	120	SE	3437	45	173	0.26
2	394348	4581637	398	127	SE	3418	41	181	-0.25
3	394348	4581658	378	117	SE	3424	44	166	-0.04
4	394363	4581677	260	129	SE	3423	45	186	-0.32
5	394383	4581688	280	122	SE	3413	37	177	0.20
6	394393	4581707	350	132	SE	3419	41	191	-0.09
7	394399	4581719	267	126	SE	3421	36	183	-0.82
8	394417	4581742	270	132	SE	3420	26	147	0.82
9	394449	4581764	295	114	SE	3421	20	163	-0.10
10	394454	4581779	255	135	SE	3422	25	186	0.12
11	394456	4581793	288	155	SE	3425	9	167	-0.37
12	394482	4581787	340	121	SE	3418	15	162	-0.44
13	394497	4581794	214	148	SE	3418	17	184	0.46
14	394510	4581803	254	125	SE	3417	18	172	-0.49
15	394515	4581819	284	102	E	3419	12	152	0.15
16	394530	4581815	211	145	SE	3414	20	184	0.38
17	394546	4581821	231	124	SE	3415	13	166	-0.09
18	394543	4581840	221	117	SE	3416	8	157	-0.24
19	394565	4581847	309	172	S	3415	16	188	0.11
20	394580	4581847	305	175	S	3414	28	211	0.31
21	394586	4581831	354	140	SE	3409	29	194	-0.03
22	394602	4581833	172	164	S	3404	32	213	0.05
23	394609	4581844	349	169	S	3407	33	215	0.19
24	394620	4581846	364	171	S	3410	25	206	-0.08
25	394629	4581845	252	154	SE	3408	31	207	0.39
26	394634	4581837	315	147	SE	3401	35	204	0.03
27	394637	4581832	248	150	SE	3398	33	206	0.79
28	394650	4581823	254	133	SE	3391	30	188	-0.58
29	394636	4581810	298	182	S	3388	23	203	-0.60
30	394610	4581804	262	153	SE	3389	24	197	0.06
31	394595	4581802	272	168	S	3390	27	208	0.12
32	394578	4581797	281	181	S	3387	25	204	-0.24
33	394566	4581813	272	151	SE	3400	44	212	0.08
34	394551	4581800	285	149	SE	3399	41	210	-0.20
35	394529	4581793	202	143	SE	3402	46	204	0.26
36	394513	4581781	205	137	SE	3402	42	197	-0.10
37	394528	4581767	285	144	SE	3386	34	200	0.07
38	394482	4581754	235	140	SE	3399	41	200	-0.27
39	394463	4581736	254	140	SE	3397	41	199	0.33
40	394438	4581727	269	144	SE	3405	40	204	0.46
41	394423	4581698	254	127	SE	3395	36	183	-0.45
42	394400	4581676	236	129	SE	3400	33	184	-0.81
43	394388	4581658	180	128	SE	3398	34	183	-0.33
44	394374	4581630	225	103	E	3397	25	149	0.42
45	394360	4581634	336	116	SE	3409	42	168	0.40
46	394329	4581617	320	110	E	3427	43	157	0.59
47	394333	4581591	247	124	SE	3414	46	179	-0.02
48	394341	4581566	60	107	E	3404	20	156	0.78
49	394386	4581584	164	109	E	3384	14	151	-0.06
50	394320	4581584	135	128	SE	3421	38	185	-0.09
51	394306	4581610	295	131	SE	3441	35	187	-0.16
52	394264	4581583	228	121	SE	3454	44	174	0.18
53	394212	4581577	228	102	E	3483	21	152	0.23
54	394205	4581552	252	128	SE	3477	52	180	-0.83
55	394184	4581528	302	122	SE	3479	51	174	-0.31
56	394171	4581516	310	141	SE	3481	45	202	-0.37
57	394169	4581502	105	137	SE	3470	48	197	-0.15
58	394161	4581485	80	128	SE	3465	37	184	0.11
59	394180	4581501	0	148	SE	3464	33	204	-0.88
60	394211	4581518	61	133	SE	3458	29	188	-0.49
61	394144	4581481	165	135	SE	3471	44	194	0.31
62	394133	4581476	185	133	SE	3476	42	193	-0.51
63	394100	4581469	105	171	S	3473	15	206	-0.45
64	394105	4581479	55	182	S	3475	10	174	-0.84

n	Easting (m)	Northing (m)	Snow Depth (cm)	Aspect (degree)	Aspect	Elevation (m)	Slope (degree)	Solar Radiation (W/m^2)	Northness
65	394104	4581514	0	278	W	3478	8	148	0.01
66	394153	4581527	105	113	SE	3493	10	158	-0.43
67	394168	4581550	30	72	E	3476	15	129	-0.57
68	394178	4581538	258	136	SE	3489	35	196	0.23
69	394193	4581568	90	58	NE	3489	12	126	0.22
70	394206	4581567	160	107	E	3484	31	158	-0.40
71	394235	4581581	210	131	SE	3470	39	189	0.74
72	394240	4581608	310	85	E	3474	25	131	-0.08
73	394255	4581630	174	55	NE	3463	16	112	0.26
74	394281	4581612	130	124	SE	3456	41	178	0.09
75	394293	4581625	280	126	SE	3454	33	182	0.35
76	394299	4581647	130	70	E	3455	12	132	-0.20
77	394329	4581650	109	115	SE	3439	39	165	-0.14
78	394336	4581681	370	123	SE	3445	25	176	0.03
79	394371	4581693	125	125	SE	3427	40	180	0.17
80	394372	4581732	105	115	SE	3443	17	163	0.02
81	394403	4581737	145	137	SE	3427	27	189	0.25
82	394399	4581768	140	129	SE	3442	28	184	-0.01
83	394436	4581770	150	151	SE	3427	12	174	-0.19
84	394449	4581806	60	146	SE	3429	33	199	0.23
85	394477	4581806	220	129	SE	3424	10	163	-0.12
86	394496	4581842	130	111	E	3423	7	152	-0.09
87	394535	4581831	242	113	SE	3417	9	156	0.64
88	394550	4581858	140	162	S	3419	15	185	-0.10
89	394584	4581839	203	171	S	3411	26	207	0.35
90	394618	4581843	246	172	S	3408	28	211	-0.04
91	394601	4581871	154	145	SE	3421	20	187	0.77
92	394628	4581897	170	158	S	3424	14	183	-0.03
93	394631	4581892	55	164	S	3422	17	191	-0.45
94	394646	4581899	0	208	SW	3424	15	181	0.73
95	394660	4581895	82	176	S	3425	25	208	-0.10
96	394671	4581883	95	150	SE	3413	32	205	0.13
97	394667	4581859	255	143	SE	3404	37	202	0.29
98	394639	4581857	155	156	SE	3412	32	210	0.33
99	394647	4581846	168	153	SE	3403	36	210	0.36
100	394653	4581817	220	119	SE	3385	40	173	0.69
101	394651	4581787	212	140	SE	3376	27	193	-0.15
102	394651	4581799	135	145	SE	3379	27	195	0.59
103	394661	4581789	384	124	SE	3373	40	180	0.24
104	394678	4581803	250	141	SE	3361	41	199	-0.01
105	394678	4581790	308	129	SE	3356	41	184	-0.18
106	394675	4581777	195	114	SE	3353	43	164	-0.17
107	394668	4581755	80	130	SE	3350	31	186	-0.24
108	394682	4581771	246	111	E	3346	42	159	0.13
109	394699	4581787	225	145	SE	3344	29	196	-0.56
110	394706	4581779	220	159	S	3341	20	191	-0.16
111	394690	4581747	301	125	SE	3333	16	168	-0.39
112	394683	4581719	228	134	SE	3327	25	184	-0.06
113	394692	4581716	84	132	SE	3326	30	186	-0.61
114	394686	4581682	302	129	SE	3315	15	169	-0.68
115	394699	4581666	270	117	SE	3306	33	168	-0.71
116	394690	4581647	90	175	S	3303	22	198	0.08
117	394696	4581639	166	157	SE	3300	29	204	-0.20
118	394670	4581631	212	140	SE	3298	14	173	0.23
119	394653	4581600	297	98	E	3299	16	148	0.14
120	394703	4581592	197	129	SE	3289	10	161	0.10
121	394725	4581588	118	134	SE	3285	13	169	0.04
122	394737	4581583	134	136	SE	3283	6	156	-0.17
123	394745	4581568	105	176	S	3282	5	159	-0.32
124	394750	4581551	145	219	SW	3280	8	161	0.62
125	394766	4581533	160	199	S	3277	4	154	-0.11
126	394940	4581617	101	290	W	3279	5	152	0.11
127	395024	4581709	150	210	SW	3308	19	186	0.16
128	395071	4581690	135	198	S	3307	23	188	-0.93
129	395098	4581716	150	192	S	3317	8	210	0.34

n	Easting (m)	Northing (m)	Snow Depth (cm)	Aspect (degree)	Aspect	Elevation (m)	Slope (degree)	Solar Radiation (W/m^2)	Northness
130	395110	4581762	170	176	S	3326	10	193	0.06
131	395140	4581792	238	182	S	3334	14	184	0.59
132	395199	4581835	225	212	SW	3342	13	184	0.01
133	395227	4581875	217	225	SW	3356	12	195	0.60
134	395277	4581935	94	207	SW	3375	12	205	0.19
135	395304	4581971	35	217	SW	3385	14	181	0.04
136	395331	4582015	138	181	S	3391	9	170	-0.46
137	395310	4582067	104	230	SW	3396	5	172	-0.54
138	395292	4582109	55	181	S	3399	7	168	0.11
139	395222	4582139	103	-1	NE	3404	0	159	-0.01
140	395224	4582107	101	79	E	3404	1	153	0.28
141	395233	4582072	112	159	S	3407	5	160	-0.08
142	395119	4582004	140	180	S	3398	27	210	-0.36
143	395088	4582005	395	152	SE	3404	44	214	-0.01
144	395059	4581982	120	162	S	3399	39	219	0.01
145	395038	4581976	120	158	S	3401	40	216	0.60
146	395005	4581954	130	158	S	3394	33	213	0.19
147	394995	4581968	143	173	S	3406	31	217	-0.10
148	394958	4581968	225	173	S	3410	35	221	-0.01
149	394942	4581966	40	175	S	3410	40	225	0.26
150	394942	4581946	78	185	S	3395	33	218	-0.22
151	394940	4581925	140	182	S	3384	26	208	0.29
152	394980	4581925	230	165	S	3383	28	209	-0.16
153	395020	4581938	180	157	SE	3382	29	207	-0.67
154	395077	4581957	275	162	S	3379	24	202	-0.34
155	395114	4581961	155	200	S	3380	22	196	0.03
156	395146	4581986	30	186	S	3393	21	200	-0.46
157	395145	4582023	301	175	S	3405	16	189	-0.04
158	395144	4582024	415	166	S	3406	16	189	-0.01
159	395120	4582019	500	167	S	3406	28	211	0.27
160	395119	4582034	235	153	SE	3411	19	190	-0.20
161	395118	4582072	55	135	SE	3417	6	159	0.13
162	395105	4582131	104	94	E	3411	1	145	-0.84
163	395113	4582159	212	48	NE	3411	2	136	0.61
164	395047	4582148	145	28	NE	3413	8	140	-0.81
165	395055	4582113	141	53	NE	3416	5	143	-0.35
166	395064	4582065	178	129	SE	3421	6	158	0.23
167	395077	4582013	343	152	SE	3414	32	208	0.27
168	395049	4582001	358	155	SE	3415	30	208	0.34
169	395027	4582046	203	113	SE	3424	8	156	0.80
170	394995	4582098	166	39	NE	3419	2	137	0.64
171	394953	4582102	194	59	NE	3420	4	141	0.13
172	394963	4582046	87	130	SE	3431	1	150	0.32
173	394974	4582009	218	132	SE	3429	10	165	-0.30
174	394984	4581993	370	161	S	3422	26	205	-0.10
175	395002	4581996	446	149	SE	3422	28	201	-0.06
176	394955	4581994	330	158	S	3428	13	181	0.11
177	394934	4581994	427	183	S	3429	20	199	-0.01
178	394920	4582016	268	118	SE	3433	6	155	-0.34
179	394879	4582047	183	168	S	3424	6	147	0.00
180	394833	4582057	115	111	E	3425	1	136	-0.53
181	394787	4582038	131	173	S	3425	3	133	0.01
182	394806	4582002	178	63	NE	3424	2	142	-0.51
183	394819	4581971	158	49	NE	3438	3	140	-0.10
184	394828	4581968	184	104	E	3438	5	151	0.42
185	394883	4581971	369	154	SE	3425	39	214	-0.54
186	394895	4582003	282	123	SE	3434	8	159	-0.89
187	394799	4581952	290	167	S	3437	32	215	-0.52
188	394777	4581940	500	163	S	3437	27	207	0.34
189	394761	4581937	398	170	S	3438	19	196	0.17
190	394745	4581926	310	177	S	3429	42	222	-0.55
191	394721	4581923	415	160	S	3430	37	217	0.19
192	394701	4581914	432	170	S	3428	36	221	-0.46
193	394693	4581929	280	220	SW	3436	8	164	0.62
194	394712	4581925	85	164	S	3436	25	206	0.26

n	Easting (m)	Northing (m)	Snow Depth (cm)	Aspect (degree)	Aspect	Elevation (m)	Slope (degree)	Solar Radiation (W/m^2)	Northness
195	394736	4581949	50	271	W	3438	2	147	0.35
196	394722	4581991	45	326	NW	3426	8	139	0.98
197	394699	4582029	105	185	S	3425	2	141	0.10
198	394665	4582066	125	274	W	3424	5	142	0.41
199	394616	4582085	95	167	S	3420	4	150	-0.30
200	394571	4582067	115	97	E	3422	4	154	0.66
201	394594	4582007	88	221	SW	3432	1	150	0.57
202	394615	4581955	55	249	W	3431	4	152	0.25
203	394634	4581916	15	195	S	3429	20	196	0.63
204	394628	4581879	89	168	S	3419	14	184	-0.19
205	394688	4581878	350	151	SE	3404	41	212	0.45
206	394674	4581890	454	155	SE	3417	42	214	-0.07
207	394667	4581867	379	143	SE	3407	35	200	0.07
208	394549	4581922	301	177	S	3425	6	166	0.02
209	394500	4581975	161	251	W	3425	1	161	-0.45
210	394421	4581943	145	168	S	3425	4	151	0.71
211	394364	4581915	74	51	NE	3426	5	148	-0.19
212	394378	4581864	163	40	NE	3429	2	145	-0.52
213	394420	4581847	118	147	SE	3425	7	136	0.07
214	394470	4581852	330	96	E	3434	15	148	-0.26
215	394511	4581875	150	117	SE	3424	16	163	-0.08
216*	394572	4581894	88	251	W	3423	8	153	0.22
217	394665	4581850	350	138	SE	3399	36	197	-0.29
218	394681	4581860	280	147	SE	3398	42	207	0.79
219	394691	4581870	314	148	SE	3400	40	209	-0.52
220	394705	4581849	342	145	SE	3377	41	205	0.07
221	394716	4581871	275	162	S	3391	44	220	0.05
222	394767	4581882	85	165	S	3381	45	223	-0.22
223	394792	4581878	112	165	S	3373	35	217	0.12
224	394832	4581875	128	160	S	3366	43	220	0.34
225	394875	4581877	138	163	S	3355	36	217	-0.70
226	394877	4581891	270	159	S	3364	37	216	0.55
227	394887	4581872	218	167	S	3349	36	217	0.37
228	394816	4581846	220	163	S	3348	32	213	0.57
229	394758	4581819	312	161	S	3345	29	207	0.26
230	394729	4581823	204	138	SE	3351	23	185	-0.12
231	394728	4581754	205	132	SE	3326	30	186	-0.44
232	394761	4581774	130	150	SE	3325	27	198	0.01
233	394829	4581782	60	177	S	3318	17	190	-0.25
234	394861	4581778	204	156	SE	3307	40	210	0.12
235	394841	4581771	120	152	SE	3313	30	204	-0.15
236	394880	4581751	45	187	S	3292	19	192	0.01
237	394927	4581766	80	212	SW	3298	15	176	-0.10
238	394905	4581679	156	260	W	3284	16	147	0.31
239	394679	4581288	201	-1	Flat	3277	0	145	0.08
240	394658	4581261	254	102	E	3271	10	153	-0.26
241	394614	4581224	301	103	E	3274	8	161	0.82
242	394634	4581290	298	57	NE	3281	10	128	0.00
243	394672	4581305	115	-1	Flat	3277	0	145	0.00
244	394639	4581321	210	57	NE	3278	7	132	0.55
245	394622	4581395	198	108	E	3284	24	157	-0.40
246	394586	4581381	260	121	SE	3295	33	174	-0.04
247	394604	4581325	75	77	E	3287	16	131	-0.08
248	394601	4581264	155	98	E	3281	18	154	0.79
249	394554	4581297	385	133	SE	3296	17	146	0.01
250	394532	4581332	274	116	SE	3310	25	166	-0.01
251	394511	4581345	130	2	N	3316	20	77	-0.40
252	394526	4581350	185	61	NE	3314	18	116	-0.01
253	394562	4581337	184	123	SE	3298	15	164	-0.16
254	394327	4581276	80	14	N	3358	24	64	-0.16
255	394297	4581247	149	38	NE	3357	23	152	0.97
256	394268	4581239	9	23	NE	3366	13	163	-0.07
257	394218	4581258	0	175	S	3372	9	152	-0.51
258	394219	4581294	10	126	SE	3385	13	166	0.40
259	394200	4581334	0	171	S	3382	12	164	-0.37

n	Easting (m)	Northing (m)	Snow Depth (cm)	Aspect (degree)	Aspect	Elevation (m)	Slope (degree)	Solar Radiation (W/m^2)	Northness
260	394204	4581363	45	149	SE	3389	19	164	-0.06
261	394195	4581388	205	148	SE	3403	32	202	-0.99
262	394191	4581396	95	150	SE	3408	31	208	-0.99
263	394208	4581420	181	141	SE	3411	36	199	0.48
264	394239	4581430	100	151	SE	3406	25	198	0.19
265	394277	4581431	145	119	SE	3399	11	160	-0.33
266	394322	4581444	278	104	E	3391	24	154	0.01
267	394360	4581444	198	255	W	3374	10	147	-0.10
268	394382	4581453	328	80	E	3374	26	124	-0.20
269	394405	4581434	211	123	SE	3360	30	176	0.65
270	394372	4581422	246	135	SE	3369	20	180	-0.28
271	394348	4581427	268	197	S	3371	8	165	-0.43
272	394313	4581403	185	147	SE	3377	37	206	0.52
273	394262	4581335	261	106	E	3370	32	154	0.20
274	394259	4581301	180	103	E	3367	34	150	-0.43
275	394237	4581307	94	99	E	3382	27	147	0.11
276	394247	4581272	271	60	NE	3375	19	104	0.00
277	394287	4581278	140	14	N	3368	49	15	0.09
278	394310	4581309	275	92	E	3353	7	139	-0.82
279	394322	4581270	188	33	NE	3361	29	64	-0.48
280	394345	4581302	73	4	N	3348	9	112	-0.08
281	394394	4581335	177	101	E	3340	13	150	0.49
282	394425	4581315	230	88	E	3339	15	140	0.38
283	394403	4581289	104	75	E	3334	11	145	-0.45
284	394452	4581340	240	38	NE	3331	28	71	-0.13
285	394451	4581317	267	116	SE	3330	24	165	0.56
286	394487	4581300	267	58	NE	3312	12	152	0.20
287	394489	4581324	226	109	E	3322	17	157	0.03
288	394484	4581351	165	23	NE	3317	18	89	0.41
289	394436	4581364	140	63	NE	3329	17	118	-0.66
290	394409	4581397	255	113	SE	3338	35	164	-0.09
291	394418	4581411	256	120	SE	3336	38	174	0.02
292	394462	4581441	324	107	E	3325	21	156	0.43
293	394451	4581413	215	102	E	3322	14	149	0.09
294	394447	4581387	271	62	NE	3324	12	125	0.16
295	394496	4581351	320	32	NE	3315	19	87	0.38
296	394532	4581368	175	25	NE	3308	15	99	0.31
297	394517	4581389	326	88	E	3309	14	141	0.36
298	394564	4581397	229	24	NE	3299	12	109	-0.20
299	394557	4581454	189	85	E	3300	25	130	0.01
300	394483	4581457	304	110	E	3317	23	159	0.81
301	394492	4581492	270	103	E	3318	25	151	0.07
302	394522	4581483	361	119	SE	3305	15	160	0.16
303	394474	4581390	135	71	E	3316	17	125	0.02
304	394578	4581515	98	134	SE	3303	20	178	-0.36
305	394560	4581511	136	183	S	3304	4	154	-0.49
306	394590	4581560	108	209	SW	3309	3	149	-0.16
307	394547	4581559	135	102	E	3323	21	151	-0.10
308	394552	4581578	230	109	E	3322	20	156	-0.21
309	394584	4581585	250	103	E	3311	17	151	0.31
310	394598	4581616	190	138	SE	3312	29	191	-0.65
311	394613	4581631	210	141	SE	3313	16	176	0.08
312	394640	4581614	281	122	SE	3305	16	166	0.21
313	394613	4581593	245	125	SE	3304	15	166	0.17
314	394603	4581563	198	108	E	3304	27	157	0.17
315	394624	4581545	201	76	E	3299	24	120	-0.23
316	394663	4581565	74	131	SE	3296	20	176	0.10
317	394677	4581519	111	158	S	3281	11	172	-0.15
318	394626	4581521	177	148	SE	3290	21	188	-0.46
319	394642	4581499	271	151	SE	3280	12	173	-0.19
320	394669	4581505	151	170	S	3279	10	170	-0.08
321	394692	4581523	114	157	SE	3279	16	182	0.04
322	394630	4581480	145	157	SE	3278	10	168	-0.52
323	394612	4581446	410	46	NE	3279	15	110	0.18
324	394642	4581458	37	-1	Flat	3277	0	142	0.00

n	Easting (m)	Northing (m)	Snow Depth (cm)	Aspect (degree)	Aspect	Elevation (m)	Slope (degree)	Solar Radiation (W/m^2)	Northness
325	394740	4581579	78	162	S	3283	5	157	0.05
326	394731	4581622	237	220	SW	3287	1	146	0.69
327	394737	4581656	164	178	S	3291	7	163	-0.10
328	394357	4581580	188	94	E	3400	23	143	-0.14
329	394392	4581608	254	111	E	3386	25	161	0.23
330	394425	4581626	249	83	E	3378	8	140	0.11
331	394442	4581672	228	144	SE	3383	19	181	-0.18
332	394494	4581714	93	128	SE	3377	22	177	0.09
333	394529	4581726	262	194	S	3370	17	184	-0.69
334	394550	4581766	310	150	SE	3377	32	200	0.10
335	394595	4581782	103	168	S	3380	26	206	-0.19
336	394615	4581790	117	150	SE	3382	27	200	0.68
337	394635	4581797	101	164	S	3382	24	202	-0.71
338	394637	4581741	97	147	SE	3353	12	173	0.19
339	394584	4581731	230	125	SE	3356	21	173	0.62
340	394549	4581722	92	112	E	3368	17	160	-0.33
341	394523	4581720	136	145	SE	3368	21	186	-0.04
342	394485	4581690	228	132	SE	3370	27	183	0.84
343	394475	4581644	114	123	SE	3363	27	174	-0.40
344	394443	4581606	133	116	SE	3366	23	165	0.62
345	394422	4581575	190	111	E	3372	33	160	0.04
346	394394	4581539	183	102	E	3378	19	150	0.21
347	394366	4581507	310	139	SE	3382	10	165	-0.36
348	394297	4581503	110	125	SE	3409	26	177	-0.16
349	394279	4581485	196	123	SE	3411	26	175	-0.32
350	394245	4581469	107	146	SE	3418	30	199	-0.18
351	394144	4581470	143	135	SE	3466	39	194	-0.67
352	394143	4581545	0	308	NW	3478	11	124	0.46
353	394156	4581572	0	354	N	3472	16	133	0.03
354	394174	4581594	57	12	N	3466	11	119	0.46
355	394191	4581614	50	86	E	3461	6	103	0.78
356	394206	4581640	0	46	NE	3455	14	76	0.26
357	394226	4581648	180	34	NE	3468	22	85	-0.03
358	394241	4581665	171	152	SE	3449	2	116	0.06
359	394265	4581681	20	26	NE	3455	3	136	-0.15
360	394294	4581701	0	80	E	3452	7	143	0.07
361	394312	4581702	78	82	E	3449	10	141	-0.17
362	394329	4581733	65	70	E	3446	3	143	0.14
363	394363	4581752	0	85	E	3445	6	145	0.11
364	394374	4581779	0	23	NE	3433	8	134	-0.13
365	394390	4581805	95	71	E	3429	8	137	-0.13
366	394421	4581818	0	43	NE	3440	4	138	-0.03
367	394444	4581831	121	52	NE	3437	7	133	-0.35
368	394472	4581847	25	113	SE	3433	17	162	-0.48
369	394492	4581871	117	120	SE	3429	10	160	-0.02
370	394534	4581896	66	146	SE	3422	6	162	-0.06
371	394555	4581921	93	184	S	3425	6	165	0.07
372	394595	4581933	0	235	SW	3429	8	160	-0.47
373	394577	4581893	15	246	SW	3423	8	155	0.06
374	394614	4581914	65	206	SW	3429	8	167	-0.23
375	394656	4581931	80	211	SW	3432	4	157	0.47
376	394676	4581906	0	165	S	3429	22	201	-0.24
377	394633	4581775	53	160	S	3372	27	205	0.02
378	394630	4581764	113	159	S	3368	29	207	-0.21
379	394646	4581743	125	140	SE	3351	25	189	-0.07
380	394638	4581744	93	155	SE	3354	23	197	0.09
381	394653	4581716	290	160	S	3334	24	199	0.78
382	394849	4581428	342	240	SW	3273	13	156	0.83
383	394872	4581481	154	241	SW	3281	10	176	0.78
384	394882	4581521	1	312	NW	3282	8	129	-0.13
385	394845	4581378	28	241	SW	3289	3	150	0.18
386	394837	4581326	190	337	NW	3291	9	118	-0.01
387	394844	4581276	220	307	NW	3279	13	146	-0.35
388	394824	4581220	203	289	W	3284	5	157	0.12
389	394799	4581197	345	258	W	3297	13	151	0.34

n	Easting (m)	Northing (m)	Snow Depth (cm)	Aspect (degree)	Aspect	Elevation (m)	Slope (degree)	Solar Radiation (W/m^2)	Northness
390	394808	4581137	241	347	N	3299	6	126	-0.06
391	394803	4581088	100	329	NW	3298	8	132	0.19
392	394789	4581033	84	273	W	3303	2	173	0.93
393	394750	4580996	157	305	NW	3303	5	152	0.91
394	394697	4580993	160	280	W	3295	13	141	0.12
395	394646	4581008	135	280	W	3281	13	137	0.00
396	394628	4581063	164	283	W	3275	8	136	0.99
397	394732	4581054	147	306	NW	3297	9	120	-0.47
398	394742	4581105	48	325	NW	3291	9	127	0.22
399	394755	4581154	90	330	NW	3284	16	130	0.66
400	394753	4581209	375	294	NW	3290	32	95	0.17
401	394721	4581250	90	290	W	3277	16	121	-0.03
402	394682	4581286	173	-1	Flat	3277	0	145	0.00
403	394723	4581322	1	-1	Flat	3277	0	145	0.00
404	394779	4581313	218	299	NW	3282	14	120	-0.10
405	394789	4581363	145	272	W	3278	26	129	-0.13
406	394790	4581414	133	263	W	3277	6	142	-0.17
407	394770	4581460	130	315	NW	3277	1	142	0.36
408	394771	4581517	122	223	SW	3277	1	146	-0.59
409	394719	4581516	58	-1	Flat	3277	0	144	-0.02
410	394714	4581463	8	-1	Flat	3277	0	144	0.00
411	394699	4581413	6	-1	Flat	3277	0	145	0.00
412	394667	4581408	4	-1	Flat	3277	0	144	0.00
413	394651	4581458	7	-1	Flat	3277	0	143	0.00
414	394607	4581431	138	24	NE	3285	23	74	-0.26
415	394591	4581476	295	116	SE	3284	19	161	-0.57
416	394625	4581516	101	140	SE	3289	19	180	0.05
417	394662	4581550	115	148	SE	3292	26	196	-0.32
418	394618	4581604	184	149	SE	3306	15	177	-0.14
419	394678	4581629	318	156	SE	3297	15	180	-0.28
420	394713	4581626	343	104	E	3289	16	153	0.35
421*	394280	4581371	173	142	SE	3374	32	198	-0.72
422	394313	4581375	80	152	SE	3364	21	191	-0.47
423	394310	4581377	80	148	SE	3365	26	196	-0.62
424	394314	4581376	83	152	SE	3364	21	191	-0.19
425	394315	4581378	84	152	SE	3364	21	191	0.18
426	394315	4581381	83	145	SE	3366	26	194	0.75
427	394315	4581381	83	145	SE	3366	26	194	0.80
428	394316	4581379	84	152	SE	3364	21	191	0.22
429	394316	4581380	79	145	SE	3366	26	194	0.40
430	394316	4581380	91	145	SE	3366	26	194	0.40
431	394317	4581380	80	145	SE	3366	26	194	0.32
432	394317	4581382	81	145	SE	3366	26	194	0.28
433	394317	4581382	69	145	SE	3366	26	194	0.32
434	394317	4581383	109	145	SE	3366	26	194	0.12
435	394318	4581384	116	152	SE	3365	19	188	0.01
436	394318	4581385	115	146	SE	3366	23	191	-0.15
437	394319	4581387	146	146	SE	3366	23	191	-0.18
438	394318	4581387	154	146	SE	3366	23	191	-0.29
439	394316	4581390	194	140	SE	3370	34	197	-0.15
440	394318	4581392	160	146	SE	3368	30	198	-0.08
441	394321	4581393	135	146	SE	3368	30	198	-0.25
442	394320	4581385	113	146	SE	3366	23	191	-0.02
443*	394499	4581442	100	69	E	3312	15	126	0.40
444*	394804	4581247	135	296	NW	3295	18	116	-0.22
445	394607	4581341	160	78	E	3286	16	132	0.01
446	394605	4581344	165	81	E	3285	16	134	-0.05
447	394601	4581347	166	82	E	3287	14	136	0.48
448	394602	4581347	168	82	E	3287	14	136	0.43
449	394601	4581346	180	82	E	3287	14	136	0.56
450	394601	4581346	185	82	E	3287	14	136	0.56
451	394599	4581346	185	82	E	3287	14	136	0.60
452	394596	4581346	194	83	E	3288	14	137	0.14
453	394595	4581353	194	89	E	3288	14	141	0.17
454	394594	4581351	186	89	E	3288	14	141	0.39

n	Easting (m)	Northing (m)	Snow Depth (cm)	Aspect (degree)	Aspect	Elevation (m)	Slope (degree)	Solar Radiation (W/m^2)	Northness
455	394595	4581349	186	89	E	3288	14	141	0.31
456	394595	4581348	190	83	E	3288	14	137	0.23
457	394591	4581349	195	90	E	3289	15	142	-0.06
458	394591	4581351	205	90	E	3289	15	142	-0.14
459	394591	4581353	217	90	E	3289	15	142	-0.15
460	394585	4581342	218	80	E	3291	18	131	0.23
461	394584	4581346	199	82	E	3290	18	132	-0.40
462	394586	4581347	199	82	E	3290	18	132	-0.56
463	394586	4581348	170	82	E	3290	18	132	-0.51
464	394584	4581351	189	89	E	3290	17	139	-0.39
465	394586	4581351	205	89	E	3290	17	139	-0.56
466	394587	4581353	217	89	E	3290	17	139	-0.25
467*	394633	4581639	296	123	SE	3311	19	169	-0.15
468	394646	4581640	307	124	SE	3308	21	172	0.05
469	394638	4581669	234	142	SE	3316	29	192	0.07
470	394647	4581670	167	167	S	3315	19	188	0.17
471	394635	4581675	187	139	SE	3322	39	198	0.49
472	394622	4581622	302	156	SE	3310	14	178	0.17
473	394782	4581541	212	181	S	3278	2	150	0.49
474	394810	4581504	199	302	NW	3283	18	109	-0.61
475	394850	4581503	135	278	W	3294	20	129	0.12
476	394869	4581540	113	326	NW	3293	9	120	0.08
477	394888	4581578	100	288	W	3276	8	136	-0.78
478	394859	4581591	160	305	NW	3286	20	102	-0.90
479	394816	4581617	248	-1	Flat	3281	0	144	0.00
480	394802	4581574	189	201	S	3280	5	158	-0.61
481	394802	4581664	125	109	E	3288	9	153	-0.46
482	394843	4581666	26	-1	Flat	3281	0	144	0.00
483	394892	4581670	122	229	SW	3281	3	151	0.15
484	394927	4581673	191	187	S	3285	6	162	0.13
485	394929	4581674	164	178	S	3286	11	176	0.28
486	395009	4581653	211	208	SW	3286	10	165	-0.02
487	395048	4581651	122	203	SW	3290	17	182	0.93
488	395006	4581607	147	163	S	3285	3	156	0.88
489	394967	4581631	205	296	NW	3290	3	142	0.02
490*	394961	4581672	304	244	SW	3287	12	157	-0.21
491	394999	4581697	194	207	SW	3300	18	186	-0.28
492	394972	4581718	170	193	S	3301	24	201	0.24
493	394979	4581745	168	180	S	3313	19	194	0.08
494	395010	4581735	117	226	SW	3313	23	180	-0.35
495	395041	4581725	72	212	SW	3322	29	199	0.06
496	395059	4581744	32	220	SW	3322	12	182	0.02
497	395034	4581775	167	203	SW	3328	14	179	-0.33
498	395020	4581798	277	200	S	3330	12	177	0.17
499	394986	4581819	322	248	W	3325	14	156	-0.47
500	394956	4581839	178	169	S	3329	26	206	0.45
501	395017	4581844	1	254	W	3339	23	154	0.39
502	395046	4581842	134	194	S	3344	13	180	0.00
503	395073	4581818	279	169	S	3336	18	191	-0.46
504	395102	4581840	62	152	SE	3340	14	177	0.30
505	395086	4581849	258	148	SE	3345	16	182	0.57
506	395060	4581879	175	182	S	3356	20	197	0.15
507	395102	4581871	246	156	SE	3350	19	191	-0.10
508	395103	4581874	248	161	S	3349	19	193	-0.40
509	395104	4581874	257	161	S	3349	19	193	-0.49
510	395108	4581871	258	176	S	3348	19	195	-0.11
511	395109	4581872	235	176	S	3348	19	195	-0.13
512	395107	4581879	244	167	S	3350	20	197	-0.34
513	395109	4581878	259	173	S	3350	20	197	-0.48
514	395109	4581879	276	167	S	3352	24	203	0.01
515	395111	4581879	240	173	S	3350	20	197	-0.18
516	395109	4581880	255	167	S	3352	24	203	0.16
517	395110	4581880	250	167	S	3352	24	203	0.33
518	395111	4581880	245	167	S	3352	24	203	0.14
519	395112	4581880	250	167	S	3352	24	203	0.16

n	Easting (m)	Northing (m)	Snow Depth (cm)	Aspect (degree)	Aspect	Elevation (m)	Slope (degree)	Solar Radiation (W/m^2)	Northness
520	395112	4581884	238	167	S	3352	24	203	0.39
521	395114	4581883	235	165	S	3352	22	199	0.15
522	395150	4581886	41	174	S	3352	24	205	-0.08
523	395170	4581896	31	208	SW	3355	17	185	-0.72
524	395198	4581943	42	184	S	3373	18	193	0.23
525	395151	4581928	323	154	SE	3368	29	205	0.70
526	395123	4581931	107	184	S	3373	19	195	0.42
527	395077	4581946	172	167	S	3374	25	205	0.18
528	395073	4581978	317	152	SE	3388	34	207	0.02
529	395124	4581992	57	185	S	3393	20	198	-0.59
530	395176	4581996	104	176	S	3397	18	194	-0.53
531	395192	4581991	231	181	S	3395	23	205	-0.14
532	395284	4582005	102	202	S	3399	8	167	0.24
533*	395286	4582008	103	202	S	3399	8	167	-0.09
534	395255	4582029	133	172	S	3402	8	171	-0.27
535	395206	4582027	127	151	SE	3404	11	174	-0.46
536	395161	4582052	176	149	SE	3411	11	174	-0.11
537	395111	4582042	156	134	SE	3416	14	172	-0.05
538	395052	4582022	256	136	SE	3420	7	161	-0.21

* Snowpit

NAD83, Zone 13N

n	Easting (m)	Northing (m)	Snow Density (kg/m^3)	Snow Depth (cm)
A1	394804	4581247	339	135
A2	394499	4581442	474	100
A3	394280	4581371	394	173
B1	394961	4581672	463	304
B2	394633	4581639	447	296
B3	395286	4582008	402	103
C1	394572	4581894	401	88